Control of matter wave tunneling in an optical lattice

Carlo Sias

Advisor:
Prof. Ennio Arimondo

Università degli Studi di Pisa
Dipartimento di Fisica *E. Fermi*
Corso di Dottorato in Fisica Applicata
V Ciclo
January 2008

Acknowledgements

When I arrived in Pisa four years ago I did not know almost anything about experiments with Bose-Einstein condensates. During my Ph.D. I had the opportunity to learn so many things on this subject, so that now I really want to acknowledge all the people that accompanied and helped me in this long way. I want to thank Prof. Ennio Arimondo, who allowed me to work in his laboratory and who encouraged me in working on such interesting topics. Oliver Morsch and Donatella Ciampini were for me as *Virgilio* and *Beatrice* for *Dante*, joining hands with me whenever the way was dark, and theoretical and experimental difficulties were overcoming me. Matteo Cristiani, Emmanuel Courtade, Hans Lignier, Yeshpal Singh, Sandro Wimberger, Alessandro Zenesini were not only my "labmates" during these years: the many scientific discussions we had day by day in the laboratory, that have been fundamental for me to understand the physics we investigated, were joined by discussions about life, so that our relationships became real, wonderful friendships. The Pisa team was like a family for me. And a part of this family were Prof. Maria Allegrini, Prof. Francesco Fuso, Francesco Tantussi (Tupi), Enrico Andreoni and Nicola Puccini. With their help we managed to recover the experiment after the *family drama*, i.e., the fire that in 2005 occurred in our laboratory. As far as the work presented in this thesis is concerned, I acknowledge Prof. Martin Holthaus and André Eckardt for the enlightening discussions we had, especially during their visit in Pisa in 2007. I want also to thank Prof. Francesco De Martini, who encouraged me to move to Pisa to learn about experimental atomic physics.

Apart from the "laboratory family", I had another family in Pisa, made of all the friends I met during these years. Our common house was the flat I developed with Sascha and Angelo. Our common time was made of sharing the happiness and disgraces of our lives (quite often while drinking a beer). Thanks to all these friends, I will always remember my time in Pisa as one of the best in my life.

But apart from the "laboratory family" and the "Pisa family", I have obviously a real one. My parents and my brother were the solid backbone that from far away supported me during all this time, and this thesis is

dedicated to them.

Contents

Introduction

Bose Einstein condensation is a phase transition emerging in systems of integer-spin particles whose temperature is lowered under a critical value [1, 2, 3]. One of the signatures of this phenomenon is the emergence of a phase coherence through the whole system, so that its behaviors can be described by single particle wavefunctions. After two-decades-long efforts in the development of laser cooling techniques [4, 5, 6], Bose-Einstein condensation was achieved in dilute gases of neutral atoms [7, 8]. Apart from its fundamental interest, this experimental result opened the way to the study of the quantum world with macroscopic samples.

In parallel with the research on cooling, the developments on laser physics led to the creation of artificial atomic crystals by use of light-induced periodic potentials, so-called optical lattices [9, 10]. These potentials were applied to Bose-Einstein condensates shortly after their discovery [11].

In the last decade, a large part of the BEC community showed a strong interest in ultra-cold atoms loaded into optical lattices [12, 13]. The periodic potentials proved to be an exceptional tool for manipulating BECs, because of their feasibility in the laboratory with the present technology, and because only few parameters govern the behavior of the sample. In fact, this is described by the interplay between two fundamental physical processes: atom-atom interactions and quantum tunneling.

The unifying theme of this thesis is the quantum tunneling in an ultra-cold gas loaded into an optical lattice. In the experiments that we performed we were able to observe effects due to quantum tunneling as well as to develop experimental techniques to control it.

The thesis is organized as follows.

Chapter 1 introduces the theoretical background of Bose Einstein condensation and gives a full description of the experimental procedure to reach this quantum phase in dilute gases. Moreover, the experimental apparatus of the Pisa BEC laboratory is described.

Chapter 2 introduces to the physics of cold atoms in periodic potentials. Its first part shows how to realize a periodic potential by light interference. Then, the theoretical description of cold atoms in an optical lattice is intro-

duced, with particular attention to the connections with solid state physics. In its final part, the chapter describes the experimental realization of an optical lattice, and the basic procedures for its characterization.

Chapter 3 describes the role of quantum tunneling in the evolution of ultra-cold atoms in an optical lattice. The chapter introduces the concepts of *intra-band* and *inter-band* tunneling, which constitute the main subject of our experimental investigations.

Chapter 4 describes an experiment on inter-band tunneling. In its first part the tunneling rate is defined by use of the Landau-Zener theory of avoided energy crossings. It is then shown that if the quantized energy levels at each lattice site are taken into account, the tunneling is expected to be resonantly enhanced over this Landau-Zener prediction. The observation of resonantly enhanced tunneling is reported. Finally, an investigation on the role of the atom-atom interactions in inter-band tunneling is described. The observation of the expected destruction of tunneling resonances when the strength of the interactions is increased is reported.

Chapter 5 is devoted to the description of an experimental investigation on the control of intra-band tunneling by strong driving of the optical lattice. First the theoretical description of cold atoms loaded into a driven lattice is given by the use of Floquet theory of time-periodic Hamiltonians. Then, the chapter describes how to measure the intra-band tunneling by letting the atoms expand into an optical lattice. The experimental realization of control of tunneling is reported, and the dependence of the tunneling on the strength and the frequency of the driving is investigated. Then, it is explained how the phase coherence of the condensate is affected by the lattice driving. The evidence of a change of the sign of tunneling is reported. Finally, the problem of adiabaticity in a driven lattice is discussed.

Chapter 6 reports on an experiment in which the complete suppression of tunneling is recovered by a "photon assistance". In its first part, the chapter describes the experimental realization of the complete suppression of tunneling by use of a linear potential, lifting the degeneracy between the single site energy levels. Then, the partial recovery of tunneling by a driving of the lattice is reported. The tunneling emerged when the energy carried by the lattice driving matched the position-dependent energy shift induced by the linear potential. An investigation on the dependence of the tunneling on the strength of the driving is described.

Chapter 1

Bose Einstein Condensation in dilute alkali gases

In 1995 the phase transition of a dilute gas of bosons to a Bose-Einstein condensate (BEC) was observed for the first time [7][8]. These experiments were the final results of a decade-long research on cooling of atomic gases. The creation of a Bose-Einstein condensate is the first step of all the experiments that will be described in this thesis. Some theoretical notes about BEC in dilute gases will be given in the first part of the chapter. In the second part the steps to experimentally realize BEC are explained. Finally the sequence used in our experiment is described.

1.1 The non interacting Bose gas

In a gas of non-interacting bosons treated as a grand canonical ensemble, the number of atoms is:

$$N = \sum_m \frac{1}{\exp(\beta\epsilon_m - \mu) - 1} \tag{1.1}$$

where ϵ_m is the m-th energy level, μ the chemical potential, $\beta = (k_B T)^{-1}$, and k_B is the Boltzmann constant. A useful approximation is to consider the energy spectrum to be a continuum, so the sum in Eq. (1.1) can be substituted by the integral:

$$N = \int_0^\infty \frac{g(\epsilon)d\epsilon}{\exp(\beta\epsilon - \mu) - 1} \tag{1.2}$$

where $g(\epsilon)$ is the density of states, which depends on the potential experienced by the bosons. Of particular interest is the case of a harmonic potential, because the traps (magnetic or optical) used in the experiments on

cold Bose gases can usually be well approximated by harmonic ones, whose energy spectrum is:

$$\epsilon_{n_x,n_y,n_z} = \left(n_x + \frac{1}{2}\right)\hbar\omega_x + \left(n_y + \frac{1}{2}\right)\hbar\omega_y + \left(n_z + \frac{1}{2}\right)\hbar\omega_z. \tag{1.3}$$

The density of states then reads:

$$g(\epsilon) = \frac{\epsilon^2}{2(\hbar\omega_{ho})^2} \tag{1.4}$$

where $\omega_{ho} = (\omega_x\omega_y\omega_z)^{1/3}$ is the mean trapping frequency.

Bose-Einstein condensation occurs when the number of atoms N_0 populating the lowest energy level $\epsilon_{0,0,0}$ becomes a macroscopic fraction of the whole system, that is when the chemical potential is $\mu = 0$. This corresponds to a system in which the number of atoms in the excited energy levels $N_{exc} = N - N_0$ is much smaller than the total number of atoms: $N_{exc} \ll N$. When this is the case, it is convenient to separate the atoms in the ground state N_0 from the total number of atoms N in Eq. (1.2):

$$N - N_0 = \int_0^\infty \frac{g(\epsilon)d\epsilon}{\exp(\beta\epsilon) - 1}. \tag{1.5}$$

Substituting the density of states (1.4) into Eq. (1.5) one can solve the integral in the latter equation and obtain:

$$N - N_0 = \zeta(3)\left(\frac{k_B T}{\hbar\omega_{ho}}\right) \tag{1.6}$$

where $\zeta(\cdot)$ is the Riemann ζ function, with $\zeta(3) \simeq 1.2$.

The gas becomes a thermal Bose gas when the temperature reaches a critical value $T = T_C$ such that $N_0 \ll N$. This value can be found by imposing $N_0 = 0$ in Eq. (1.6):

$$k_B T_C = \hbar\omega_{ho}\left(\frac{N}{\zeta(3)}\right) \cong 0.94\hbar\omega_{ho}N^{1/3}. \tag{1.7}$$

Eq. (1.7) shows that for a large enough number of atoms N the critical temperature is much larger than the energy levels separation: $k_B T_c/(\hbar\omega_{ho}) \simeq 0.94N^{1/3} \gg 1$. Then the phase transition from a thermal cloud to a Bose Einstein condensate can be achieved in experiments with cold bosonic gases trapped in harmonic potentials.

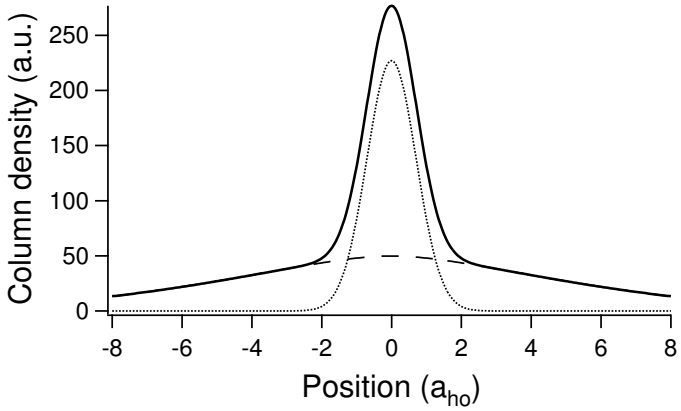

Figure 1.1: Column density of a noninteracting Bose gas at $T = 0.95T_c$ as a function of the position. The dotted line is the density of the condensed fraction, the dashed line the density of the thermal fraction, and the continous line the total density of the gas.

Emergence of condensation

The wave function of the condensed gas fraction corresponds to the ground state of the harmonic oscillator:

$$\phi_0(\mathbf{r}) = \left(\frac{m\omega_{ho}}{\pi\hbar}\right)^{3/4} \exp\left(-\frac{m}{2\hbar}(\omega_x x^2 + \omega_y y^2 + \omega_z z^2)\right). \tag{1.8}$$

Therefore, the condensed atoms have a density distribution $n_c(\mathbf{r}) = N_0|\phi_0(\mathbf{r})|^2$. The thermal fraction of the system can be estimated for $T < T_C$ by substituting Eq. (1.7) in Eq. (1.6):

$$N - N_0 = N\left(\frac{T}{T_C}\right)^3 \tag{1.9}$$

whose density distribution is:

$$n_T(\mathbf{r}) = \frac{1}{\lambda_T} g_{3/2}(e^{-\beta V_{ext}(\mathbf{r})}) \tag{1.10}$$

where $\lambda_T = [2p\hbar^2/(mk_BT)]^{1/2}$ is the thermal wavelength, $g_{3/2}$ is a function of the type: $g_\alpha(x) = \sum_{n=1}^{\infty} x^n/n^\alpha$[14], and $V_{ext}(\mathbf{r})$ is the potential experienced by the gas, i.e., the harmonic potential $V_{ext}(\mathbf{r}) = 1/2m(\omega_x x^2 + \omega_y y^2 + \omega_z z^2)$. A plot of the gas density integrated along one direction (column density) is given in figure (1.1) for $T < T_c$: the condensate appears as a peaked spatial distribution over the wider distribution of the thermal fraction.

1.2 The interacting Bose gas: mean field theory

The many-body Hamiltonian that describes a system of N interacting particles in a potential V_{ext} is:

$$\hat{H} = \int d\mathbf{r}\hat{\Psi}^{\dagger}(\mathbf{r})\left[-\frac{\hbar^2}{2m}\nabla^2 + V_{ext}\right]\hat{\Psi}(\mathbf{r}) + \frac{1}{2}\int d\mathbf{r}\hat{\Psi}^{\dagger}(\mathbf{r})\hat{\Psi}^{\dagger}(\mathbf{r}')V(\mathbf{r}-\mathbf{r}')\hat{\Psi}(\mathbf{r}')\hat{\Psi}(\mathbf{r}) \tag{1.11}$$

where $V(\mathbf{r}-\mathbf{r}')$ is the inter-particle interaction potential and $\hat{\Psi}^{(\dagger)}(\mathbf{r})$ is the boson field operator that annihilates (creates) a particle at the position $\mathbf{r}$. This can be written as:

$$\hat{\Psi}^{(\dagger)}(\mathbf{r}) = \sum_{\alpha}\Psi_{\alpha}(\mathbf{r})\hat{a}_{\alpha} \tag{1.12}$$

where $\Psi_{\alpha}(\mathbf{r})$ is the single particle wave function of the α-th energy level, and $\hat{a}_{\alpha}$ is its corresponding boson annihilation operator, obeying the commutation relations: $[\hat{a}_{\alpha}, \hat{a}^{\dagger}_{\alpha'}] = \delta_{\alpha,\alpha'}$, and $[\hat{a}_{\alpha}, \hat{a}_{\alpha'}] = [\hat{a}^{\dagger}_{\alpha}, \hat{a}^{\dagger}_{\alpha'}] = 0$, $\forall\alpha, \alpha'$. The problem of calculating the ground state of the Hamiltonian (1.11) can be solved analitically by use of a mean field approximation. If the gas is in the BEC phase, that is if $N_0 \gg 1$, the boson creation and annihilation operators of the fundamental state $\hat{a}_0, \hat{a}^{\dagger}_0$ can be considered as complex numbers. Hence the boson field operator $\hat{\Psi}(\mathbf{r})$ can be written as a sum of a complex function for the condensed fraction and a field operator for the atoms in the excited states:

$$\hat{\Psi}(\mathbf{r}, t) = \Phi(\mathbf{r}, t) + \hat{\Psi}'(\mathbf{r}, t). \tag{1.13}$$

The wavefunction of the condensate is defined as $\Phi(\mathbf{r}, t) \equiv \langle\hat{\Psi}(\mathbf{r}, t)\rangle$. The boson field operator in (1.13) is written in the Heisenberg picture, so it is straightforward to write the Heisenberg equation:

$$\begin{aligned} i\hbar\frac{\partial}{\partial t}\hat{\Psi}(\mathbf{r}, t) &= \left[\hat{\Psi}, \hat{H}\right] \\ &= \left(-\frac{\hbar^2\nabla^2}{2m} + V_{ext}(\mathbf{r}) + \int d\mathbf{r}'\hat{\Psi}^{\dagger}(\mathbf{r}', t)V(\mathbf{r}' - \mathbf{r})\hat{\Psi}(\mathbf{r}', t)\right)\hat{\Psi}(\mathbf{r}, t). \end{aligned} \tag{1.14}$$

The integral in Eq. (1.14) is the interaction term. Assuming a dilute gas, the relevant interactions are two-body scattering processes, and the interaction potential can be approximated as:

$$V(\mathbf{r}' - \mathbf{r}) = \frac{4\pi\hbar^2 a_s}{m}\delta(\mathbf{r}' - \mathbf{r}) \tag{1.15}$$

where a_s is the s-wave scattering length. Moreover, if the term $\hat{\Psi}'(\mathbf{r},t)$ in Eq. (1.13) is small, then the operator $\hat{\Psi}(\mathbf{r},t)$ can be substituted with the complex function $\Phi(\mathbf{r},t)$[15]. Therefore the problem (1.14) becomes the so-called *Gross-Pitaevskii Equation*:

$$i\hbar\frac{\partial}{\partial t}\Phi(\mathbf{r},t) = \left(-\frac{\hbar^2\nabla^2}{2m} + V_{ext}(\mathbf{r}) + g\left|\Phi(\mathbf{r},t)\right|^2\right)\Phi(\mathbf{r},t) \tag{1.16}$$

where $g = (4\pi\hbar^2 a_s)/m$. The Gross Pitavskii equation is a Schrödinger equation with a nonlinear term which takes into account the interactions. It is valid if the total number of atoms is much larger than 1, and if the s-wave scattering length is much smaller than the mean distance between atoms. The latter condition corresponds to having a dilute gas, that is, the number of atoms contained in a volume of size a_s must be very small: $\overline{n}|a_s|^3 \ll 1$, where $\overline{n}$ is the mean spatial density.

Thomas-Fermi approximation

The Gross-Pitaevskii equation describes the condensate behavior when the assumption of dilute gas holds. However, this does not mean that the interactions are weak. The gas can be dilute but exhibit strong interactions: this is the case when the interaction energy $E_{int} \propto gN_0\overline{n} \sim gN_0^2/a_{ho}^3$ is much larger than the kinetic energy $E_{kin} \propto N_0\hbar\omega_{ho}$.Therefore the key parameter to estimate the strength of the interactions is:

$$\frac{E_{int}}{E_{kin}} \propto \frac{N_0|a_s|}{a_{ho}}. \tag{1.17}$$

For atoms with a repulsive interaction ($a_s > 0$) in a dilute gas ($\overline{n}|a_s|^3 \ll 1$) the kinetic energy term in the Gross Pitaevskii equation can be neglected. This is known as the *Thomas Fermi approximation*. Under this assumption the density distribution of the condensate reads:

$$\begin{aligned} n(\mathbf{r}) = |\Phi(\mathbf{r})|^2 &= g^{-1}(\mu - V_{ext}(\mathbf{r})) \quad \text{for } \mu > V_{ext}(\mathbf{r}) \\ &= 0 \qquad\qquad\qquad\qquad\quad \text{for } \mu < V_{ext}(\mathbf{r}). \end{aligned} \tag{1.18}$$

For a harmonic potential this corresponds to:

$$n(\mathbf{r}) = \frac{\mu}{g}\left[1 - \frac{x^2}{R_x^2} - \frac{y^2}{R_y^2} - \frac{z^2}{R_z^2}\right] \tag{1.19}$$

where R_i is the so-called Thomas Fermi radius of the condensate along the direction i:

$$R_i = \sqrt{\frac{2\mu}{m\omega_i^2}}. \tag{1.20}$$

The chemical potential can be evaluated by imposing the normalization $\int n d\mathbf{r} = N_0$:

$$\mu = \frac{\hbar\omega_{ho}}{2}\left(\frac{15N_0a_s}{a_{ho}}\right)^{2/5}. \tag{1.21}$$

1.3 Atom cooling by spontaneous emission

The experimental realization of Bose-Einstein condensation in dilute gases has been the final result of a decade-long effort in the research on cooling atomic gases. The first idea on this subject was to exploit the light absorption of the atoms and the Doppler effect due to their motion [16]. In the ideal model an atom in its ground state and with a transition at frequency ω_0 is irradiated by laser light at frequency ω_L. If the detuning $\Delta = \omega_L - \omega_0$ is negative (the laser is *red detuned*), an atom has the maximum probability to absorb a photon when it moves in the opposite direction with respect to the laser propagation, because of the Doppler effect that shifts the laser frequency closer to the atomic transition frequency. Thus, the probability to absorb a photon increases. When this is the case, the atom gains momentum in a direction opposite to its motion, and its velocity is reduced.

This idea can be explained in a more rigorous treatment by considering the radiation pressure of the light by solving the optical Bloch equations [17]. For a small detuning ($\Delta \ll \omega_0$) a process of absorption and spontaneous emission on one atom changes its momentum by:

$$\delta p = \hbar k_L(1 - \cos(\theta)) \tag{1.22}$$

where $\mathbf{k}_L = k_L\hat{\mathbf{z}}$ is the laser wavevector and θ is random. This randomness causes the effect of the photon emission by the atom to average to zero. Therefore the force exerted on the atom is:

$$\mathbf{F} = \frac{\Gamma}{2}\frac{\hbar k_L\Omega_R^2/2}{\Delta^2 + \Gamma^2/4 + \Omega_R^2/2}\hat{z} \tag{1.23}$$

where Γ is the natural linewidth of the excited atomic state, $\Omega_R = \wp E_0/\hbar$ the Rabi frequency of the atomic transition, $\wp$ the electric dipole moment and E_0 the amplitude of the light electric field.

It is interesting to consider the case of two counterpropagating laser beams. In this case the total force is the sum of the forces exerted by the two beams. In order to take into account the Doppler effect, it is convenient to make the substitution $\Delta \to \Delta - k_L v_z$ in Eq. (1.23), where v_z is the atom velocity along

the z direction. One then finds:

$$\begin{aligned}\mathbf{F} &= \mathbf{F}_+ + \mathbf{F}_- \\ &\approx \hbar k_L^2 \Gamma \Delta \frac{\Omega_R^2}{\left(\Gamma^2/4 + \Delta^2\right)^2} v_z \hat{z} \\ &= -\gamma v_z \hat{z}.\end{aligned} \tag{1.24}$$

For red detuning, i.e. $\Delta < 0$, Eq. (1.24) states that the laser fields work as a viscous medium for the atom. Such a system is known as an *optical molasses* [18]. It can be evaluated [19] that the theoretical lowest temperature achievable in an optical molasses is:

$$k_B T_D = \frac{1}{2}\hbar\Gamma \tag{1.25}$$

usually referred to as the Doppler temperature.

1.3.1 SubDoppler cooling

When experimentally realized, 3D optical molasses exhibited a surprising behavior: temperatures far below the Doppler limit (1.25) were observed [20]. The explanation of this experimental evidence was found by treating the atom-light interaction in the so-called dressed atom model [21]. In particular, the sub Doppler cooling was explained as an effect due to a light polarization gradient [22] along the atomic cloud. This process, usually referred as *Sisyphus cooling*, can be easily understood in the case of a *lin* $\perp$ *lin* configuration of the laser beams, that is, the two counterpropagating laser beams have linear, mutually orthogonal polarization. In this case, the overall electric field carried by the laser light is:

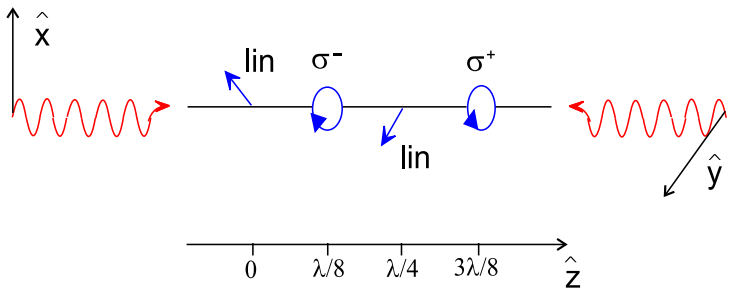

Figure 1.2: Space dependence of the local polarization of the light field in the *lin* $\perp$ *lin* configuration of the laser beams.

$$\begin{aligned}\mathbf{E}(\mathbf{r},t) &= E_0\hat{\mathbf{x}}\cos(\omega_L t - k_L z) + E_0\hat{\mathbf{y}}\cos(\omega_L t + k_L z) \\ &= E_0[(\hat{\mathbf{x}} + \hat{\mathbf{y}})\cos\omega_L t\cos k_L z + (\hat{\mathbf{x}} - \hat{\mathbf{y}})\sin\omega_L t\sin k_L z]\end{aligned} \tag{1.26}$$

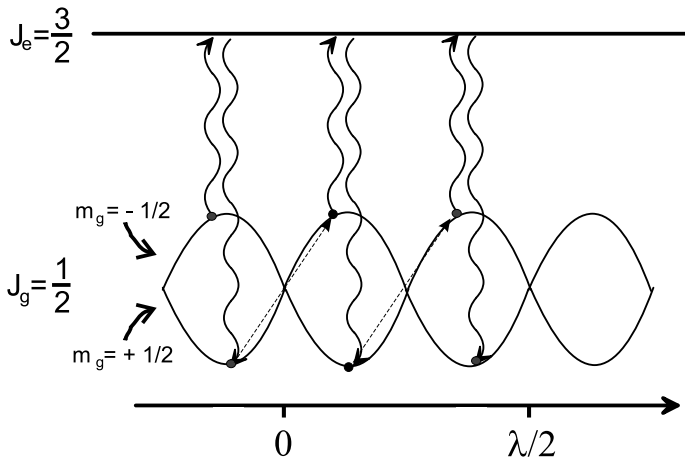

Figure 1.3: Energy of the ground state sublevels of a $J_g = 1/2$ atom in a $lin \perp lin$ laser fields configuration.

so the light polarization changes in space from circular to linear (see Fig. (1.2)). Let us consider the atoms to have a ground and an excited state with total angular momentum $J_g = 1/2$ and $J_e = 3/2$ respectively. As shown in figure (1.3), the two Zeeman sublevels of the ground state have different energy depending on the local polarization of the laser field, and they cross where the local polarization is linear. It can be shown that the maximum probability for an atom to experience a photon absorption is when it is in the higher energy sublevel. Every time an atom spontaneously decay to the lower sublevel after an absorption, it loses the kinetic energy used to climb the potential hill corresponding to the difference in energy between the two ground state sublevels. Then the atom during its motion climbs again the potential hill and the process is repeated. Averaged in time, this sequence causes a cooling of the gas below the Doppler limit. In fact, the steady state kinetic energy is of the order of few times the recoil energies $E_{rec} = \hbar k_L^2/(2m)$, where $k_L = 2\pi/\lambda$ is the light wavevector [23], leading to a temperature (for ^{87}Rb) $T \sim 1\,\mu$K

1.4 The Magneto-Optical Trap

Cooling in optical molasses is based on the dependence of the detuning seen by the atoms on their velocity (1.24). In order to trap the atoms, a good strategy is to make this detuning dependent on the spatial position of the atoms. This can be realized by use of a magnetic gradient b'. In a one dimensional system this corresponds to having a magnetic field varying in space: $\mathbf{B} = b'z\hat{\mathbf{x}}$. Thus the Zeeman energy shift depends on the position of

the atom:

$$\Delta E_Z = \mu_B g_F m_F b' z \tag{1.27}$$

where μ_B is the Bohr magneton, g_F is the Landé factor and m_F is the x component of the angular momentum. The energy shift (1.27) changes the detuning seen by the atoms. Let us assume that two counterpropagating circularly polarized laser beams create an optical molasses along the same z axis. Referring to Fig. (1.4), the detuning for the $\sigma^{(\pm)}$ polarized beams become:

$$\Delta \mp \gamma v_z \pm \mu_B g_F m_F b' z/\hbar, \tag{1.28}$$

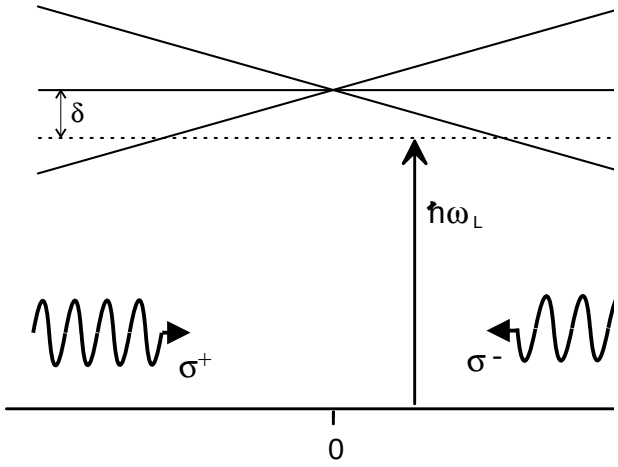

Figure 1.4: Principle of a one dimensional MOT for a $F = 0 \rightarrow F' = 1$ transition. The inhomogeneous magnetic field induces a space-dependent shift of the Zeeman sublevels, producing a space-dependent force on the atoms.

In order to understand how trapping occurs, let us consider the atoms to have the ground state and the excited state with total angular momentum $J_g = 0$ and $J_e = 1$ respectively. The molasses laser beams become resonant to the $m_J = 0 \rightarrow m_J = 1$ transition for $z < 0$ and to the $m_J = 0 \rightarrow m_J = -1$ transition for $z > 0$. If the polarizations of the two molasses beams are circular: σ^+ and σ^-, the atoms absorb photons only when they move away from the $B = 0$ position, and only from the molasses beam that counterpropagates with respect to their motion. This effect can be extended to a three dimensional system with three counterpropagating pairs of laser beams, resulting in a force exerted to the atoms:

$$\mathbf{F} = (-\gamma v + m\omega^2 \mathbf{r}) \tag{1.29}$$

where:

$$\begin{aligned} \gamma &= -\hbar k_L^2 \Gamma \Delta \frac{\Omega_r}{\left(\Gamma^2/4 + \Delta 2\right)^2} \\ \omega^2 &= \frac{\mu g_F m_F b'}{m \hbar k_L} \gamma. \end{aligned} \tag{1.30}$$

The atoms are then trapped around the $B = 0$ point. This trap is known as Magneto-Optical Trap (MOT)[24].

1.5 Evaporative cooling

In order to achieve Bose-Einstein condensation it is necessary to cool the atomic sample far below the temperature reachable in an optical molasses. The technique used in the first observations of Bose Einstein condensation

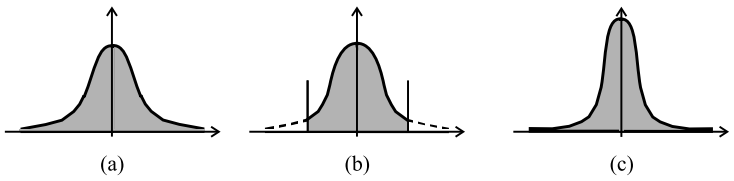

Figure 1.5: The evaporative cooling process: the edges of the thermal velocity distribution of the atoms are cut by expelling the atoms with higher energy. The system then re-thermalizes and the final temperature is lowered

[7][8] was evaporative cooling [25]. The idea is to expel from the whole system the atoms with the highest energy, i.e., by "cutting" the edges of the thermal velocity distribution, as shown in fig. (1.5). The truncated distribution is not in equilibrium, and the remaining atoms undergo a process of thermalization that creates again a Boltzmann distribution of the energies. In order to have an efficient evaporation that lowers the temperature of the system as much as possible with the minimum loss rate, the energy of the system must be varied adiabatically with respect to the thermalization process. The latter depends on the elastic collision rate, so a dense atomic sample is needed for fast evaporation. However, it must be noted that excessive densities cause strong atom losses from the sample due to inelastic and three body collisions.

In order to realize evaporative cooling experimentally, there must be a physical parameter that can be varied in order to expel the most energetic atoms from the trap. This can be done in several ways; in our experiment evaporative cooling was realized both in a magnetic and in an optical trap. These two setup will be explained subsequently.

1.6 The TOP trap

All the optical processes of trapping and cooling have a lower limit corresponding to the recoil energy $E_{rec} = \frac{\hbar^2 k^2}{2m}$ gained by an atom in the absorption of a photon. Cooling below this limit can be achieved by performing evaporative cooling in an all-magnetic trap. The easiest way for trapping neutral atoms without the use of light-assisted processes is to implement a quadrupole trap. A spherical quadrupole field creates a magnetic gradient resulting in a field:

$$\vec{B} = 2b'z\hat{z} - b'y\hat{y} - b'x\hat{x} \tag{1.31}$$

where $\hat{z}$ is called *strong axis* because of the factor 2. The potential is: $U = -\vec{\mu}\vec{B}$, and the energy of the atoms is then:

$$E = \mu_B g_F m_F B. \tag{1.32}$$

Hence the atoms in a state with $g_F m_F > 0$ are trapped, because they will have a minimum of the energy in the origin, where $B = 0$. Note that it is not possible to trap atoms having a state such that $g_F m_F < 0$ because it would be necessary to have a local maximum of the magnetic field, which is forbidden by Maxwell's laws. During their motion, the atoms see the magnetic field always changing in modulus and direction; their magnetic dipole must follow the magnetic field in order to avoid spin flips that would cause a change of the atomic state from trapped to untrapped. This condition is satisfied if the variation of the magnetic field experienced by the atoms is less than the Larmor frequency ω_{Lar}:

$$\frac{d\theta}{dt} < \frac{\mu B}{\hbar} = \omega_{Lar}, \tag{1.33}$$

where θ is the orientation of $\mathbf{B}$. In the $B = 0$ point the derivative of the magnetic field has a discontinuity, therefore the condition (1.33) is not satisfied, causing spin flips and then a loss of atoms from the trap.

In the Time-Orbiting-Potential (TOP) trap [26] the losses of the quadrupole trap are avoided by use of a rotating magnetic bias field B_{TOP} added to the quadrupole field (see fig. 1.6). The $B = 0$ point moves, because of the rotating bias field, in a trajectory called the *circle-of-death*, because the atoms that cross it undergo a spin flip and then are lost from the trap. The radius of the circle of death is $r_{cod} \propto (B_{top}/b')^{1/2}$. The displacement speed of the $B = 0$ point must be such that the atoms cannot follow its trajectory; the potential felt by the atoms then corresponds to the instantaneous potential integrated in time:

$$U(x, y, z) = \int U(x, y, z, t)dt \tag{1.34}$$

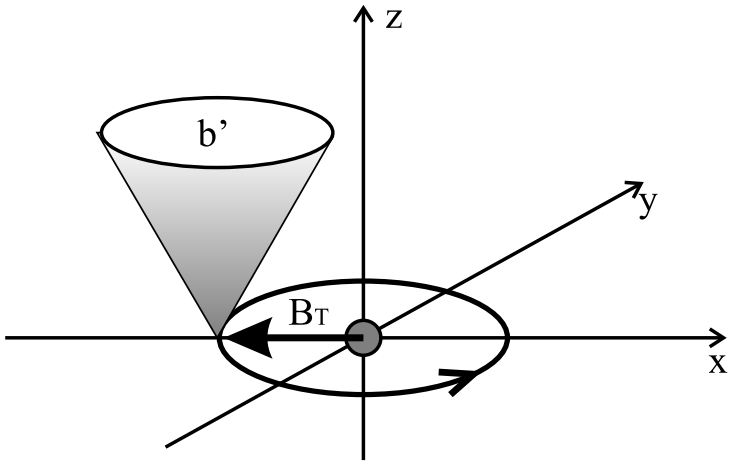

Figure 1.6: The TOP trap. A rotating magnetic bias field causes a continuous displacement of the $B = 0$ point in order to avoid spin flip losses at the center.

It can be shown that the shape of the integrated potential is, close to its minimum, parabolic, with its minimum $B_{min} \neq 0$, and with average frequency:

$$\omega_{ho} = (\omega_x \omega_y \omega_z)^{1/3} = \frac{b'}{\sqrt{B_{TOP}}} \sqrt{\frac{\mu}{m}} \tag{1.35}$$

1.7 The dipolar trap

An alternative method for trapping cold atoms without using spontaneous emission processes is to exploit the dipolar force that emerges when the atoms are illuminated by a laser beam [27]. This force emerges due to the electric field carried by light:

$$\mathbf{E}(\mathbf{r}, t) = \mathbf{E}_\omega e^{-i\omega t} + \mathbf{E}_{-\omega} e^{i\omega t} \tag{1.36}$$

where $\mathbf{E}_{-\omega} = \mathbf{E}_\omega^*$. The resulting potential experienced by the atoms is:

$$U = -\mathbf{d}\mathbf{E}_\omega \tag{1.37}$$

where $\mathbf{d}$ is the atomic electric dipole. Because of the potential (1.37), the ground state of the atoms changes as:

$$\Delta E_g = \sum_e \langle g|\mathbf{d}\mathbf{E}_\omega|e\rangle \frac{1}{E_g - E_e + \hbar\omega} \langle e|\mathbf{d}\mathbf{E}_{-\omega}|g\rangle, \tag{1.38}$$

where the sum is over all the excited states. In fact in Eq. (1.36), the classical field $\mathbf{E}_\omega e^{-i\omega t}$ corresponds to the absorption of a photon in a quantum

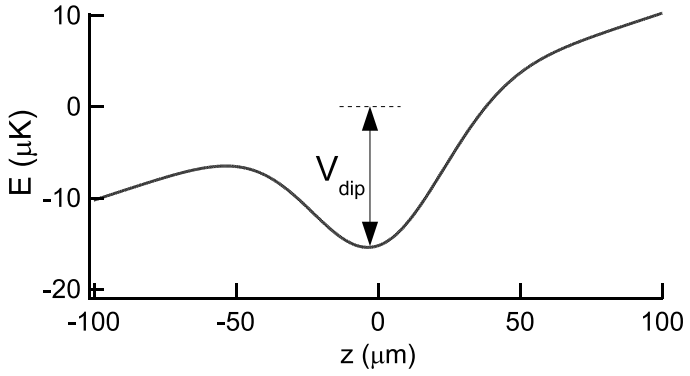

Figure 1.7: Dipolar confinement along the gravity (z) direction created by a laser beam with $\lambda = 1030\,\mathrm{nm}$, $w_0 = 46\,\mu\mathrm{m}$ and of power $P = 1.1\,\mathrm{W}$. V_{dip} is the resulting trap depth.

mechanical treatment, while the field $\mathbf{E}_{-\omega}e^{i\omega t}$ corresponds to the emission of a photon.

After some calculations, Eq. (1.38) becomes:

$$\Delta E_g = -\frac{1}{2}\alpha(\omega)\langle E^2(\mathbf{r},t)\rangle_t \tag{1.39}$$

where $\mathbf{E} = E\hat{\epsilon}$, $\langle\cdot\rangle_t$ corresponds to a time average and $\alpha(\omega)$ is the atomic polarizability:

$$\alpha(\omega) = \sum_e \frac{2(E_e - E_g)\left|\langle e|\mathbf{d}\hat{\epsilon}|g\rangle\right|^2}{(E_e - E_g)^2 - (\hbar\omega)^2}. \tag{1.40}$$

The change in energy of the ground state of the atoms can be seen as being due to the presence of an effective potential V_{eff}. Therefore, the atoms experience a force:

$$\mathbf{F} = -\nabla V_{eff} = -\frac{1}{2}\alpha(\omega)\nabla\langle E^2(\mathbf{r},t)\rangle_t. \tag{1.41}$$

It is important to note from Eq. (1.40) that the dipolar force (1.41) is *attractive* if $\hbar\omega < E_e - E_g$, i.e. the optical field is red detuned, while it is *repulsive* if $\hbar\omega > E_e - E_g$, i.e. the optical field is blue detuned. In the description given above, the effect of spontaneous emission has been ignored. This approximation is valid in the limit that the detuning of the optical field is much larger than the frequency of the atomic transition:

$$|\Delta| = |\hbar\omega - (E_e - E_g)| \gg (E_e - E_g). \tag{1.42}$$

Therefore, within this approximation the light excites the atoms to virtual energy levels, and then the atoms decay to the ground state with a stimulated

emission process. The absence of spontaneous emission processes, i.e., photon scattering, makes the heating of the sample negligible.

Therefore, a red detuned optical laser creates a trap for the atoms. This trap is usually called *dipolar trap*. Its depth in Kelvin is:

$$V_{dip} = \frac{\hbar\Gamma^2}{\pi\Delta I_{sat} k_B} \frac{P}{w_0^2} \tag{1.43}$$

where P is the power of the laser beam and w_0 its waist. The radial frequency of the dipolar trap is:

$$\omega_{dip} = \sqrt{\frac{2\Gamma^2\hbar}{\pi|\Delta|mI_{sat}}} \frac{\sqrt{P}}{w_0^2}. \tag{1.44}$$

1.8 The Experiment

The first step of our experiments is the production of Bose-Einstein condensates of ^{87}Rb atoms. This is an alkali element, i.e., of the group 1A in the Mendeleev periodic table, with the valence electron in the $5^2S_{1/2}$ orbital. The lowest energy transitions are hence to the $5^2P_{1/2}$ and to the $5^2P_{3/2}$ levels, usually called the D1 and D2 lines, centered at 795 nm and 780 nm respectively. The optical transition we used to cool the atoms was the D2 line, whose spectrum is shown in figure (1.8), where the hyperfine levels of the $5^2S_{1/2}$ and $5^2P_{3/2}$ states are called F and F' respectively. The ground state hyperfine level used in our experiment was $|F = 2\rangle$. Therefore, the frequency of the light used for the optical molasses and the MOT was near resonant to the transition $|F = 2\rangle \rightarrow |F' = 3\rangle$, the so-called laser cooling transition, and hence only the atoms in the $|F = 2\rangle$ level were trapped in the MOT. However, this laser cooling transition is not closed: the atoms can be off-resonantly excited to the $|F' = 2\rangle$ level, then decaying to $|F = 1\rangle$. This effect would cause a depletion of the number of atoms in the MOT. In order to circumvent this problem, a light near resonant to the $|F = 2\rangle \rightarrow |F' = 2\rangle$ transition was added to the laser cooling light, hence re-pumping the atoms in the $|F = 1\rangle$ level to the $|F = 2\rangle$ one. This light is called *re-pumper*.

1.8.1 Laser sources

The light for the laser cooling and the re-pumper was provided by two master lasers, whose output was then optically amplified in order to have the power needed for the experiment. A master laser was composed of a commercial laser diode, whose natural linewidth was of the order of few MHz. In order to reduce the linewidth, the diode output was sent to a grating creating an

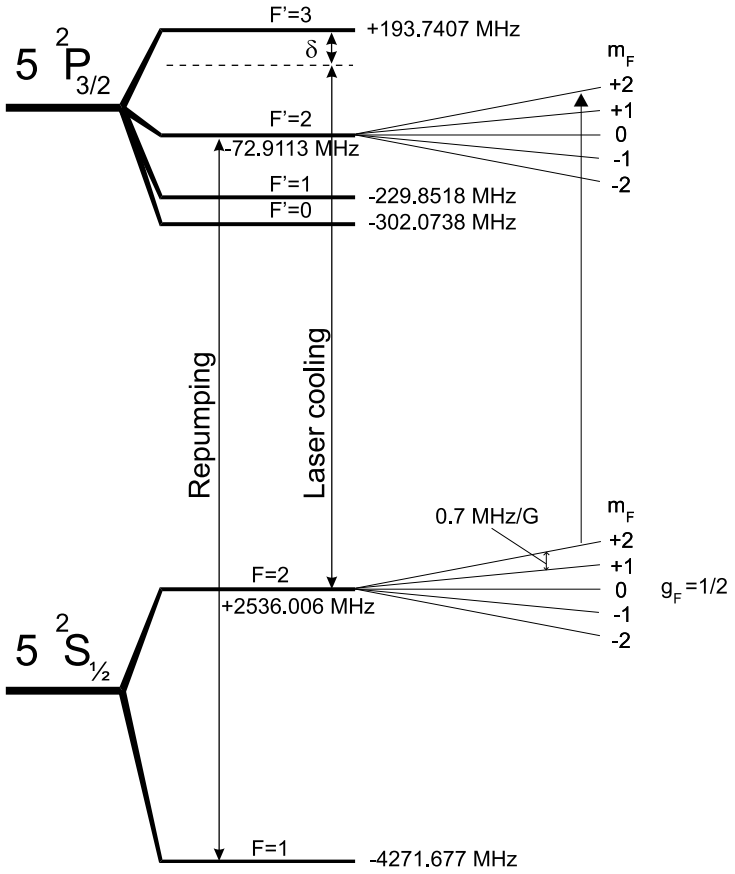

Figure 1.8: Scheme of the D2 line of ^{87}Rb

external cavity with its first order of diffraction. At the back of the grating a piezo electric transducer was placed to vary the cavity length. The diode and the grating were placed in a home-made mount, stabilized in temperature with two Peltier elements with more than 0.01K of precision. Moreover, the current was supplied by external batteries rather than power supplies in order to avoid any coupling to the usual line noise.

The stability of the frequency of the master laser output is a crucial point in a cold atoms experiment. This goal was fulfilled by locking the laser frequency to an atomic transition. This was realized by sending a small portion of the laser output to an optical circuit. There, two beams were sent almost counterpropagating to a cell containing thermal vapor of Rb, one of them being stronger than the other. This beam (pump) saturated the transition, so it was possible to measure the saturated absorption spectrum by measuring the power of the weaker beam with a photodiode. Its output was used to create an error signal then sent to the piezoelectric transducer.

The output power of the two master lasers was $\sim 20\,\mathrm{mW}$. The re-pumper light was then amplified by injecting a slave laser diode, whose output power

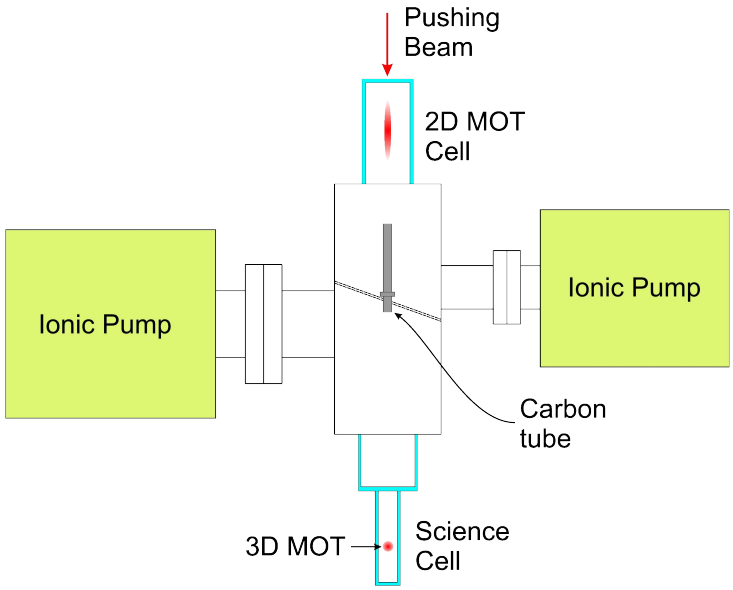

Figure 1.9: Scheme of the vacuum chamber. The magnetic field coils and both the 2D and 3D MOT laser beams are not shown.

was $\sim 55\,\mathrm{mW}$. The master used for generating the laser cooling light was amplified in two stages: the master light injected a slave diode laser whose output was in turn used to inject a MOPA amplifier, whose output power was up to 600 mW. This light was used for all the purposes of the experiment, by splitting it and varying its frequency with acousto-optic modulators (AOMs).

1.8.2 The vacuum chamber

The apparatus was composed of two quartz vacuum cells placed at opposite sides of a central body. This was made of steel and internally devided by a septum (see Fig.(1.9)) that divided the vacuum chamber into two parts, connected only by a hole placed in the center of the internal septum, where a carbon tube was placed. The two cells had a square section and different sizes: $(49 \times 49 \times 100)\,\mathrm{mm}$ and $(24 \times 24 \times 90)\,\mathrm{mm}$. Two ionic pumps were connected with the two parts of the vacuum chamber, in order to have a pressure $\sim 10^{-9}\,\mathrm{mbar}$ in the big cell and $\sim 10^{-11}\,\mathrm{mbar}$ in the science cell , where the experiments are performed (for this reason called the "science cell").

The Rb atoms were provided by two pairs of dispensers: electric resistances whose surface was covered with Rb, which was emitted when an electric current flowed in them. The dispensers were placed close to the big cell, where a two dimensional MOT was created by two pairs of counterpropagating laser

beams circularly polarized with waist $w_0 = 12\,\mathrm{mm}$. These were detuned by $\Delta = -2.4\Gamma$ from the $|F = 2\rangle \rightarrow |F' = 3\rangle$ transition ($\Gamma = 6.065\,\mathrm{MHz}$ is the natural linewidth of the $|F' = 3\rangle$ level), and a repumper beam was added to them. The 2D MOT magnetic gradient was $b' = 11\,\mathrm{G/cm}$.

In the 2D MOT the atoms were collected in a cigar shaped cloud, whose long axis was parallel to the carbon tube. In the same direction, a near resonant laser beam (the "pushing beam") was sent in order to push the atoms from the 2D MOT cell to the science cell through the carbon tube. The corresponding atomic flux was collected by a 3D MOT in the science cell.

1.8.3 The 3D MOT

The 3D MOT was created by splitting a $\sim 30\,\mathrm{mW}$ beam into six beams of waist $w_0 = 8\,\mathrm{mm}$. The beams were directed to the cell as three mutually orthogonal counterpropagating pairs. A repumper light was added to two of these three pairs. The 3D MOT beams were detuned by $\Delta = -2.5\,\Gamma$ from the $|F = 2\rangle \rightarrow |F' = 3\rangle$ transition. The magnetic gradient for the MOT was $b' = 6.6\,\mathrm{G/cm}$.

The flux of atoms from the 2D MOT led to a continuous loading of the 3D MOT. This loading process was counteracted by an atoms loss process that was mainly due to collisions with background atoms. After $\sim 90\,\mathrm{s}$ of loading the MOT reached a stationary size, and up to $2 \cdot 10^9$ atoms were trapped.

A portion of the light scattered by the atoms was collected by a lens and sent to a photodiode, whose signal was proportional to the number of atoms in the MOT. This reference was used in order to start the experiments with clouds of roughly the same size. Loading times of $25 - 40\,\mathrm{s}$ were usually sufficient in order to trap enough atoms before starting sub-Doppler and evaporative cooling.

1.8.4 The magnetic field

For trapping, cooling and displacing the atomic cloud several magnetic fields were used in the experiment.

- The quadrupole field. This was created by six cylindrical pancake-shaped coils placed along the direction of gravity z, that was hence the strong axis with the largest field gradient. In order to create a spatial magnetic gradient, the three coils above the science cell were in anti-Helmholtz configuration with respect to the three coils below the science cell (see Fig.(1.10)). The coils were made of copper and were covered with an insulating sock. The wires used for the coils

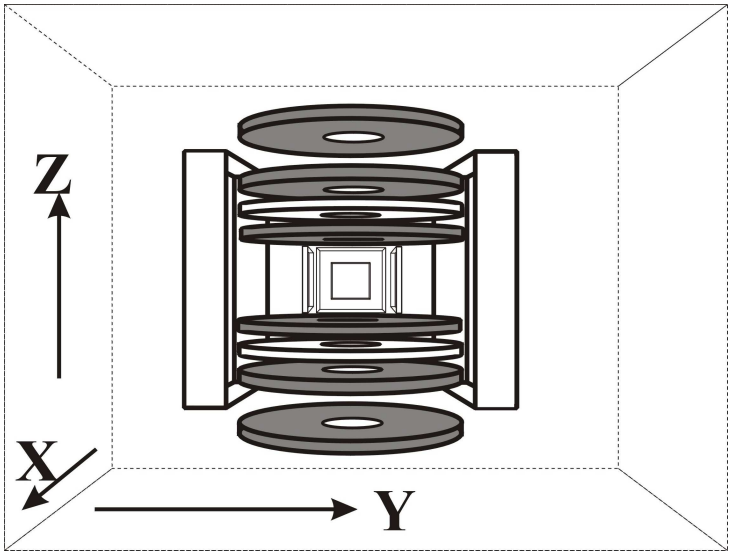

Figure 1.10: Schematic diagram of the mount of the coils for the magnetic gradient (shaded) and the rotating bias field (white). The science cell is at the center of the coils.

were hollow, and a continuous water flow inside them cooled the coils. The resulting magnetic gradient had cylindrical symmetry so that its modulus in the z direction (the strong axis) was $2b'$, while in the x, y directions it was b'. Magnetic gradients up to $b' = 366\,\mathrm{G/m}$ were created when the current was 226 A. This value was reached in 4 ms, while the time for switching off the field was of the order of $10\,\mu$s.

- The rotating bias field. This field B_{TOP} was created by two pairs of coils: a pair of circular coils that were placed in between the quadrupole coils, and a pair of square coils in the orthogonal direction (see Fig.(1.10)), both in Helmholtz configuration. The current flowing in each pair oscillated in time, and the pairs were mutually dephased by $\pi/4$: $I_{circular} = I_{TOP}\sin(\omega t)$, $I_{squared} = I_{TOP}\sin(\omega t + \pi/4)$, with $\omega = 10\,\mathrm{KHz}$. The maximum value of the field was $B_{TOP} = 38\,\mathrm{G}$. The cooling of the coils was assured by their contact with the water-cooled quadrupole coils.

- The compensation coils. These were three muthually orthogonal pairs of coils in the Helmholtz configuration. The current flowing in these coils was of the order of 100 mA. The magnetic field created by these coils was used to compensate the external fields, such as the earth's magnetic field and the magnetic field created by the ion pumps.

- The extra-compensation coil. This was a single coil placed above and

parallel to the quadrupole coils. Its role was to create a magnetic field that was varied during the experiment in order to be able to change the position of the cloud along the z-axis and hence to minimize the losses when the trap was changed, e.g., when passing from the TOP to the dipolar trap.

1.9 The experimental sequence

After that $\sim 10^9$ atoms were trapped in the MOT, sub-Doppler and evaporative cooling were used in order to create a Bose Einstein condensate, which was the starting point for all the experimental investigations reported in this thesis. The different stages for driving the atoms through the BEC phase transition constituted a temporal sequence during which several experimental parameters (laser frequency and intensity, magnetic fields etc.) were changed. Every single experiment performed was destructive, so the whole process had to be restarted from the 3D MOT loading.

The experimental sequence was controlled by a computer, which controlled in time (within a resolution of $10\,\mu$s) all the experimental parameters. In the following, the experimental sequence for the creation of a Bose-Einstein condensate is listed in chronological order.

- The compressed MOT (C-MOT). During this phase the size of the MOT was reduced by decreasing the magnetic gradient (to $b = 2.6\,\mathrm{G/cm}$) and increasing the detuning (to $\Delta = -4.8\,\Gamma$) of the laser. This phase was 200 ms long. This compression was done in order to optimize the loading into the TOP trap.

- The Molasses. During this phase, which was 6 ms long, the magnetic gradient was switched off and the detuning of the laser increased to $\Delta = -5.0\,\Gamma$. The sample was cooled to the sub-Doppler regime, reaching at the end of the stage a temperature around $15\,\mu$K. Moreover, during the molasses phase the capacitors of the quadrupole field power supply were charged, in order to reduce the rising time of the magnetic gradient in the TOP trap.

- Optical pumping. This phase consisted of three light pulses that pumped the atoms into the $|F = 2, m_F = 2\rangle$ state. The light frequency was resonant with the $|F = 2\rangle \rightarrow |F' = 2\rangle$ transition, and the quantization axis was defined by the rotating bias field B_{TOP} that was switched on with amplitude $B_{TOP} = 3.8\,\mathrm{G}$. In order to pump the atoms into the $|F = 2, m_F = 2\rangle$ state, the selection rule for the light-induced atomic transition had to be $\Delta m_F = +1$. This condition was realized when the

light was circularly polarized $\sigma^{(+)}$ and the magnetic field was pointing in the same direction as the light wavevector. Because the direction of B_{TOP} rotated with frequency 10 KHz, the optical pumping was realized by sending to the atoms three light pulses of 10 μs duration and synchronized with the B_{TOP} field in order to illuminate the atoms only when B_{TOP} was pointing in the desired direction.

- The TOP trap. At the end of the optical pumping stage the atoms were loaded into the TOP trap. This was done by increasing the magnetic gradient in 1 ms to $b' = 73$ G/cm, while the rotating bias field was turned on at its maximum value, in order to maximize the circle of death. After the loading, the trap frequencies were first increased in order to enhance the collision rate, and hence to create the conditions for an efficient evaporative cooling. The evaporative cooling was then realized by reducing the circle of death. At the end of the process the cloud contained $\sim 6 \cdot 10^5$ atoms at a temperature $T = 2.5\,\mu$K.

- The Dipolar trap. After the evaporative cooling in the TOP trap, the atoms were loaded into the dipolar trap. This was created by use of a Yb:YAG laser, with a maximum power of 5W and emitting at $\lambda = 1030$nm, i.e., far off-resonance from the Rb transitions. Its output was split into two beams, and each of them was sent to an acousto-optic modulator, and then to the atoms. There the two beams intersected at an angle $\sim 90°$, creating hence an optical trap for the atoms. After passing through the science cell, each beam was collected and sent to a photodiode, whose signal was sent to a PID circuit. In this circuit the photodiode signal was compared to a reference from the computer, and the PID output was then used to control the power of the radiofrequency input of the corresponding AOM and hence the power of the dipolar beam. By these feedback circuits the power of each beam was controlled by the computer, and the noise in the beam powers was reduced to a signal-to-noise ratio $S/N \sim 10^{-4}$. The dipolar beams had a maximum power of 1.2W each, and were focalized to the atoms with a waist $w_0 \cong 46\,\mu$m. The corresponding maximum depth of the optical trap was 7 μK, while the maximum mean frequency was $\bar{\omega} = 490$ Hz.

1.9.1 Bose-Einstein condensation

Once the atoms were loaded into the dipolar trap, evaporative cooling started in this trap as well. This was performed by ramping down in time the power of both the dipolar beams, so both the depth and the frequencies of the optical trap were reduced. The overall ramp was formed by four linear ramps of

decreasing gradient. This cooling stage was 2.5 s long, and at its end a Bose Einstein condensate of up to 10^5 atoms was created. Fig.(1.11a)) reports the CCD image of a sample formed by a thermal part over which a condensate fraction emerges. The density profile reported in Fig. (1.11 a)) shows the typical bimodal distribution (see Fig.(1.1)) in which the Bose Einstein condensate emerges as a density peak surrounded by a broader distribution of thermal atoms. Fig. (1.11 b)) shows the CCD image of an almost pure condensate.

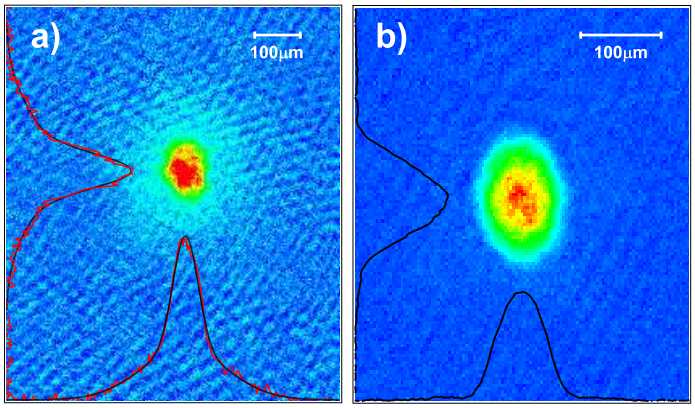

Figure 1.11: Absorption images of the cloud at the end of the evaporative cooling in the dipolar trap. The lines correspond to the density profiles. a) Image of a cloud in which $\sim 30\%$ of the atoms are condensed. The line over the density profile is a fit with a sum of two gaussian functions. b) Image of a cloud which is an almost pure BEC.

Imaging the cloud

At the end of the evaporative cooling the atoms were released from the trap and allowed to expand in free space, in order to decrease the density of the cloud. After a certain time (called *time of flight*) of the order of $\sim 10-20$ ms a resonant light pulse of 10 μs duration was sent to the atoms and then collected by a CCD camera, in which the shadow of the atomic cloud was imaged. This signal was proportional to the column density of the condensate. The CCD camera was purchased from DTA, featuring a Kodak Chip (KAF 1400) with pixel size 6.8 $\times$ 6.8 μm, whose quantum efficiency was 40% at 780 nm. In front of the CCD camera an objective (Rodenstock Aporadagon) of focal length $f = 75$ mm and f-number $f/\# = 4.5$ was placed. The objective was optimized for 1:2 reduction, but it was used reversed in order to have a magnification of ~ 2. The system was focused by minimizing the apparent size of small atomic clouds imaged on the CCD. The calibration of the image

size was done by performing an experiment of free fall of the condensate under gravity.

Chapter 2

Optical lattice

The experiments described in this thesis were performed on Bose Einstein condensates in a periodic potential. This was created optically by the interference of two laser beams, far detuned from the atomic transitions. This chapter gives both the theoretical and the experimental background of the physical system that forms the basis of our experiments.

2.1 Introduction

At the end of the 1970s, the technological developments in experimental laser physics allowed to realize experiments on the interactions between atomic beams and standing waves created by the interference of laser beams [28]. The study of the interactions between atoms and light of frequency near resonant to some atomic transition eventually led to the realization of laser cooling [4, 5, 6].

On the other hand, the study of the interactions of atoms and far off-resonant light also paved the way towards "atom optics" [9, 29]. Within this subject, many predicted effects were observed using atomic beams as a sample [10, 30]. This interest was renewed once cold atomic clouds were realized, and the periodic potentials created by light interference (usually called *optical lattices*) were used to observe basic phenomena of solid state physics [31, 32, 33].

More recently, Bose-Einstein condensates were loaded into optical lattices [11]. The coherence of the BECs permitted to study more accurately solid state physics effects [12], as well as the physics of strongly interacting systems [34]. Within this research field, the emergence of phase transitions such as the superfluid-Mott insulator [35] led to the use of optical lattices for studying the physics of phase transitions.

2.2 Atom optics

A standing wave is created by the interference of two laser beams at frequency $\omega_L = 2\pi c/\lambda$. If the two beams propagate along the x axis and have the same polarization $\hat{\epsilon}$, the resulting total electric field carried by the light is

$$\mathbf{E}(\mathbf{r}, t) = E_0 \sin(k_L r + \omega_L t)\hat{\epsilon} + E_0 \sin(k_L r - \omega_L t)\hat{\epsilon}, \tag{2.1}$$

where E_0 is the amplitude of each field, and $k_L = 2\pi/\lambda$ the light wavevector. Under the hypothesis that the frequency of the laser beams is far off-resonant from the closest atomic transition at frequency ω, i.e. $|\Delta| = |\omega_L - \omega| \gg \omega$, then spontaneous emission can be neglected. Therefore, the stimulated emission process in which j photons are transferred from one laser beam to the second one causes a change of the atomic momentum of $\Delta p = 2j\hbar k_L$ [36]. In this *atom optics* approach the atomic states are plane waves that experience Bragg diffraction from the standing wave. In a j-th order diffraction process, energy conservation reads:

$$\frac{\hbar^2 p^2}{2m} = \frac{\hbar^2 (p + \Delta p)^2}{2m} = \frac{\hbar^2 (p + 2j\hbar k_L)^2}{2m}. \tag{2.2}$$

The condition (2.2) leads to the atom optics analogue of the Bragg law:

$$p = -j\hbar k_L. \tag{2.3}$$

Let us consider a first-order diffraction process in which the initial atomic momentum is $\hbar k_L$. The state of the system after a time t is:

$$\Psi(x, t) = c(-1, t)|-1, g\rangle + c(0, t)|0, e\rangle + c(1, t)|1, g\rangle \tag{2.4}$$

where $|n, g(e)\rangle$ is the free particle state of the ground (excited) level with momentum $n\hbar k_L$. Under the dipole approximation, the Hamiltonian of the system is [29]:

$$\begin{pmatrix} \hbar\omega_0 & -ie^{-i\omega_L t}\hbar\Omega_r/2 & ie^{-i\omega_L t}\hbar\Omega_r/2 \\ ie^{i\omega_L t}\hbar\Omega_r/2 & -\hbar\omega_{rec} & 0 \\ -ie^{i\omega_L t}\hbar\Omega_r/2 & 0 & \hbar\omega_{rec} \end{pmatrix}, \tag{2.5}$$

where:

$\Omega_r = \wp E_0/\hbar$	single beam Rabi frequency
$\wp$	electric dipole moment
$\omega_{rec} = E_{rec}/\hbar$	recoil frequency
$E_{rec} = \hbar^2 k_L^2/2m$	recoil energy

If at $t = 0$ the atomic momentum is $\hbar k_L$, so that the initial state is:

$$\psi(x, t = 0) = |1, g\rangle, \tag{2.6}$$

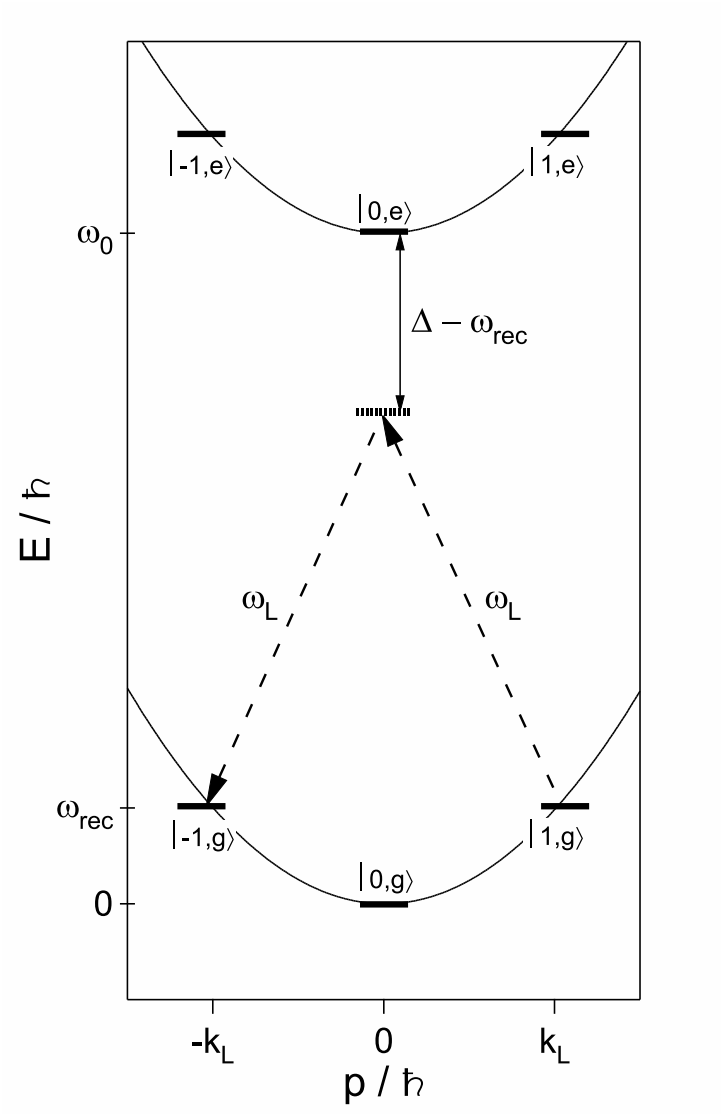

Figure 2.1: First order Bragg transition. The atom initially in the state $|1, g\rangle$ absorbs a photon, thus reaching the virtual level represented by the dotted line. A subsequent stimulated emission of one photon into the other beam forming the standing-wave field takes the particle to the level $|-1, g\rangle$.

then the state of the system at time t is:

$$\begin{aligned} c(-1,t) &= ie^{-i\Omega_r^{(2)}/2} \sin\left(\frac{\Omega_r^{(2)} t}{2}\right) \\ c(0,t) &= 0 \\ c(1,t) &= e^{-i\Omega_r^{(2)}/2} \cos\left(\frac{\Omega_r^{(2)} t}{2}\right), \end{aligned} \tag{2.7}$$

where the two photon Rabi frequency $\Omega_r^{(2)}$ is given by:

$$\Omega_r^{(2)} = \frac{\Omega_r^2}{2\Delta}. \tag{2.8}$$

The atomic momentum oscillates in time from $\hbar k_L$ to $-\hbar k_L$, and the probability of finding the atoms in the initial state is thus:

$$P(p = \hbar k_L, t) = \sin\left(\frac{\Omega_r^{(2)}}{2} t\right) \tag{2.9}$$

This process is known as *Pendellösung oscillation* [37] and it is the analogue of the Rabi oscillations in a two-level system.

2.3 Solid state approach

The effects of a standing wave on an atomic sample can be studied by use of the *dressed-atom* approach [21], for which the light interaction results in a change of the atomic adiabatic levels. Let us consider a system with one ground state $|g\rangle$ and one excited state $|e\rangle$. The Hamiltonian reads:

$$H = \begin{pmatrix} -\hbar\Delta & \hbar\Omega_r \sin(k_L x) \\ \hbar\Omega_r \sin(k_L x) & 0 \end{pmatrix}, \tag{2.10}$$

where x is the mean value of the position and can therefore be considered as a parameter. If one solves the problem by adiabatically eliminating the excited state $|e\rangle$, the energy of the ground state is:

$$E_g = \hbar\frac{\Omega_r^2}{\Delta}\sin^2(k_L x). \tag{2.11}$$

The eigenvalue (2.11) can be considered as a conservative potential experienced by the atoms in the ground state. In the case of far off-resonant light, the population of the excited level is infinitesimally small, therefore the Hamiltonian of the system is:

$$H(x) = \frac{p^2}{2m} + \frac{V_0}{2}\cos(2k_L x), \tag{2.12}$$

where

$$V_0 = \hbar\frac{\Omega_r^2}{\Delta} = 2\hbar\Omega_r^{(2)} \tag{2.13}$$

is the lattice depth, usually expressed in units of recoil energies $E_{rec} = \hbar^2 k_L^2/(2m)$.

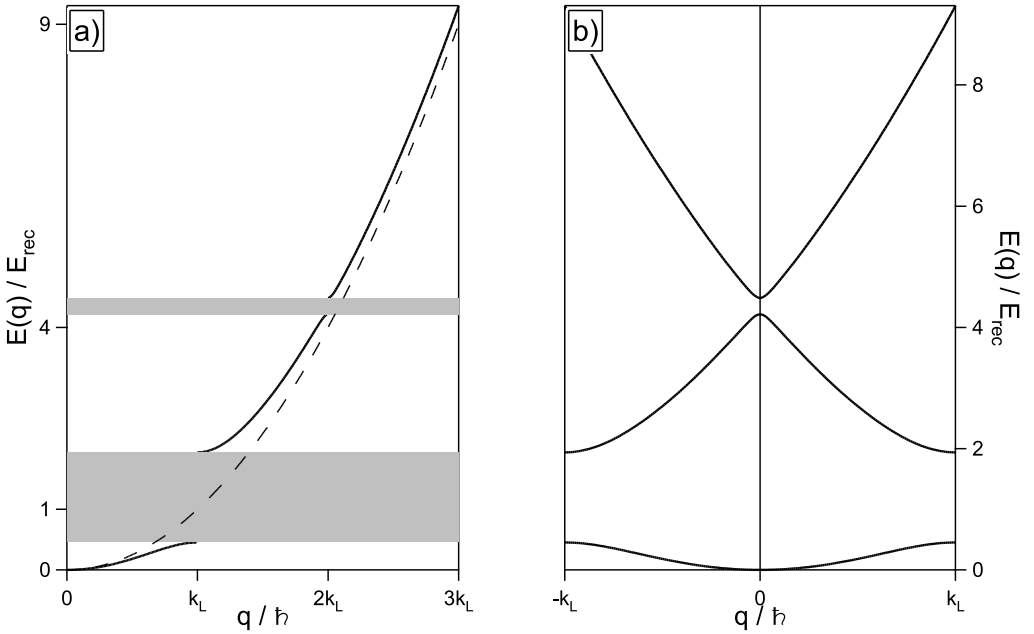

Figure 2.2: a) the dispersion law for the free particle (dashed line) is plotted together with the energy-vs-momentum curve in the presence of the periodic potential (continuous line): the shaded regions correspond to energy gaps; b) the energy spectrum is folded into the first Brillouin zone

Before solving the eigenvalue problem of the Hamiltonian (2.12), let us reanalyze the first order Bragg scattering process within this picture. As stated in the previous section, if the atomic momentum is $\hbar k_L$ the evolution of the atomic wavefunction involves only the states with momentum $\pm\hbar k_L$. In the base formed by the plane waves $|k_L\rangle$, $|-k_L\rangle$, the Hamiltonian (2.12) reads:

$$H = \begin{pmatrix} E_{rec} & V_0/4 \\ V_0/4 & E_{rec} \end{pmatrix}. \tag{2.14}$$

The eigenvalues and eigenfunctions of this Hamiltonian are:

$$\begin{array}{ll} E_1(k_L) = E_{rec} - \frac{V_0}{4}; & |\psi_{1,k_L}\rangle = \frac{1}{\sqrt{2}}(|+k_L\rangle - |-k_L\rangle) \\ E_2(k_L) = E_{rec} + \frac{V_0}{4}; & |\psi_{2,k_L}\rangle = \frac{1}{\sqrt{2}}(|+k_L\rangle + |-k_L\rangle). \end{array} \tag{2.15}$$

Let us call $|\psi(t)\rangle$ the atomic wavefunction. The initial condition is $|\psi(t=0)\rangle = |k_L\rangle$, in which the plane wave $|k_L\rangle$ can be expressed in terms of the eigenvectors (2.15):

$$|k_L\rangle = \frac{1}{\sqrt{2}}\left(|\psi_{1,k_L}\rangle + |\psi_{2,k_L}\rangle\right). \tag{2.16}$$

The atomic wavefunction at time t is therefore:

$$|\psi(t)\rangle = \frac{1}{\sqrt{2}} e^{iE_{rec}t/\hbar}(e^{-iV_0t/4\hbar}|\psi_{1,k_L}\rangle + e^{iV_0t/4\hbar}|\psi_{2,k_L}\rangle). \tag{2.17}$$

The probability at time t that the atomic momentum has at the initial value $\hbar k_L$ is:

$$|\langle +k_L|\psi(t)\rangle|^2 = \sin^2\left(\frac{V_0}{4\hbar}t\right), \tag{2.18}$$

that is equal to the probability (2.9) that was found in the atom optics picture.

Apart from demonstrating that the Hamiltonian (2.12) describes this physical system as the atom optics picture does, the previous calculations allow us to observe one of the key features of the energy spectrum of this problem. The Hamiltonian (2.14) has two eigenvalues $E_1(k_L)$ and $E_2(k_L)$ that are not degenerate, but have a difference in energy $\Delta E_1 = E_2(k_L) - E_1(k_L) = V_0/2$. This corresponds to an *energy gap* in the dispersion law, because a region of forbidden energies emerges. Energy gaps of different sizes emerge in the dispersion law periodically with period $\hbar k_L$ (see Fig.(2.2)). The dispersion law is therefore divided into branches, called *energy bands*, that can be labeled by an index n: in first order Bragg scattering the two eigenvalues (2.15) correspond to the first ($n = 1$) and the second ($n = 2$) band. The energy bands can be folded into the region $[-\hbar k_L, \hbar k_L]$ of momentum space, called first Brillouin zone, and the momentum p is substituted by the *quasimomentum* $q = p + \hbar\mathcal{K}$, where $\mathcal{K} = jk_L$, j integer, is a generic reciprocal lattice vector.

The band structured dispersion law of an atom in an optical lattice recalls the dispersion law of an electron in a crystal. In fact, as in this physical system, the Hamiltonian (2.12) is periodic in space: $H(x) = H(x + d_L)$, where $d_L = \lambda/2$ is the lattice constant. Therefore the Bloch theorem holds [38], and the eigenstates of the Hamiltonian (2.12) are of the form:

$$|\psi_{n,q}(x)\rangle = \sum_q e^{iqx}|u_{n,q}(x)\rangle \tag{2.19}$$

where the functions $|u_{n,q}(x)\rangle$ are periodic in space: $|u_{n,q}(x)\rangle = |u_{n,q}(x + d_L)\rangle$. In the case of a sinusoidal potential as in Hamiltonian (2.12), the wavefunctions (2.19) are the *Mathieu functions* [39]. It is interesting to point out the link between the atom optics and the solid state approach. This can be done by expanding the periodic functions $|u_{n,q}(x)\rangle$ in the Fourier series:

$$|u_{n,q}(x)\rangle = \sum_j u_{n,q}(j)e^{i2jk_Lx}. \tag{2.20}$$

The exponential terms in (2.20) correspond to plane waves of momentum $2j\hbar k_L$:

$$|u_{n,q}(x)\rangle = \sum_j c_{n,q}|2jk_L\rangle. \tag{2.21}$$

Therefore the eigenfunctions (2.19) can be written as a sum of plane waves:

$$|\psi_{n,q}\rangle = \sum_j c_{n,j}(q)|q/\hbar + 2jk_L\rangle. \tag{2.22}$$

The analogies between the problem of an atom in an optical lattice and an electron in a crystal suggest that solid state physics can be explored in a different framework. In fact, with respect to solid state experiments, there are several advantages in studying solid state physics using a condensate in an optical lattice. First, the optical lattice can be easily manipulated: its depth and lattice constant can be varied, it can be switched on and off in a short time, and different lattice structures can be implemented [40]. Moreover, an optical lattice has no impurities, resulting in an increase of the mean free path. Finally, the dynamics of the atoms can be observed both in real and momentum space, and the role of nonlinearity in the system can be explored.

2.4 The tight-binding approximation

In the previous section the Mathieu functions $|\psi_{n,q}(x)\rangle$ were expanded in the basis of the plane waves $|q/\hbar+2jk_L\rangle$. Another full basis of the system is given by the Wannier functions. The Wannier function $|\phi_n(x-x_l)\rangle$ is centered at the l-th lattice site of coordinate x_l, and it is defined as the Fourier transform of the Mathieu function [38]:

$$\phi_n(x-x_l) = \frac{1}{2\hbar k_L}\int_{-\hbar k_L}^{\hbar k_L} dq e^{-ild_Lq}\psi_{n,q}(x). \tag{2.23}$$

The Wannier functions are localized, and Wannier functions centered at different lattice sites are orthogonal:

$$\langle\phi_n(x-x_l)|\phi_n(x-x_j)\rangle = \delta_{l,j}. \tag{2.24}$$

Because the Wannier functions form a complete set, the Mathieu functions can be expanded in this basis:

$$|\psi_{n,q}(x)\rangle = \sum_l c_l|\phi_n(x-x_l)\rangle = \frac{1}{\sqrt{N}}\sum_l e^{ild_Lq}|\phi_n(x-x_l)\rangle. \tag{2.25}$$

The Hamiltonian (2.12) can be expressed in the Wannier basis as well. The Hamiltonian matrix elements are:

$$H_{l,j} = \langle\phi_1(x-x_l)|H|\phi_1(x-x_j)\rangle, \tag{2.26}$$

where for simplicity we restricted the analysis to the fundamental band, i.e., $n = 1$. In the case of a deep lattice one can neglect all the interactions between lattice sites that are not nearest neighbors:

$$H_{l,j} = 0 \qquad \text{for } j \neq l,\, l \pm 1. \tag{2.27}$$

This is a *tight binding* approximation that makes the Hamiltonian matrix tri-diagonal. The terms of the principal diagonal of the matrix are:

$$H_{l,l} = \langle \phi_1(x - x_l)|H|\phi_1(x - x_l)\rangle = E_0, \tag{2.28}$$

while the off-diagonal terms are:

$$H_{l,l\pm1} = \langle \phi_1(x - x_l)|H|\phi_1(x - x_{l\pm1})\rangle = \gamma. \tag{2.29}$$

The off-diagonal terms connect neighboring lattice sites. The physical process that is behind these connections is the inter-well tunneling. This point will be cleared when the Bose-Hubbard model will be introduced. The dispersion law for the fundamental band can be calculated by use of the expansion of the Mathieu function for $n = 1$ in the Wannier basis (2.25) [38]:

$$E_1(q) = \langle \psi_{1,q}(x)|H|\psi_{1,q}(x)\rangle = E_0 + 2\gamma\cos(qd/\hbar). \tag{2.30}$$

2.4.1 The Bose-Hubbard model

In 1998 Jaksch *et al.* [41] proposed to use a tight-binding-like approximation to write an Hamiltonian for a condensate of N interacting bosons loaded in a deep lattice. The starting point is the many-body Hamiltonian for the Bose-field operators:

$$\begin{aligned} H = &\int d^3r\hat{\Psi}^\dagger(\mathbf{r})\left(-\frac{\hbar^2}{2m}\nabla^2 + \frac{V_0}{2}\cos(2k_L x)\right)\hat{\Psi}(\mathbf{r}) + \\ &+ \frac{1}{2}\frac{4\pi a_s\hbar^2}{m}\int d^3r\hat{\Psi}^\dagger(\mathbf{r})\hat{\Psi}^\dagger(\mathbf{r})\hat{\Psi}(\mathbf{r})\hat{\Psi}(\mathbf{r}), \end{aligned} \tag{2.31}$$

where $\hat{\Psi}(\mathbf{r})$ is the Bose field operator in a three dimensional space of coordinate $\mathbf{r} = (x, y, z)$, and the 1D optical lattice is along the x direction. The 3D Hamiltonian (2.31) is separable in three 1D Hamiltonians. In the y, z directions the Bose-field operator can be approximated by a single particle wavefunction $\Phi(y, z)$ as shown when the Gross-Pitaevskii equation was derived. In the x direction, the Bose field operator can be expanded in terms of the boson creation and annihilation operators $a_l^\dagger$, a_l at the single lattice site:

$$\hat{\Psi}^{(\dagger)}(x) = \sum_l a_l^{(\dagger)}\phi_l(x - x_l) \tag{2.32}$$

where the amplitude of each term is given by the corresponding Wannier function. The expansion (2.32) can be now substituted into the Hamiltonian (2.31). If, as in the tight binding approximation, only the interactions between next neighboring sites are considered, then the Hamiltonian along the x axis is:

$$H = -J \sum_{\langle l,j \rangle} a_l^\dagger a_j + \frac{U}{2} \sum_l n_l(n_l - 1) \tag{2.33}$$

where:

- the sum $\langle l, j \rangle$ is over nearest neighbor sites
- $n_l = a_l^\dagger a_l$ is the number operator that counts the number of atoms in the n-th site
- $J = \int dx \phi(x - x_l) \left(-\frac{\hbar^2}{2m} \nabla^2 + \frac{V_0}{2} \cos(2k_L x) \right) \phi(x - x_j)$ is the hopping matrix element that considers the tunneling from one lattice site to a neighboring one. J is equal to the off diagonal term γ (2.29) of the Hamiltonian that was found in the tight binding approximation.
- $U = \frac{1}{2} \frac{4\pi a_s \hbar^2}{m} \int dx \, |\phi(x)|^4$ is the interaction energy of two atoms occupying the same lattice site.

The Bose-Hubbard Hamiltonian (2.33) expresses therefore that the dynamics of cold atoms in a deep lattice depend only on two parameters: the on-site interaction U and the tunneling between lattice sites J. Their dependence on the lattice depth V_0 is [42]:

$$\begin{aligned} J &= \frac{4}{\sqrt{\pi}} E_{rec} \left(\frac{V_0}{E_{rec}} \right) \exp \left(-2 \sqrt{\frac{V_0}{E_{rec}}} \right) \\ U &= \frac{8}{\sqrt{\pi}} k a_s E_{rec} \left(\frac{V_0}{E_{rec}} \right)^{1/4} \end{aligned} \tag{2.34}$$

The preceding formulas demonstrate how the evolution of an atomic sample in an optical lattice can be controlled by just varying the lattice depth. Experimentally, this can be done very easily by changing the power of the laser beams creating the lattice. However, by changing the lattice depth *both* U and J are varied at the same time. The interaction U can be controlled independently by using a Feshbach resonance [43, 44], that allows to vary the scattering length a_s. On the other hand, one can control independently the tunneling parameter J by strongly driving the lattice. This technique has been explored in an experiment described in Chapter 5.

2.5 The lattice and a force

The flow of an electric current in a conductor is one of the fundamental problems of solid state physics. Theoretically, this results in the problem of a crystal Hamiltonian to which an external force is added. This same physical system can be implemented in an experiment of cold atoms in an optical lattice by applying a force F to the atoms.

One of the first solid state phenomena that was observed in an atomic physics experiment were the *Bloch oscillations* [32]. In order to observe how this effect emerges, let us start from the problem of an atom loaded into an optical lattice and on which a force is exerted. The force leads to a linear potential that must be added to the optical lattice Hamiltonian (2.12):

$$H = H_{lattice} + H_F = \frac{p^2}{2m} + \frac{V_0}{2}\cos(2k_L x) - Fx. \tag{2.35}$$

Let us assume that one atom is loaded in the fundamental band of an optical lattice with initial quasimomentum $q = 0$, and to exert at $t = 0$ a constant force F on the atom. At time t the atomic wavefunction is:

$$|\psi(x)\rangle_t = \exp\left(-\frac{i}{\hbar}(H_{lattice} + H_F)t\right)|\psi_{q=0}(x)\rangle_{t=0}. \tag{2.36}$$

The exponential operator into Eq.(2.36) can be transformed in a product of exponential operators by use of the Baker-Campbell-Hausdorff formula [45]. In this operator product, all the terms containing the momentum operator p give no contribution. Therefore, Eq.(2.36) reduces to:

$$\begin{aligned} |\psi(x)\rangle_t &= \exp\left(-\frac{i}{\hbar}H_{lattice}t\right)\exp\left(-\frac{i}{\hbar}H_F t\right)|\psi_{q=0}(x)\rangle_{t=0} \\ &= \exp\left(-\frac{i}{\hbar}H_{lattice}t\right)\exp\left(\frac{i}{\hbar}Fxt\right)|\psi_{q=0}(x)\rangle_{t=0} \\ &= \exp\left(-\frac{i}{\hbar}H_{lattice}t\right)|\psi_{q(t)}(x)\rangle. \end{aligned} \tag{2.37}$$

The state of the atom remains an eigenstate of the Hamiltonian $H_{lattice}$ but with quasimomentum changing in time according to

$$q(t) = Ft. \tag{2.38}$$

In the more general case of a time dependent force $F(t)$ Eq.(2.38) becomes:

$$q(t) = \int F(t)dt. \tag{2.39}$$

Eq.(2.37) states that the evolution of the wavefunction of the atom corresponds to an evolution of its quasimomentum in momentum space. Let us follow this evolution in the case of a constant force step by step:

- At $t = 0$ the quasimomentum is $q = 0$ and the constant force F is switched on.
- At $t = \hbar k_L/F$ the quasimomentum is $q = \hbar k_L$, i.e., the atom is at the first Brillouin band edge.
- The atomic quasimomentum jumps from $q = \hbar k_L$ to $q = -\hbar k_L$, while the atom remains in the fundamental band.
- At $t = 2\hbar k_L/F$ the quasimomentum is equal to its initial value: $q = 0$.

The quasimomentum is therefore periodic in time with period:

$$\tau_B = \frac{h}{F d_L}. \tag{2.40}$$

τ_B is called *Bloch time*. The mean velocity of an atom in the $|\psi_{n,q}(x)\rangle$ state is:

$$\langle v_{n,q} \rangle = \frac{1}{\hbar} \frac{dE_n(q)}{dq}. \tag{2.41}$$

Therefore the time periodic evolution of the quasimomentum causes both the mean velocity and the position of the atom to oscillate with a frequency $\nu_B = \tau_B^{-1}$. This effect is known as *Bloch oscillations*.

While predicted in the 1930s [46], Bloch oscillations were observed for the first time only in the early 1990s in semiconductor superlattices [47, 48, 49], because in natural crystals the Bloch time is much longer than the time of scattering from crystal impurities. Later on, Bloch oscillations were observed in cold atoms in an optical lattice [32, 50, 51] and, more recently, with use of a Bose Einstein condensed sample [52].

It must be noted that in the derivation of the Bloch oscillations given previously, it was assumed that during the time evolution atom always stayed in the fundamental band. However, when a force is exerted on an atom loaded into an optical lattice, at the band edge tunneling through the energy gap to the upper band can occur. This inter-band tunneling will be discussed in detail in the next chapter.

2.6 Experimental realization of an optical lattice

This section is devoted to the description of how an optical lattice can be implemented. First, the setup of the Pisa experiment is described. Then, the problem of adiabatically loading a Bose-Einstein condensate into an optical lattice is discussed. Finally, some experiments performed to measure the lattice depth are presented.

2.6.1 The setup

The optical lattice was created by crossing two (independent) laser beams. The experimental setup is shown in Fig.(2.3). The lattice beams originated from the same laser, a Master Oscillator Power Amplier (MOPA), purchased from Toptica (model TA100). The laser output was single mode at a wavelength centered around $\lambda = 852.2\,\text{nm}$, and its power was up to 750 mW. The laser beam passed first through an optical insulator in order to avoid any back reflection that could affect the light mode. The beam was then split by use of a $\lambda/2$ waveplate and a polarizing beam splitter. Each of the two beams then created was sent to an acousto-optic modulator (AOM) (Crystal Technologies) that diffracted the input beam and detuned it from its initial frequency. Each AOM had its own radio-frequency (RF) source (Agilent 3325A and Stanford DS345). Both the AOMs were aligned in order to optimize the first order of diffraction and had RF input centered at 72 MHz. Therefore the lattice beams were at the same frequency, apart from the cases in which a detuning between them was voluntarily imposed. The zero-th order diffracted light of one AOM was sent to a Fabry Perot cavity that was used to monitor the single mode output of the laser. Each first order diffracted beam was sent to a single mode, polarization preserving optical fiber (OZ Optics). The optical setup described until now was mounted on a different optical table than the one in which the vacuum chamber was placed.

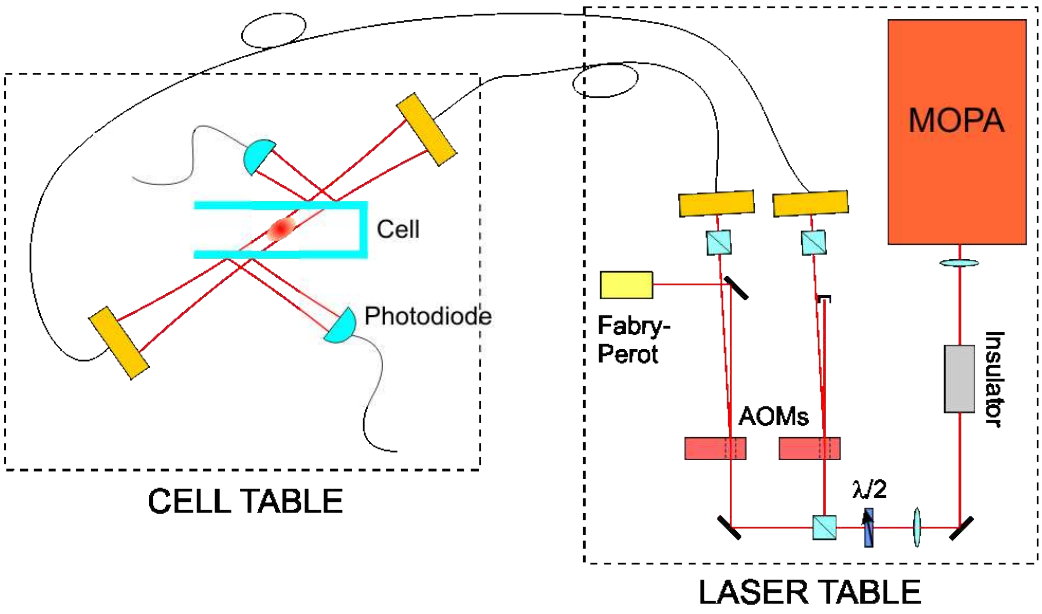

Figure 2.3: Scheme of the experimental setup implemented in our laboratory for the creation of an optical lattice.

The optical fiber outputs were mounted at a distance of 18 cm from the center of the cell, where the condensates were created. The power of each beam at the output was up to 80 mW. In front of each fiber output a polarization cube was placed in a rotating mount as a polarization filter. The two beams were focused onto the atoms, and each beam had a waist of 110 μm at the center of the cell. For each beam, a small portion of the beam that was reflected by the cell was sent to a photodiode, whose signal was sent to a PID circuit with a reference signal provided by the computer. The output of the PID was sent to an attenuator that controlled the RF power at the AOM input, and hence its diffraction efficiency. The PID circuits allowed us to control the power of each lattice beam independently during the experiment, and to reduce the light amplitude noise to a signal-to-noise ratio $S/N \sim 10^{-4}$.

The optical lattice created by the intersection at an angle ϕ of the two laser beams had lattice constant

$$d_L = \frac{\lambda}{2\sin\left(\frac{\phi}{2}\right)}. \tag{2.42}$$

In particular, when the lattice beams were counterpropagating, $d_L = \lambda/2$.

2.6.2 Adiabaticity of loading

Let us suppose that the lattice is suddenly switched on at $t = 0$ at a lattice depth V_0, and that the initial state of the BEC is a plane wave $|p/\hbar\rangle$. The plane waves are not eigenstates of the Hamiltonian of the lattice (2.12). Therefore, the state of the atoms in the basis of the Bloch states $|\psi_{n,q}\rangle$ is:

$$|\psi\rangle_{t=0} = \sum_n |\psi_{n,q}\rangle\langle\psi_{n,q}|q/\hbar\rangle \tag{2.43}$$

where q is the initial momentum p of the atoms in the first Brillouin zone. The probability for the atoms to be in the $|\psi_{n,q}\rangle$ Bloch state is therefore $\langle\psi_{n,q}|p/\hbar\rangle$.

However, in most of the experiments described in this thesis, the atoms had to populate a single Bloch state instead of being in a superposition of many Bloch states as in Eq.(2.43). This can be achieved by loading the lattice in a time τ_{on} such that the atom wavefunction follows the instantaneous adiabatic state. When this is the case the initial free particle state $|p/\hbar\rangle$ is connected to one Bloch state $|\psi_{n,q}\rangle$ whose band index n and quasimomentum q are such that:

$$|p| = (n-1)\hbar k_L + |q|. \tag{2.44}$$

The adiabatic condition can be expressed analytically by use of the adiabaticity criterion [32]:

$$\left|\langle\psi_{n',q}|\frac{d}{dt}|\psi_{n,q}\rangle\right| \ll \frac{|E_{n'} - E_n|}{\hbar}. \tag{2.45}$$

Therefore the loading of the optical lattice is adiabatic if the condition (2.45) holds for any Bloch state with $n' \neq n$. However, the most restrictive condition is for the closer band, that is for $n' = n \pm 1$. Let us suppose that we are interested in loading the condensate in the $|\psi_{1,0}\rangle$ state of the fundamental band. Therefore, the loading will be adiabatic if the condition (2.45) holds for $n' = 2$, i.e., for the Bloch state of quasimomentum $q = 0$ in the first excited band. In the limit of a shallow lattice, the gap between the fundamental and the first excited state can be approximated with its value in the free particle case: $|E_{n'} - E_n| \simeq 4E_{rec}$. Therefore the condition (2.45) can be written [50]:

$$\frac{d}{dt}\frac{V_0}{E_{rec}} \ll 32\sqrt{2}\frac{E_{rec}}{\hbar}. \tag{2.46}$$

If the lattice is ramped up linearly in a time τ_{on}, the condition (2.46) reduces to the following condition for τ_{on}:

$$\tau_{on} \gg \tau_{ad} = \frac{1}{32\sqrt{2}\omega_{rec}}\frac{V_0}{E_{rec}} \tag{2.47}$$

where $\omega_{rec} = E_{rec}/\hbar$. For instance, for typical parameters in our experiment such as $d_L = 426.1\,\text{nm}$, $V_0 = 5E_{rec}$ the condition (2.47) becomes: $\tau_{on} \gg 5\,\mu\text{s}$. It must be noted that the condition (2.47) was found for $q = 0$, i.e., for the value of quasimomentum for which the gap between the fundamental and the first excited band is maximum. In fact, the adiabaticity condition for loading the atoms into the fundamental band becomes more restrictive when $q \neq 0$. In particular, for $|q| = \hbar k_L$ the time τ_{ad} diverges and the adiabatic loading is impossible. This is true for every point in the band structure for which the bands are degenerate in the free particle case.

The adiabaticity condition (2.47) is valid even for the time τ_{off} in which the lattice is switched off. In fact, if $\tau_{off} \ll \tau_{ad}$ the wavefunction of the atoms will be formed by the plane wave decomposition, i.e., the Fourier transform, of the wavefunction of the atoms in the lattice. On the other hand, if $\tau_{off} \gg \tau_{ad}$ the wavefunction of the atoms follow instantaneously the adiabatic state, and hence if the wavefunction of the atoms in the lattice was a single Bloch state, the wavefunction of the atoms when the lattice is switched off is a single plane wave.

Depending on the loading time τ_{on} and on the time τ_{off}, the behaviors of the sample change [53]. The regimes realized in our experiments are listed in the following.

- τ_{on}, $\tau_{off} \ll \tau_{ad}$. In this case the initial state of the atoms is a superposition of many Bloch states, as in Eq.(2.43). Then, if the system is allowed to evolve in time inside the lattice, each of these Bloch states evolve with a different phase, and after a time t the state of the atoms is:

$$|\psi\rangle_t = \sum_n e^{-iE_n(q)t/\hbar} |\psi_{n,q}\rangle\langle\psi_{n,q}|q/\hbar\rangle. \tag{2.48}$$

  After a fast switching off of the lattice, the atomic wavefunction is the Fourier transform of Eq.(2.48). Thus the probability for the atoms to be in the state $|p/\hbar + 2jk_L\rangle$ is:

$$P_{p+2j\hbar k_L} = \left| \sum_n e^{-iE_n(q)t/\hbar} \langle p/\hbar + 2jk_L|\psi_{n,q}\rangle\langle\psi_{n,q}|q/\hbar\rangle \right|^2 . \tag{2.49}$$

  The probability (2.49) for $p = \hbar k_L$ and $j = 0$ corresponds to the probability (2.9). Measurements in this regime can be used to measure the lattice depth by exploiting the Kapitza-Dirac effect [10, 12].

- τ_{on}, $\tau_{off} \gg \tau_{ad}$. In this case the atomic wavefunction at the end of the experiment is equal to the atomic wavefunction before the lattice was switched on. Measurements in this regime were used in the experiment to test the adiabaticity of loading.

- $\tau_{on} \gg \tau_{ad}$, $\tau_{off} \ll \tau_{ad}$. This is the regime of most of the measurements performed in our experiments. The wavefunction of the atoms in the lattice is one Bloch state $|\psi_{n,q}\rangle$, because of the adiabatic loading. On the other hand, the atomic state observed after switching off the lattice is the Fourier transform of $|\psi_{n,q}\rangle$. The probability for the atoms to be in the $|p/\hbar + 2jk_L\rangle$ state is:

$$P_{p+2j\hbar k_L} = |\langle p/\hbar + 2jk_L|\psi_{n,q}\rangle|^2 . \tag{2.50}$$

2.6.3 Measuring matter waves in an optical lattice

In the experiments described in this thesis we observed the behavior of ultracold atoms loaded into an optical lattice. In the measurements performed, the condensate was detected by absorption imaging techniques. We used two type of measurements to obtain information on the sample:

- *In situ* measurements. In these measurements the atoms were released from the dipolar trap and from the optical lattice at the same time, and the cloud was imaged immediately afterwards (i.e., after a time of flight t_{tof} such that the free expansion of the atoms was negligible). In these measurements the sample was thus observed in real space.

- *Time of flight* measurements. In these measurements the lattice and dipolar trap were switched off as in the in situ measurements, but the time of flight t_{tof} was now such that the atomic wavefunction decomposition in plane waves was visible. In fact, after that the atoms were released from the lattice, each plane wave component of momentum p in the lattice frame had velocity in the laboratory frame $v = v_{lat} + p/m$, where v_{lat} is the final velocity of the lattice in the laboratory frame. After a time of flight t_{tof} the atoms displaced in an interference pattern in which the distance between the different plane wave components was:

$$\delta x = \frac{2\hbar k_L}{m} t_{tof} \propto d_L^{-1}. \tag{2.51}$$

  Each plane wave component is called also *class of velocity*. It is important to note that the decomposition in plane waves can be observed only if the state of the sample is a coherent superposition of Bloch states. If the phase coherence is broken, the interference pattern disappears. This is the case, for instance, when the inter-well tunneling is suppressed and the matter wave of each lattice site evolves independently [54]. However, in this case the interference pattern can have a revival if the sample is let evolve in the lattice for a time such that the single site phases become equal all along the lattice.

2.6.4 Measurements of the lattice depth

The lattice depth was defined in Eq.(2.13) considering an atom as a two level system. However, the actual energy spectrum of an atom is more complicated. A full calculation gives:

$$V_0 = \zeta \hbar \Gamma \left(\frac{I}{I_{sat}} \right) \left(\frac{\Gamma}{\Delta} \right) \tag{2.52}$$

where

ζ	is a numerical factor (depending on the Clebsh-Gordan coefficients)
Γ	is the line width
I_{sat}	is the single beam saturation intensity.

In our experiments, the lattice depth was always measured before the actual measurements were performed. We used different techniques, briefly described in the following.

Rabi Oscillations

If the lattice is switched on suddenly, i.e., $\tau_{on} \lesssim \tau_{ad}$, and the atoms are loaded with quasimomenentum $q = \hbar k_L$, the atomic wavefunction $|\psi\rangle$ is a

superposition of the two Bloch states $|\psi_{0,\hbar k_L}\rangle$ and $|\psi_{1,\hbar k_L}\rangle$. In the plane wave decomposition of $|\psi\rangle$, the time evolution of the wavefunction is a Rabi-like oscillation between the initial state $|k_L\rangle$ and the diffracted state $|-k_L\rangle$ [55]. Eq.(2.9) gives the probability for the atoms to be in the initial state $|k_L\rangle$. By switching the lattice off abruptly, i.e., $\tau_{off} \lesssim \tau_{ad}$, we were able to observe this oscillation by measuring the number of atoms N_0 belonging to the class of velocity $v_{rec} = \hbar k_L/m$ and the number of atoms N_1 belonging to the class of velocity $-v_{rec}$. The frequency Ω_R of the oscillation is proportional to the lattice depth in the shallow lattice limit, for which [56]:

$$V_0 = 2\hbar\Omega_R. \tag{2.53}$$

In Fig.(2.4) the measurement of the ratio N_1/N_{tot}, where N_{tot} is the total number of atoms in the sample, is reported as a function of the time the condensate spent in the lattice.

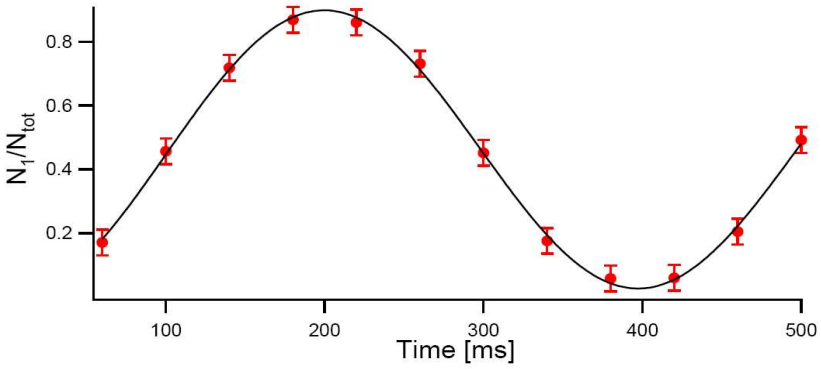

Figure 2.4: Rabi oscillations of the number of atoms in the class of velocity $-v_{rec}$ as a function of time.

Ground state analysis

Assume that a BEC is loaded into an optical lattice and has an initial wavefunction that is a Bloch state $|\psi_{0,0}\rangle$. If $k_M + 1$ lattice sites are occupied with uniform filling, the atomic Bloch state can be written in a tight binding approximation as a sum of gaussian functions of equal width σ centered at each lattice site:

$$|\Psi_{0,0}(x)\rangle \propto \sum_{n=-k_M}^{k_M} \exp\left(-\frac{(x-x_n)^2}{2\sigma^2}\right), \tag{2.54}$$

where x_n is the position of the n-th site. The Fourier transform of the expression (2.54) is [57]:

$$\begin{aligned}\Psi_{0,0}(p_x) &\propto \exp\left(-\frac{p^2\sigma^2}{2\hbar^2}\right)\frac{\sin\left[(2k_M+1)pd_L/2\hbar\right]}{\sin\left(pd_L/2\hbar\right)} \\ &= \exp\left[-\frac{\pi^2}{2}\left(\frac{p}{p_B}\frac{\sigma}{d_L}\right)^2\right]\frac{\sin\left[(2k_M+1)\pi\frac{p}{p_B}\right]}{\sin\left[\pi\frac{p}{p_B}\right]}\end{aligned} \tag{2.55}$$

where $p_B = 2\hbar k_L$. The interference pattern that is observed in a time of flight measurement after that the lattice is switched off abruptly is therefore a structure of peaks of the form $\sin(x)/x$ spaced by $\delta x = t_{tof} \cdot p_B/m$, and whose amplitude is given by a gaussian envelope centered at $p = 0$. The amplitude of the first side peaks ($p = \pm p_B$) with respect to the amplitude of the central one is:

$$P_{\pm 1} = \exp\left(\frac{-4\pi^2\sigma^2}{d_L^2}\right). \tag{2.56}$$

The value of sigma depends on the potential depth [57] and can be estimated variationally. It is possible to show [56, 58] that the σ satisfies the following relation:

$$\exp\left[-\left(\frac{\sigma}{\sigma_h}\right)^2\sqrt{\frac{E_{rec}}{V_0}}\right] = \left(\frac{\sigma}{\sigma_h}\right)^{-4}, \tag{2.57}$$

where:

$$\sigma_h = \frac{d}{\pi}\left(\frac{V_0}{E_{rec}}\right)^{-1/4}. \tag{2.58}$$

By use of the relation (2.56), the Eq.(2.57) can be written as:

$$P_{\pm 1}^{-1/4} = (\ln P_{\pm 1}^{1/4})^2\frac{V_0}{E_{rec}}. \tag{2.59}$$

Therefore by measuring the ratio between the number of atoms in the first order diffracted classes of velocity and the number of atoms in the central peak we were able to measure the lattice depth.

Chapter 3

Quantum tunneling in an optical lattice

The work of this thesis is based on three experiments we performed in the Pisa BEC laboratory. All the experiments explored the effects of tunneling in a BEC loaded into an optical lattice. This subject is of interest both as a fundamental physical concept (quantum tunneling) and for the experimental progress in manipulating cold atoms in an optical lattice. In this chapter an overview of the theoretical ideas is given that form the basis of the experiments to be discussed in subsequent chapters.

3.1 Which tunneling?

The physical system of a Bose Einstein condensate loaded into an optical lattice is formally similar to the problem of electrons in a solid. In both cases the wavefunctions of the matter waves obey the Bloch theorem, while the dispersion relation is structured in bands separated by energy gaps. A BEC in an optical lattice is an ideal tool to study both solid state physics and fundamental quantum theory. This thesis is devoted to the experimental study and control of quantum tunneling in such systems.

The effects of tunneling that we observed in our experiment were of two types:

- *Inter-band* tunneling: this effect emerges when the atoms tunnel through an energy gap from one energy band to the upper/lower one.

- *Intra-band* tunneling: this effect emerges when the atoms tunnel from a lattice site to a neighboring one through the sinusoidal barrier. In fact this type of tunneling leads to delocalization and hence to the formation of energy bands.

Fig. (3.1) shows these two processes schematically. The main difference is that in intra-band tunneling an atom passes through an avoided region in space, while in inter-band tunneling an atom passes through an avoided region in energy. Therefore, intra-band tunneling connects energy levels that are almost degenerate, while inter-band tunneling connects different energy levels. The aim of this thesis is to show how both tunnelings can be experimentally observed and controlled in an optical lattice. How these effects emerge in an optical lattice will be explained in the rest of this chapter.

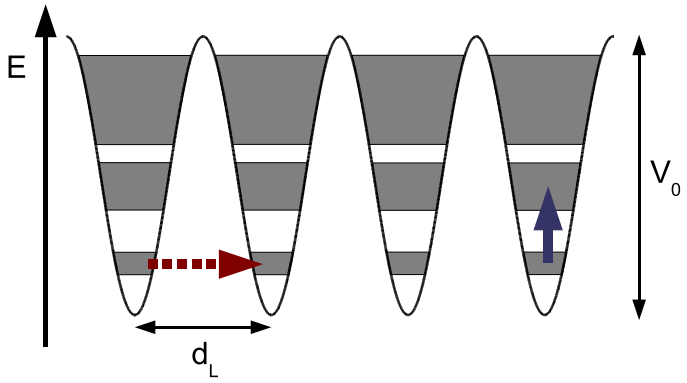

Figure 3.1: Scheme representing the two types of tunneling investigated in this thesis. In *intra-band* tunneling (dashed arrow) the atoms tunnel through the sinusoidal barrier from one lattice site to a neighboring one, whose energy levels are degenerate. On the other hand, in *inter-band* tunneling (solid arrow) the atoms tunnel from one energy band to an upper/lower one through an energy gap.

3.2 Intra-band tunneling

Let us start from the easiest problem in quantum mechanics: the free particle in one-dimensional space. This problem is defined by a Hamiltonian containing only the kinetic term: $H_{FP} = p^2/(2m)$. The particle can have any value of energy, which is connected to the particle momentum k by the one-to-one dispersion relation $E = \hbar^2 k^2/(2m)$; also the particle is delocalized in space, i.e., the probability for the particle to be at position x is non-zero for any value of x. If an infinite optical lattice is turned on, the Hamiltonian becomes:

$$H = \frac{p^2}{2m} + V_0 \sin^2(k_L x). \tag{3.1}$$

A spatial periodicity is now imposed on the system. As far as the energy spectrum is concerned, the spatial periodicity causes the emergence of values

of energy that the particle can not have, i.e., the energy gaps. The dispersion relation also becomes periodic, but in the quasi-momentum q, and it is structured in energy bands $E_n(q)$. It is important to note that, as well as the free particle eigenfunctions, the eigenstates $|\psi_{n,q}(x)\rangle = \exp(iqx)u_{n,q}(x)$ of the Hamiltonian (3.1) describe a spatially delocalized particle. Moreover, they are stationary states, because for a fixed value of $\tilde{q}$, each energy level $E_n(\tilde{q})$ has an *infinitesimal* width. If the particle, in our case the atom, has an energy that is lower than the lattice depth V_0, the delocalization occurs by tunneling through the sinusoidal barriers that divide the lattice sites. In order to see how the tunneling emerges one has to observe the atom at the single lattice site. This can be done by use of the Wannier functions, because they are spatially localized: the Wannier function $\phi_{n,l}(x)$ describes one atom in the n-th energy level of the l-th lattice site. It is important to note that the Wannier functions do not depend on the quasimomentum q, just like the energy levels of a single lattice site potential. In fact, the energy levels in a single lattice site have a finite width that is equal to the corresponding band width (see Fig. (3.2)) [31]. The energy levels width implies a decay of the corresponding Wannier states. This decay is the tunneling to the neighboring sites.

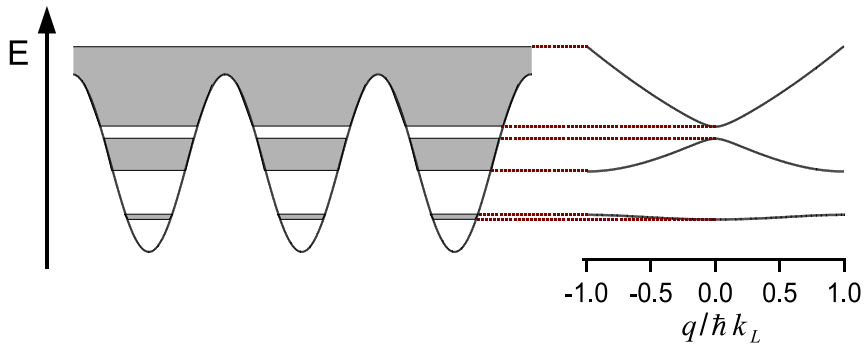

Figure 3.2: Comparison between the single site energy levels and energy bands. The band widths correspond to the width of the single site energy levels, that is $2J$ for a one dimensional lattice. The energy bands are calculated for a lattice of depth $V_0/E_{rec} = 10$. The dotted lines are guides for the eye.

In the previous section, the intra-band tunneling was introduced in a different way. Within the Bose-Hubbard model, the tunneling rate J was defined in the fundamental band as [41]:

$$J = \int dx \phi_{1,l}(x) \left(\frac{p^2}{2m} + V_0 \sin^2(k_L x) \right) \phi_{1,l+1}(x). \tag{3.2}$$

The tunneling rate (3.2) refers to the probability of tunneling from the l-th to the $(l+1)$-th site. On the other hand, the fundamental band width $(E_1(q=\hbar k_L) - E_1(q=0))$ corresponds to the decay of the single site state, and it is therefore equal to the tunneling rate to both the $(l+1)$-th and $(l-1)$-th sites. Therefore, the width of the fundamental band is $(E_1(q=\hbar k_L) - E_1(q=0)) = 2J$.

In an optical lattice, the energy levels of the single site potentials are all degenerate to each other, and therefore the intra-band tunneling can emerge. However, if this degeneracy is partially destroyed, then the tunneling is reduced. In order to see how this suppression of tunneling emerges, consider an energy shift ΔE_{shift} between neighboring sites (see Fig.(3.3)). The energy shift can be created by use of a linear potential $V_{shift} = \Delta E_{shift} x/d_L$. Thus the tunneling (3.2) becomes:

$$J_{shifted} = \int dx \phi_{1,l}(x) \left(\frac{p^2}{2m} + V_0 \sin^2(k_L x) + \frac{\Delta E_{shift}}{d_L} x \right) \phi_{1,l+1}(x). \quad (3.3)$$

The new contribution to the tunneling $\int dx \phi_{1,l} V_{shift} \phi_{1,l+1}$ has positive sign, and therefore decreases the tunneling rate:

$$J_{shifted} \leq J. \quad (3.4)$$

This simple idea for varying the tunneling is at the base of our experiments

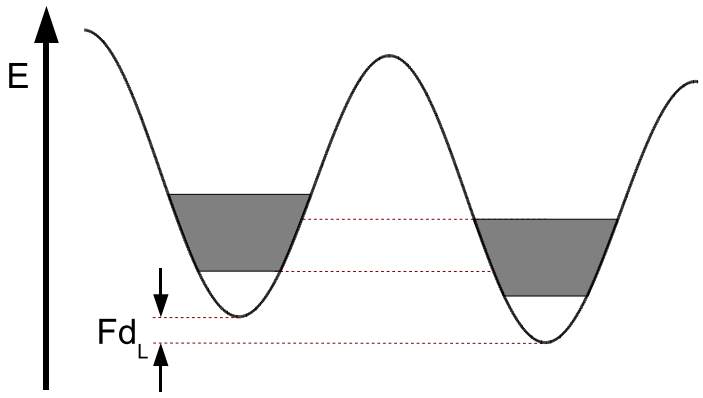

Figure 3.3: Partial suppression of intra-band tunneling. The energy shift Fd_L partially lifts the degeneracy of the energy levels at neighboring lattice sites and the tunneling rate is reduced. The dotted lines are guides for the eye.

on intra-band tunneling, and we implemented it in several ways. In Chapter 6 it is reported an experiment in which the complete suppression of tunneling was realized by use of a linear potential. On the other hand, in Chapter 5 it is described an experiment in which an energy shift was implemented by use

of a sinusoidal potential, leading to a rather complicated transformation of tunneling.

3.3 Inter-band tunneling

The energy spectrum of an atom in an optical lattice is characterized by the energy bands $E_n(q)$. These are separated by energy gaps $\Delta_n = E_{n+1}(q) - E_n(q)$ that emerge, within the first Brillouin zone, at $q = \pm\hbar k_L$ when n is odd and at $q = 0$ when n is even. In fact, for these values of the quasimomentum the free particle energies at different Bragg planes are degenerate:

$$\frac{\hbar^2 k^2}{2m} = \frac{\hbar^2 (k+G)^2}{2m} \tag{3.5}$$

where $G = \pm 2nk_L$, n integer, is a reciprocal lattice vector. The energy degeneracies are lifted by the emergence of avoided crossings, corresponding to the energy gaps.

Let us suppose that the atom is loaded in the fundamental band of the lattice and with initial quasimomentum $q = 0$. At $t = 0$ an external and constant force F is switched on, resulting in a change of the quasimomentum of the atom:

$$q(t) = Ft. \tag{3.6}$$

The evolution of Eq.(3.6) is adiabatic, i.e., the atom remains in the fundamental band, if the force F satisfies the adiabatic theorem:

$$\left| \langle u_{0,q} | \frac{d}{dt} | u_{1,q} \rangle \right| \ll \frac{E_1(q) - E_0(q)}{\hbar}, \tag{3.7}$$

which can be written in the form [50]:

$$|F| \ll \frac{k_L}{8} \frac{V_0^2}{E_{rec}}. \tag{3.8}$$

During its motion, the atom first crosses the energy gap with the first excited band at $t = \hbar k_L / F$. Let us suppose that this is the only energy gap crossed by the atom. The probability for the atom to tunnel through the gap, i.e., to be in the first excited band at $t = \infty$, is given by the Landau-Zener formula [59, 60]:

$$r = \exp(-F_c/F) \tag{3.9}$$

where F_c is the critical force [31]. In the shallow lattice approximation the energy gap is $E_1(q = \hbar k_L) = V_0/2$, and the critical force is

$$F_c = \frac{\pi}{4} \frac{k_L}{8} \frac{V_0^2}{E_{rec}} \tag{3.10}$$

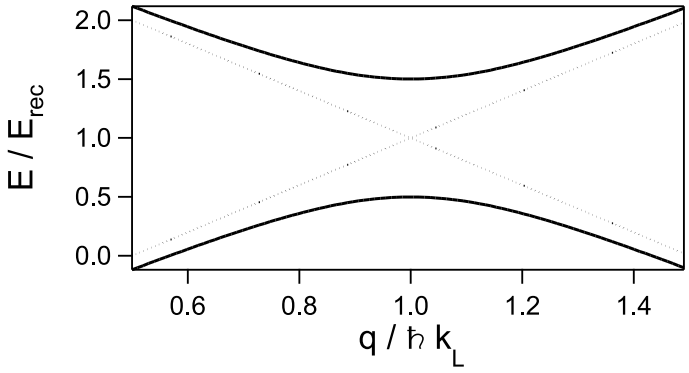

Figure 3.4: Fundamental and first excited energy bands for a lattice of depth $V_0/E_{rec} = 4$ in the proximity of $q = \hbar k_L$ where an energy gap occurs. The dotted lines correspond to the free particle dispersion law.

which is proportional to the adiabatic condition (3.8).

The Landau-Zener formula has already been tested experimentally with BECs loaded into an optical lattice [52, 56]. However, in our experiment we observed deviations from the Landau-Zener prediction of Eq. (3.9). These deviations are caused by resonances between single site energy levels at different lattice sites. In fact, the linear potential $V_{shift} = Fx$ associated with the force F creates an energy shift $\Delta E_{shift} = Fd_L$ between neighboring lattice sites. Let $\Delta E_1^{(site)}$ be the gap between the first and the second energy levels in the single lattice site potential. If this energy gap is equal to Δi times the energy shift created by the force:

$$\Delta i F d_L = \Delta E_1^{(site)}, \tag{3.11}$$

then the ground energy level of each lattice site is degenerate with the first excited level of its Δi-th neighboring lattice site. This degeneration makes it possible for the atoms to tunnel through the potential barrier to the excited state of the Δi-th neighboring site. This tunneling through a *spatial* barrier results in an enhancement of the tunneling *in energy* to the excited level with respect to the Landau Zener formula. This enhancement of tunneling emerges only when the force F satisfies the condition (3.11). Therefore, with respect to the force, this effect has a resonance-like behavior. We observed this resonant enhancement of tunneling in an experiment that is reported in Chapter 4.

Chapter 4

Resonantly enhanced tunneling

In this chapter the observation of resonantly enhanced tunneling using a BEC loaded into an optical lattice is reported. The tunneling was measured by applying an acceleration to the lattice. When the resulting linear potential matched the difference between energy levels at different lattice sites, a resonance in the tunneling was observed. Resonances in the tunneling from the fundamental and the first two excited bands were measured. Finally, the effect of nonlinearity on the resonances is reported.

4.1 Landau-Zener theory in an optical lattice

Landau-Zener theory describes the behavior of a physical system that passes through an avoided energy crossing during its time evolution[59, 60], i.e., such that the energy levels are separated by a gap. This situation can occur when the Hamiltonian depends on some variable parameter $q(t)$, and the crossing energy levels are coupled by some interaction in the Hamiltonian. The Landau-Zener formula predicts that the probability for the system to tunnel through the energy gap from one energy level to an adjacent level depends exponentially on the velocity $dq(t)/dt$ and on the square of the gap.

This ideal problem is realized in a system of cold atoms in a one dimensional optical lattice:

$$H = -\frac{\hbar^2\nabla^2}{2m} + \frac{V_0}{2}\cos(k_L x) \tag{4.1}$$

In this physical system, the energy spectrum has a band structure $E_n(q)$, periodic in the quasimomentum q. Neighboring bands $E_n(q)$, and $E_{n+1}(q)$ have avoided energy crossings at $q = \pm\hbar k_L$ when n is odd, and at $q = 0$ when n is even (within the first Brillouin Zone)[38]. The prediction of the Landau Zener formula can be tested by considering the quasimomentum as the varying parameter. In fact, if an external force is applied to the atoms,

their quasimomentum changes as:

$$q(t) = q(t=0) + Ft = q(t=0) + 2\pi\hbar\frac{F_0\nu_{rec}}{d_L}t, \tag{4.2}$$

where $F_0 = F/(E_{rec}d_L^{-1})$ is the dimensionless force and $\nu_{rec} = E_{rec}/h$ is the recoil frequency. If N atoms are in the n-th band and experience a force F, they will pass through an avoided energy crossing with the $(n+1)$-th band at some time. Because of tunneling through the energy gap $\Delta E_n = E_{n+1}(q = \hbar k_L) - E_n(q = \hbar k_L)$, a fraction of the sample will populate the $(n+1)$-th band. According to the Landau-Zener formula the number of atoms that will tunnel to the $(n+1)$-th excited bands will be:

$$N_{n+1} = N_{tot}r_n = N_{tot}e^{-\frac{a_c}{a}}, \tag{4.3}$$

where $a_c = F_c/m = d/(4\hbar^2)\Delta E_n^2$ is the critical acceleration [50, 56], and $a = (1/m)dq/dt$ is the acceleration of the atoms. Therefore the number of atoms that remain in the n-th band will be:

$$N_n = N_{tot}\,(1 - r_n) = N_{tot}\left(1 - e^{-\frac{a_c}{a}}\right). \tag{4.4}$$

4.2 The Landau-Zener tunneling rate

The ideal situation of the previous paragraph becomes more complicated in a real experiment because the atoms pass through many avoided energy crossings. A good example is to study the problem of N atoms prepared in the fundamental band of a one dimensional optical lattice and with initial quasimomentum $q(t=0) = 0$. At $t = 0$ a uniform force is switched on, so the quasimomentum evolves for $t > 0$ according to Eq.(4.2).

The typical time-scale is given by the Bloch time: $\tau_B = v_B/a$, with $a = F/m$, corresponding to the time for the quasimomentum to scan an entire Brillouin zone. By use of the dimensionless force F_0, the Bloch time may be written: $\tau_B = (F_0\nu_{rec})^{-1}$.

- At $t = \tau_B/2$ the atoms have quasimomentum $q = \hbar k_L$. At this value of q the fundamental band E_1 has an avoided crossing with the first excited band E_2. Therefore, following Eq. (4.4), $N_2 = N \cdot r_1$ atoms tunnel to the first excited band.

- At $t = \tau_B$ the atoms have quasimomentum $q = 0$ (within the first Brillouin zone) and occupy the fundamental and the first excited band. The first excited band has an avoided energy crossing with the second excited band for $q = 0$, so $N_3 = N_2 \cdot r_2 = N \cdot r_1 \cdot r_2$ atoms tunnel through the energy gap ΔE_2 to the second excited band. It is interesting to

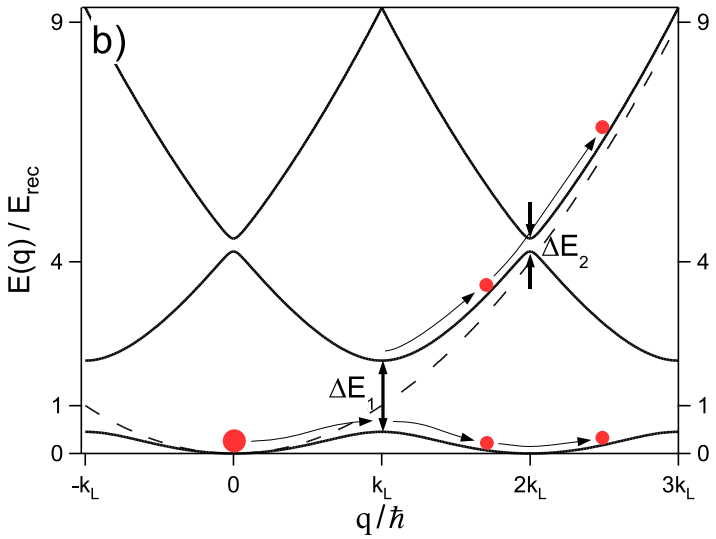

Figure 4.1: Dynamics of a BEC in an accelerated optical lattice in the extended zone representation. When the BEC quasimomentum crosses the lowest energy gap (for $q = \hbar k_L$) part of the cloud is tunneled to the first excited band. When these atoms cross the lowest energy gap with the second excited band (for $q = \frac{3}{2}\hbar k_L$) they are almost completely tunneled to the second excited band because $\Delta E_2 \ll \Delta E_1$.

compare this tunneling with the one at $t = \tau_B/2$. The Landau-Zener formula (4.4) states that the probability of tunneling depends exponentially on the square of the energy gap. In our experiment, when the atoms were prepared in the fundamental band the lattice depth was in the range: $V_0/E_{rec} = 1 - 10$. Within this range one has always $\Delta E_2^2 \ll \Delta E_1^2$. For instance, in a lattice of depth $V_0/E_{rec} = 3$, the square of the first and the second energy gaps are: $(\Delta E_1/E_{rec})^2 \sim 2$, $(\Delta E_2/E_{rec})^2 \sim 0.08$. Thus, if the N_2 atoms that tunneled at $t = \tau_B/2$ from the fundamental to the first excited band are a non-negligible fraction of the whole sample, that is if $r_1 \sim 1$, then almost all these N_2 atoms will tunnel at $t = \tau_B$ to the second excited band, because $r_2 \gg r_1$. For example, if the atoms are loaded in a $V_0/E_{rec} = 3$ deep lattice and then accelerated at $a = 14\,g$, where g is the acceleration due to gravity, the probabilities of tunneling through the first and the second energy gaps are: $r_1 \sim 0.5$,$r_2 \sim 0.98$. A plot of the probability of tunneling r_n as a function of the lattice depth is shown for $n = 1, .., 4$ in Fig. (4.2), for an acceleration $a = g$. This plot shows that in a lattice whose depth is such that the probability of tunneling r_n from the n-th band is in the range $0.1 < r_n < 0.9$, the probabilities of tunneling from the other bands are out of this range. Usually in the experiments, the

accelerations were in the range $a = 0.5 - 20\,g$.

- At $t = 3/2\tau_B$ the atoms have quasimomentum $q = \hbar k_L$. Neglecting the fraction that remained in the first excited band, the atoms populate the fundamental and the second excited band. These have avoided crossings with the first and the third excited band respectively. The first excited band is again populated by $E_1 \rightarrow E_2$ tunneling events. On the other hand, all the atoms in the second excited band tunnel to the third excited band because $r_3 > r_2$.

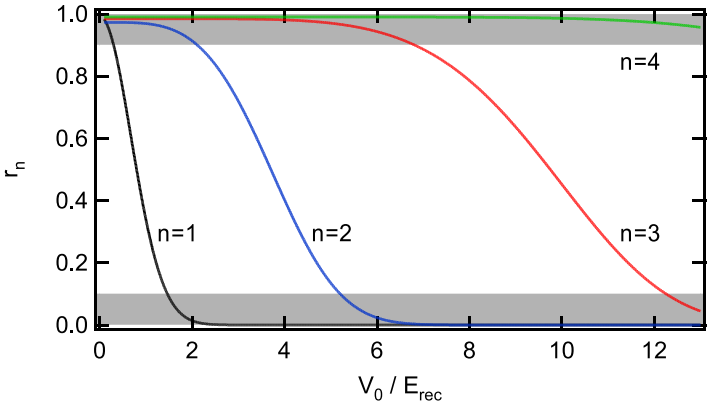

Figure 4.2: Probability of tunneling r_n for $n = 1, .., 4$ and for different values of the lattice depth V_0. The two shaded strips highlight the regions where $0.9 < r_i < 1$ and $0 < r_i < 0.1$. When one of the probabilities is in the range $0.1 < r_i < 0.9$, all the other probabilities are close to 0 or to 1. All the curves were calculated for the acceleration of gravity: $a = g$.

For $t \gg \tau_B$ and $t = n\tau_B$, where n is an integer number, the atoms that are still in the fundamental band are hence [56]:

$$N_1(t) = N_{tot}\left(1 - e^{-\frac{a_c}{a}}\right)^{\frac{t}{\tau_B}} \tag{4.5}$$

because the atoms that tunneled through the gap ΔE_1 in the $n = t/\tau_B$ energy crossings with the first excited band tunneled in turn through the gap ΔE_2 and therefore never tunneled back to the fundamental band. By expanding in series the right hand term of Eq. (4.5) for $t \ll 1$ one obtains:

$$N_1(t) \cong N_{tot}\left(1 + \ln\left(1 - e^{-a_c/a}\right)\frac{t}{\tau_B}\right). \tag{4.6}$$

Eq.(4.6) can be further on expanded in series for $\exp(-a_c/a) \ll 1$, thus becoming:

$$N_1(t) \cong N_{tot}\left(1 - e^{-a_c/a}\frac{t}{\tau_B}\right). \tag{4.7}$$

The right-hand side of Eq.(4.7) can be considered as the first two terms of the expansion in series of an exponential function. Therefore the number of atoms in the fundamental band becomes:

$$N_1(t) \cong N_{tot} e^{-\Gamma_{LZ} t}, \tag{4.8}$$

where

$$\Gamma_{LZ} = \tau_B^{-1} e^{-\frac{a_c}{a}}. \tag{4.9}$$

In Eq.(4.8,4.9) a Landau-Zener *tunneling rate* has been introduced that allows us to characterize the decay from the initial energy band. By use of the approximated formula for the wavefunctions and the energy gap ΔE_1 in the limit of shallow lattices ($\Delta E_1 \sim V_0/2$), the Landau-Zener tunneling rate for the $E_1 \rightarrow E_2$ transition is:

$$\Gamma_{LZ} = F_0 \nu_{rec} e^{-\pi^2 (V_0/E_{rec})^2/32 F_0}. \tag{4.10}$$

As stated above, the main assumption behind the introduction of the tunneling rate is to consider that for the population of the fundamental band the tunneling to the first excited band acts as a depletion. This argument holds even if the atoms are initially loaded at the center of the n-th band $E_n(q)$, $n \neq 1$, and one considers the tunneling to the $E_{n+1}(q)$ band. In fact, the only difference now is that the tunneling to the lower band $E_n \rightarrow E_{n-1}$ must be considered as well. However, the tunneling to the higher band is always larger than the tunneling to the lower band, because the energy gap ΔE_n decreases with increasing n. Therefore, if the probability of tunneling to the higher band is such that a non-negligible fraction of the sample tunnels, that is $r_n \simeq 1$, the probability to tunnel to the lower band is negligible: $r_{n-1} \ll 1$. In this regime the tunneling to the lower band can be ignored, and the tunneling rate formula (4.8) can be written:

$$N_n(t) = N_{tot} e^{-\Gamma_n t} \tag{4.11}$$

where Γ_n is the tunneling rate from the n-th band.

4.3 Resonantly enhanced tunneling

In the previous paragraph the tunneling between energy bands has been studied starting from the energy spectrum of the Hamiltonian (4.1), and then varying the quasimomentum by use of an external force (4.2). This approach is not formally correct, because the force was not inserted in the Hamiltonian of the system. In fact, the force was only used to vary the quasimomentum in the energy spectrum of the Hamiltonian without the force. Going beyond

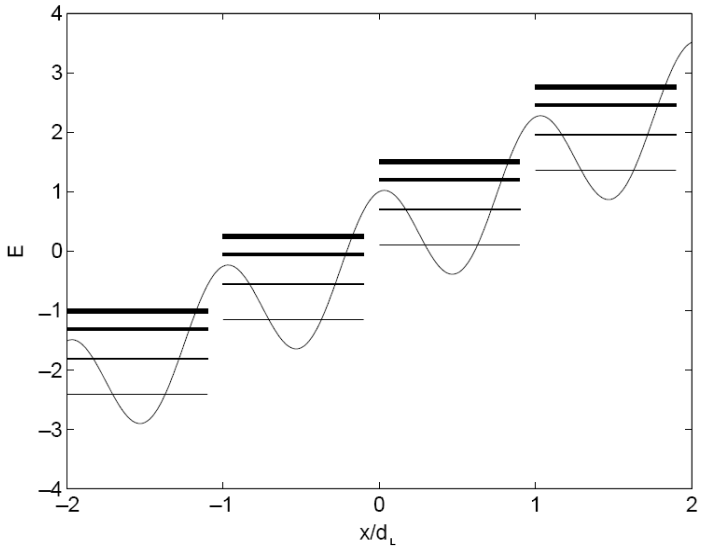

Figure 4.3: Schematics of the energy spectrum of an optical lattice in the presence of an external force. The optical lattice potential is tilted in energy and the Wannier-Stark ladder emerges (from ref. [61]).

this approximation, the physical system of cold atoms loaded into an optical lattice and subjected to an external force is described by the Hamiltonian

$$H = \frac{\hbar^2 \nabla^2}{2m} + \frac{V_0}{2} \cos\left(k_L x\right) + F \cdot x, \tag{4.12}$$

whose eigenfunctions and energy spectrum are different from the $F = 0$ case.

The eigenfunctions of the Hamiltonian (4.12) are the Wannier-Stark functions. There are two differences of particular interest between these functions and the Bloch functions. Firstly, the Wannier-Stark functions are not delocalized all along the lattice as the eigenfunctions of a lattice with $F = 0$, but are localized at the lattice sites [61]. This effect, known as Wannier-stark localization, emerges because the force F corresponds to an energy tilt of the lattice potential. Thus neighboring lattice sites are shifted in energy by Fd_L, and the interwell-tunneling is reduced because the degeneracy of the single site energy levels is lifted. Secondly, the Wannier-Stark states are not stationary, and hence have a finite lifetime $1/\Gamma$, where Γ is the tunneling rate (4.11). In fact the eigenvalues of the Hamiltonian (4.12) are complex functions whose real part forms a ladder of energy levels localized at the different lattice sites [61], while the imaginary part is the tunneling rate Γ that corresponds to the widths of these levels (see Fig.(4.3)).

The Wannier-Stark localization, the tunneling rate and hence the lifetime of the Wannier-Stark states depend on the strength of the force. It is of particular interest when this is such that the ground state at one lattice site

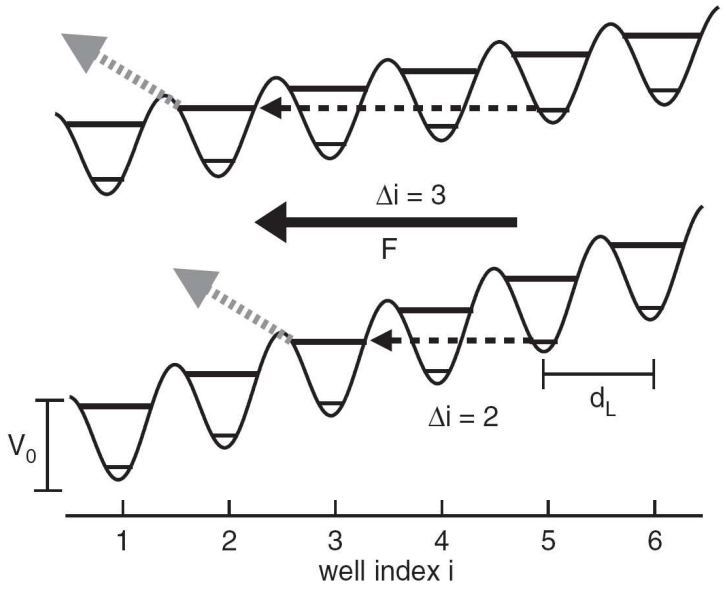

Figure 4.4: Resonantly enhanced tunneling in an optical lattice. When the tilt in energy caused by the force exerted on the system creates a degeneracy in energy between neighboring sites, the tunneling rate is enhanced.

and the excited state at the Δi-th neighboring site become degenerate in energy. This occurs when:

$$F d_L \Delta i = \Delta E \tag{4.13}$$

where ΔE is the difference in energy between levels in the single well, and Δi is the distance, expressed in units of lattice sites (see Fig.(4.4)).

When the condition (4.13) holds, the lower and the higher energy levels are resonantly coupled, and hence the probability of tunneling increases[62]. In figure (4.5) the tunneling rate Γ calculated by two different methods is plotted against the force. In the first (dashed line) the Landau-Zener formula is used, and Γ has an exponential behavior as expected. In the second (solid line) Γ is evaluated by numerically solving the eigenvalue problem of the Hamiltonian (4.12), and the tunneling rate is resonantly enhanced when the condition (4.13) holds.

This effect is known as *Resonantly Enhanced Tunneling* (RET), and has interested the solid state community for a long time. It was observed experimentally first in semiconductors, by use of superlattice structures [63, 64, 65], and with quantum wells [66]. More recently, a first evidence of RET has been observed with a cold thermal cloud loaded in an optical lattice [67]. In our experiment [68] we study the resonantly enhanced tunneling with BECs loaded into an optical lattice, and we observe for the first time the effect of interactions, i.e., of the intrinsic nonlinearity of a BEC.

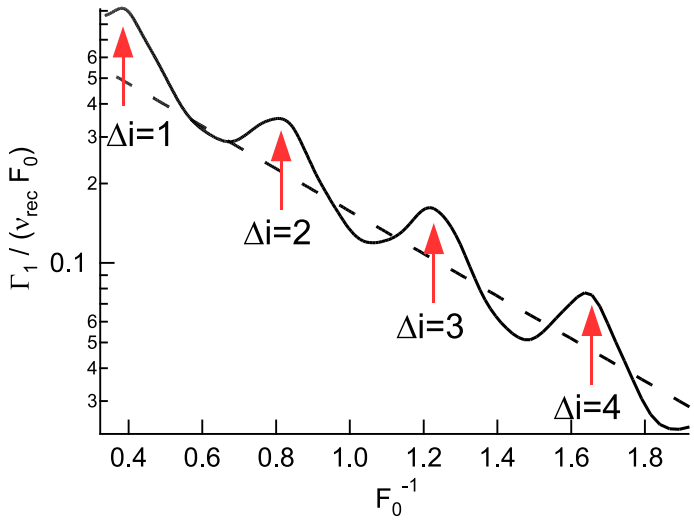

Figure 4.5: Tunneling rate as a function of the force. The dashed line corresponds to the Landau-Zener theory. The solid line corresponds to the numerical solution of the eigenvalue problem of the Hamiltonian (4.12). The tunneling is enhanced when the force is such that the condition (4.13) is satisfied. The curves were calculated for a lattice of depth $V_0/E_{rec} = 2.5$.

4.4 Measuring the tunneling rate

It has been stated previously that the atoms that tunnel from the n-th to the $n+1$-th band subsequently tunnel to the higher energy bands with almost 100% probability. As a consequence, after a certain time these atoms occupy an energy band that is above the lattice depth, i.e., in the continuum, where the energy gaps are infinitesimally small. This implies that these atoms do not experience Bloch oscillations anymore, but are uniformly accelerated in the lattice rest frame due to the force, i.e., they are stationary in the laboratory frame.

In order to measure the tunneling rate, the time sequence of a typical experiment was the following:

- Once the BEC was created, the trap frequencies were adiabatically changed in order to confine the sample in a cigar-shaped trap, with longitudinal frequency $\nu_{long} \sim 20Hz$ and radial frequency ν_{rad} varying in the range $80 - 250Hz$.

- A one-dimensional optical lattice was loaded adiabatically along the long axis of the cigar, in order to maximize the number of lattice sites occupied. Typically, 50 sites were occupied, with a mean occupation number of 1000 atoms per site. The time of loading t_{load} was in the

range $1-50$ ms, depending on the lattice depth and on the interactions between the atoms [69], and the atoms were loaded into the n-th band of the lattice. The choice of the time for the lattice loading as well as the procedure for loading the atoms in the n-th band will be explained later in this chapter.

- The optical lattice was accelerated by varying the detuning $\Delta\nu_L$ between the two laser beams creating the lattice: $a = d_L(d\Delta\nu_L/dt)$. This acceleration results in the lattice rest frame as a force exerted on the atoms: $F = md_L(d\Delta\nu_L/dt)$. This technique is of great advantage with respect to the application of external forces, e.g., by use of a magnetic gradient, because of the precision in the strength of the force and its homogeneous application to all the sample. The main disadvantage of this procedure is that the atoms are displaced by the lattice, and therefore the acceleration can not hold for long time because of the finite dimensions of the CCD camera and because the displacement causes the trapping potential experienced by the atoms to change in time. However, the time scales of our experiments are such that both effects are negligible.

- The lattice was accelerated for a time $t_{acc} = n\tau_B$, n integer. At the end of the acceleration, both the lattice and the dipolar trap were suddenly switched off, in order to make the atoms expand. The time-of-flight was ~ 20 ms in order to distinguish the peaks of the interference pattern.

A typical picture is shown in figure (4.6). The atoms that were still in

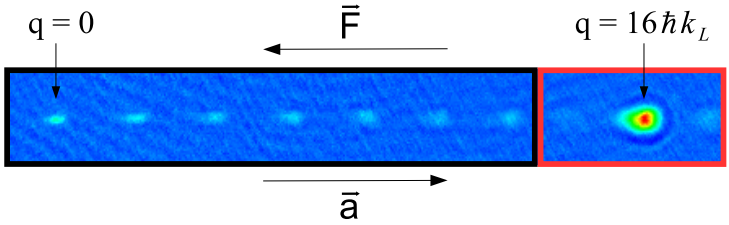

Figure 4.6: Image of the condensate after acceleration for $t = 8\tau_B$ and a Time of Flight of 15 ms. The atoms that are still dragged by the lattice, i.e. that are still in the fundamental band, are the ones in the right-side box, while the atoms in the left-side box are the ones that tunneled to the first excited band (and subsequently to higher bands).

the fundamental band at the end of the acceleration were dragged by the lattice until the end of the acceleration, and were released from the lattice

at a velocity

$$v_{drag} = \frac{F t_{acc}}{m} = \frac{t_{acc}}{\tau_B}\frac{\hbar k_L}{m} = 2n v_{rec} \tag{4.14}$$

in the laboratory frame. In the CCD image, the atoms dragged by the lattice were considered the ones with momentum $p = -2\hbar k_L, 0, 2\hbar k_L$ in the lattice frame (right box in Fig. (4.6)), to take into account the interference pattern of the atoms released from the lattice. In fact, for the lattice depth used in our experiments ($V_0/E_{rec} \leq 23$), the atoms with momentum $|p| > 2\hbar k_L$ in the interference pattern were less than the 3% of the whole sample. The atoms in the other velocity classes (left box in Fig.(4.6)) were the ones that had tunneled from the n-th band and then passed to the continuum. The velocities of these atoms in the laboratory frame corresponded to the velocity of the lattice at the moment that they tunneled to the continuum, i.e. when they stopped being accelerated by the lattice.

By measuring the number of atoms N_{tot} in the whole sample and the number of atoms N_{drag} that were still occupying the fundamental band at the end of the acceleration, it was possible to calculate the value of the tunneling rate Γ_n by use of Eq. (4.11). Here and in the following this is expressed in units of the recoil frequency $\nu_{rec} = E_{rec}/h$.

Experimental resolution

The measurement of the tunneling rate boils down to a measurement of numbers of atoms. Therefore the resolution achievable depended on the minimum number of atoms that were distinguishable from the background in the CCD images. This number was between 500 and 1000, depending on the dimension of the region where the atoms were distributed. Another limitation in measuring Γ_n was given by the minimum and maximum value for t_{acc}. The minimum acceleration time was $t_{acc} = 2\tau_{Bloch}$, in order to distinguish the tunneled fraction from the whole cloud. On the other hand the maximum constraint for t_{acc} was given by the dimension of the CCD images. In fact, if t_{acc} was too long, the atoms were displaced out of the image after the time-of-flight. For usual accelerations, this limit was $t_{acc} < 12\tau_{Bloch}$. Taking into account these limitations, we were able to measure Γ_n between ν_{rec} and $10^{-2}\nu_{rec}$.

4.5 Resonantly enhanced tunneling in the weakly nonlinear regime

One of the main characteristics of BECs in dilute gases is the atom-atom interaction, whose effect can be taken into account as a mean field term in

the Schrödinger equation, then called Gross-Pitaevskii equation:

$$i\hbar\frac{\partial}{\partial t}\psi(t) = \left[-\frac{\hbar^2\nabla^2}{2m} + g\left|\psi\right|^2\right]\psi(t) \tag{4.15}$$

where $g = 4\pi\hbar^2 a_s/m$ is the coupling parameter, and a_s is the s-wave scattering length. One can introduce a dimensionless parameter C that reflects the nonlinearity in the natural energy units of the problem, i.e., the recoil energy E_{rec} [70]:

$$C = \frac{n_0 a_s d_L^2}{\pi} = \frac{n_0 g}{8E_{rec}} \tag{4.16}$$

where n_0 is the peak density of the condensate, $\propto N_{tot}^{2/5}\overline{\nu}^{6/5}$ in the Thomas-Fermi regime. The strength of the nonlinearity depends on two physical quantities: the number of atoms in the condensate N_{tot} and the mean trapping frequency $\overline{\nu} = (\nu_x\nu_y\nu_z)^{1/3}$.

Three techniques have been used in our experiment in order to vary the nonlinearity:

1. Varying the trap frequency. As stated previously, the lattice was ramped up in the longitudinal direction of a cigar shaped cloud. Along the lattice the leading frequency was the single site frequency that was an order of magnitude larger than the frequency of the dipolar confinement ν_{long}. Therefore, at a given lattice depth and for a given number of atoms, the density of the sample and hence the nonlinearity depended on the frequency of the radial confinement ν_{rad}. In the experiment this was varied in the range $80 - 250$Hz, causing a change in C of up to a factor ~ 2.5.

2. Varying the lattice spacing d_L. In fact, d_L depends on the angle of intersection ϕ between the two laser beams that create the optical lattice: $d_L = \lambda/(2\sin(\phi/2))$. In our experiment the measurements were performed with two lattice constants: $d_L = 0.426\,\mu$m (when the two beams were counterpropagating: $\phi \cong 180°$), and $d_L = 0.620\,\mu$m (when $\phi \cong 87°$). In the latter case C was enhanced by a factor ~ 2 with respect to the counterpropagating case.

3. Varying the number of atoms. The BECs created in our experiment had up to $5 \cdot 10^4$ atoms, that is ~ 2 orders of magnitude bigger than the minimum number of atoms measurable. Therefore we were able to vary C up to a factor $100^{2/5} \simeq 6$ by changing the size of our sample.

The latter technique has the strong disadvantage that by reducing the number of atoms one reduces the experimental resolution. Therefore, in order to

test linear resonantly enhanced tunneling, the measurements were performed with the lowest radial frequency: $\nu_{rad} = 80\,\mathrm{Hz}$. This solution was sufficient to find good agreement with the linear theoretical predictions.

4.5.1 Tunneling from the fundamental band

The tunneling rate from the fundamental band was measured by using the experimental procedure previously explained. The lattice was linearly ramped up in 1ms, the atoms were loaded into the fundamental band, and the lattice was then accelerated for t_{acc}. In order to observe the resonances in the tunneling rate, a natural choice was to measure Γ_1 for different values of the force. Figs. (4.7) and Fig. (4.8) show the measurement of the tunneling rate from the fundamental band in the weakly nonlinear regime and in a lattice of depth $V_0/E_{rec} = 2.5$ and $V_0/E_{rec} = 4$ respectively. In both fig-

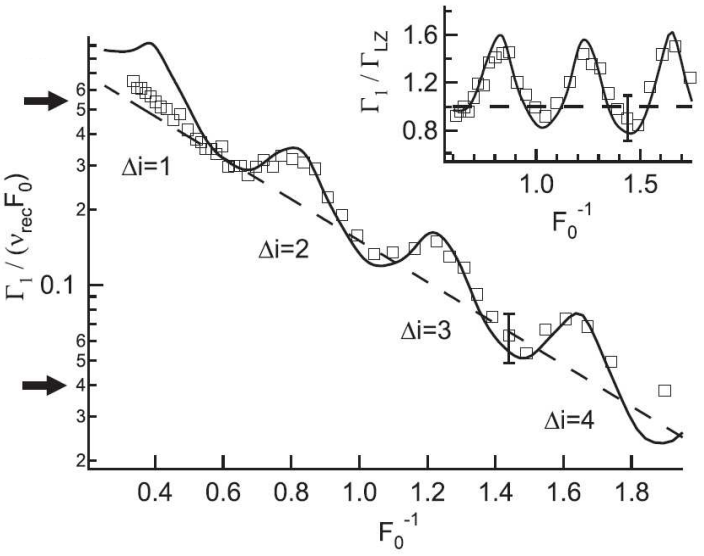

Figure 4.7: Tunneling rate from the fundamental band in the weakly nonlinear regime. The solid line corresponds to the numerical solution of the eigenvalue problem from Hamiltonian (4.12), while the dashed line corresponds to the Landau-Zener theory given by Eq. (4.9). The experimental points are an average of three measurements. The lattice depth was $V_0/E_{rec} = 2.5$. The acceleration time t_{acc} was varied in the experiment within the range $4 - 8\tau_B$, depending on the value of the tunneling rate. In order to highlight the deviation from the Landau-Zener prediction when the tunneling is resonantly enhanced, the same experimental data of the main figure but divided by their Landau-Zener theoretical prediction are plotted in the inset.

ures the experimental data are compared with two theoretical predictions: the Landau-Zener formula (dashed line) and Γ_1 calculated by numerically

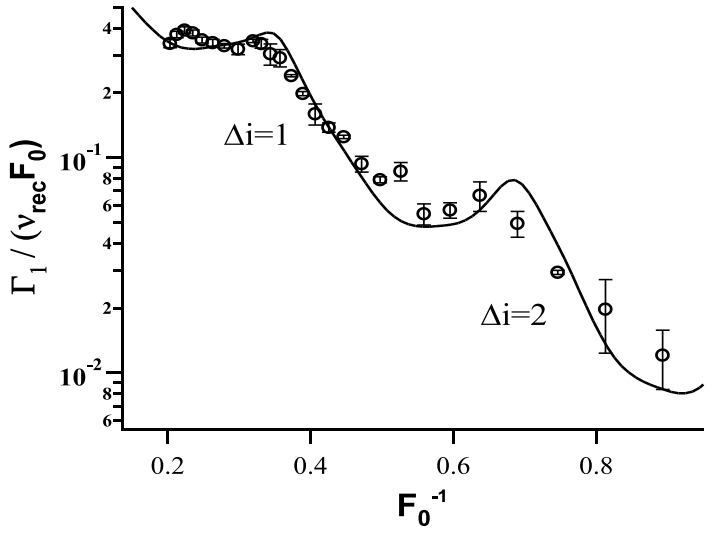

Figure 4.8: Tunneling rate from the lowest band. The experiment is equivalent to the one in Fig.(4.7), but with lattice depth $V_0/E_{rec} = 4$. In this experiment, the acceleration time t_{acc} was varied within the range $5 - 11\tau_B$, depending on the value of the tunneling rate.

solving the eigenvalue problem of the Hamiltonian (4.12)(solid line). The experimental data agrees with the latter one, and an enhancement of tunneling over the Landau-Zener prediction is evident when the resonance condition (4.13) is fulfilled. The two theoretical curves were independently evaluated and are not a fit to the experimental data. However, Fig.(4.7) shows that in a small region of forces the measured tunneling rate disagrees with the theory, and there is no evidence of the $\Delta i = 1$ peak. We interpreted this disagreement as being due to the value of Γ_1 that is, at the top of this resonance peak, out of our experimental resolution. This is highlighted in Fig. (4.7) by the two black arrows on the vertical axis.

The same measurement of figures (4.7),(4.8) was performed for different lattice depths and lattice constants: $V_0/E_{rec} = 4, 6, 9$ with $d_L = 0.426\mu$m, and $V_0/E_{rec} = 2.5, 10$ with $d_L = 0.620\mu$m. The experimental results always followed the theoretical predictions, within the experimental resolution.

For lattice depths $V_0/E_{rec} > 10$ the tunneling rate Γ_1 was out of our experimental resolution. In order to partially test the theory at deeper lattice depths, we increased the time of the acceleration t_{acc} by applying the force back and forth. In these experiments, the atoms were first accelerated for $t \simeq 20\,\tau_B$. Then, the lattice was accelerated in the opposite direction by applying a frequency chirp to the lattice beam whose frequency was fixed during the first acceleration. The second acceleration stage was $t \simeq 25\,\tau_B$ long in order to separate the dragged fraction of the sample from the whole cloud.

Apart from its sign, the acceleration was constant during each measurement. At the end of this procedure not all the atoms in the sample were imaged, because in the time-of-flight measurements the maximum separation between the density peaks was larger than the CCD size. Therefore, it was not possible to measure the absolute value of the tunneling rate Γ_1. However, it was possible to measure the number of the dragged atoms N_{drag}, that was reduced when the resonance condition (4.13) held. Thus it was possible to measure the positions of the resonances, and these corresponded to the expected values. This measurement was performed for $V_0/E_{rec} = 16$ with $d_L = 0.426\,\mu$m, and $V_0/E_{rec} = 12$ and 14 with $d_L = 0.620\,\mu$m.

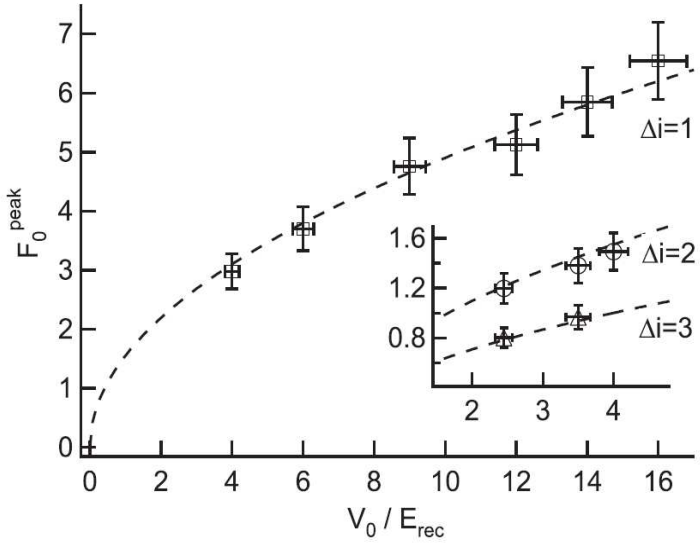

Figure 4.9: $\Delta i = 1$ peak positions plotted versus lattice depth. The relative error in the lattice depth is estimated to be 0.05. The dashed line is a fit with a square root function of the lattice depth (see text). The same measurement for the $\Delta i = 2$ and $\Delta i = 3$ interference peaks is shown in the inset.

The positions of the tunneling resonances of the orders $\Delta i = 1, 2, 3$ are plotted in Fig. (4.9) versus the lattice depth. There the dashed lines are independent fits of the experimental data with the function

$$\Delta i F d_L = \alpha E_{rec} \sqrt{\frac{V_0}{E_{rec}}}. \tag{4.17}$$

Our experimental data could be fitted with $\alpha \simeq 1.5$. If the separation between the energy levels in a single site ΔE is calculated by approximating each lattice site as an harmonic oscillator, one would expect $\alpha = 2$. Our measurement is consistent with the fact that only few energy levels were bound in our lattice, and hence the single site potential was highly anharmonic, which leads to a reduction of the actual value of ΔE.

The widths of the resonance peaks of the order $\Delta i = 1$ are plotted in Fig. (4.10) versus the lattice depth. The experimental data used for the measurement of the widths were the number of the atoms dragged by the lattice N_{drag}, whose decrease in correspondence with a resonance was fitted with a single gaussian function. The empty circles are the theoretical predictions obtained by numerical integration of the eigenvalue problem of the Hamiltonian (4.12). The width of the resonance peaks decreases for deeper lattices; this behavior corresponds to the one expected for the width of the Wannier-Stark states, which decreases when the lattice depth is increased. However, this behavior was not observed for lattice depths in the range $V_0/E_{rec} = 4-8$, within which the numerical calculations predict that the lattice width is almost constant. Apart from the numerical calculations, there is not a theoretical explanation of this behavior, as far as we know.

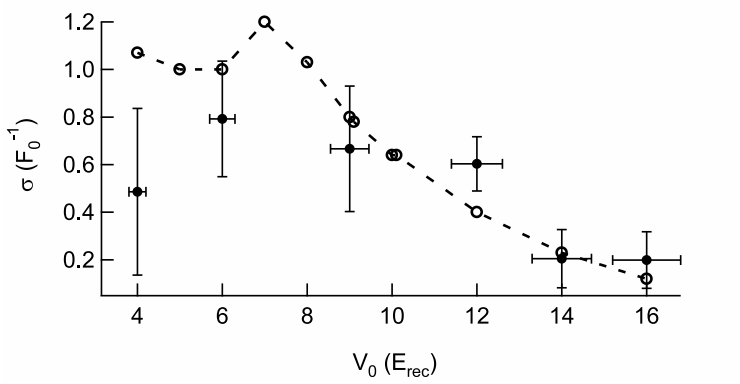

Figure 4.10: Measurement of the width of the resonant peaks of order $\Delta i = 1$ as a function of the lattice depth. The filled circles are the experimental data, while the empty ones are the theoretical prediction. The dashed line is a guide for the eyes.

4.5.2 Tunneling rate from excited bands

The experimental procedure in the measurement of the tunneling rate from the excited bands corresponded to the one described previously for the tunneling from the fundamental band. The only difference in this case concerned the preparation of the sample, which had to be initially loaded in the n-th band of the lattice. This was done by ramping up the lattice with a fixed detuning $\Delta\nu$ between the two lattice beams [51]. In the lattice frame this corresponded to a momentum p of the atoms of $md_L\Delta\nu$. If p was outside the first Brillouin zone, conservation of energy and momentum led to the atoms populating higher energy bands. In particular, the atoms were loaded into

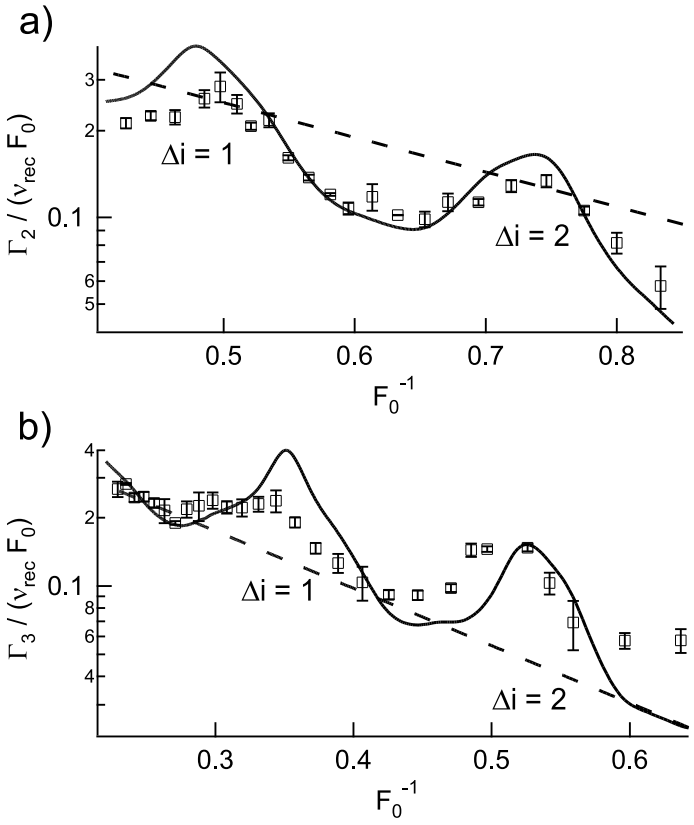

Figure 4.11: Measurement of the tunneling rate from the first and the second excited bands. The lattice depths were $V_0/E_{rec} = 10$ and $V_0/E_{rec} = 23$, respectively. The solid line is the numerical prediction, while the dashed line is the Landau-Zener prediction.

the n-th band, where $n = [p/(\hbar k_L)]$, and $[\cdot]$ is the integer part function (see Fig.(4.1), where the Bloch bands and the free particle dispersion relation are plotted). However, it is important to note that if for the momentum p there is an avoided energy crossing between two bands, that is if $p = j\hbar k_L$ (j integer), the atoms split and populate both bands. Therefore, in order to load the atoms into a single band, p must be equally distant from the Brillouin zone boundaries. In order to load the atoms into the first and the second excited bands we imposed to the lattice a constant velocity $d_L \Delta\nu = 1.5\, v_{rec}$ and $d_L \Delta\nu = 2.5\, v_{rec}$, respectively. This procedure was tested by measuring the number of tunneled and dragged atoms after separating the atoms belonging to different bands by accelerating the lattice in appropriate conditions. In order to test the loading into the first excited band, for instance, the lattice depth and acceleration had to be such that the probability of tunneling from the first excited band to the fundamental one was $r_1 \ll 1$, while the proba-

bility of tunneling from the first to the second excited band was $r_2 \sim 1$. As an example, this was the case for a lattice of depth $V_0/E_{rec} = 3$ and a force $F_0 = 0.92$, for which $r_1 \simeq 0.05$ and $r_2 \simeq 0.90$. Efficiencies of loading into the first and second excited bands of up to 90% were reached.

Fig.(4.11 a)) shows the measurement of the tunneling rate from the first excited band as a function of the force. The same measurement but from the second excited band is reported in Fig. (4.11 b)). The lattice depths were $V_0/E_{rec} = 14$ and $V_0/E_{rec} = 23$, respectively, with $d_L = 0.620\,\text{nm}$. In both cases the resonances were observed where expected by the theory.

4.5.3 The crossing-anticrossing scenario

The energy spectrum of the Hamiltonian (4.1) of a BEC in an optical lattice is characterized by the band structure. This results from the spatial symmetry of the optical lattice potential, which makes the energy spectrum periodic in quasimomentum. Because of the coupling through the potential, the degeneracy that occurs when bands of different orders cross is lifted in avoided crossings (or anticrossings) characterized by the energy gaps.

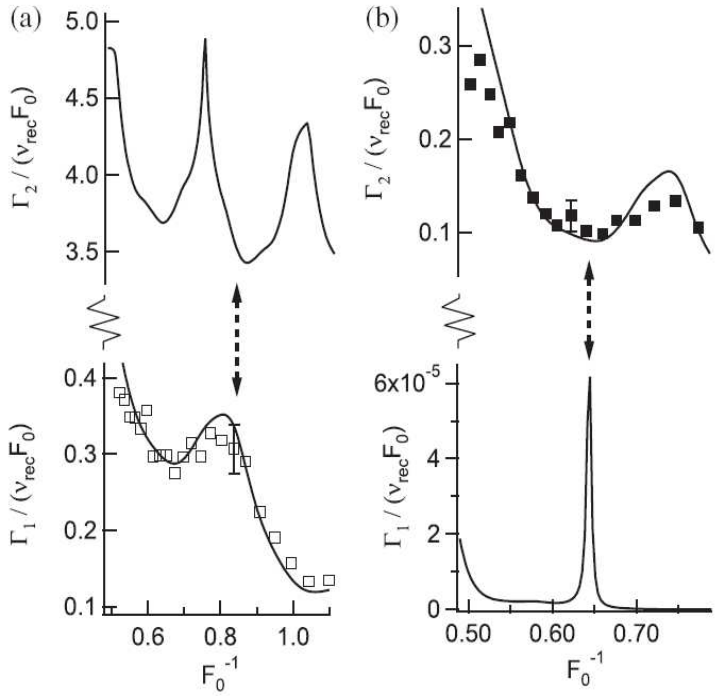

Figure 4.12: Anticrossings of the tunneling rate in resonantly enhanced tunneling. (a): theoretical plot of $\Gamma_{1,2}$ and experimental data of Γ_1 for a lattice depth of $V_0/E_{rec} = 2.5$. (b): theoretical plot of $\Gamma_{1,2}$ and experimental data of Γ_2 for a lattice depth of $V_0/E_{rec} = 10$.

In the Hamiltonian (4.12) of a BEC in an optical lattice and subject to an external force, the spatial symmetry is broken. Therefore, the quasimomentum not longer plays the role of a parameter for the energy spectrum. In fact, this now depends on two parameters: the lattice potential V_0 and the strength of the external force F. The eigenvalues of the Hamiltonian are now complex functions whose real part is the energy level while the imaginary part corresponds to the width of the energy levels, i.e. the Wannier-Stark states. Indeed, these have a mean life Γ_n^{-1}.

When the force F is such that a resonance in tunneling occurs, i.e., the resonance condition (4.13) is fulfilled, the Wannier-Stark ladders cross [71][66]. It is interesting to note that this crossing can be of two types [72][73]:

1. The energy levels have an avoided crossing and the tunneling rates have a real crossing.

2. The tunneling rates have an avoided crossing and the energy levels a real one.

In our experimental range of parameters, the crossings we observed were always of the second type. It has been predicted that at resonance the mean life of the two crossing states have opposite behavior: the lower one has a strong depletion, while the upper one reduces its decay rate (because it is coupled with the lower state that is more stable) [62]. In our experiment we were not able to measure for the same set of parameters the Γ of two different levels, because of lack of experimental resolution. Fig. (4.12) shows the measurement of Γ_1 and Γ_2 with the theoretical prediction for the two bands. The experimental data, while not complete, are in agreement with the theory. In order to prove this behavior directly it would be necessary to expand the range of measurable Γ, for instance by increasing the time of acceleration. This could be realized in experiments in which, with respect to our experiment, larger displacements of the cloud due to the lattice acceleration can be achieved [74].

4.6 Resonantly enhanced tunneling in the strongly nonlinear regime

The intrinsic nonlinear behavior of Bose-Einstein condensates has been widely studied since the first experimental realizations of BEC in dilute gases. When loaded into an optical lattice, ultracold atoms experience many effects due to nonlinearity, such as the dynamical instability [76, 77, 78]. In our experimental study of resonantly enhanced tunneling we investigated how the

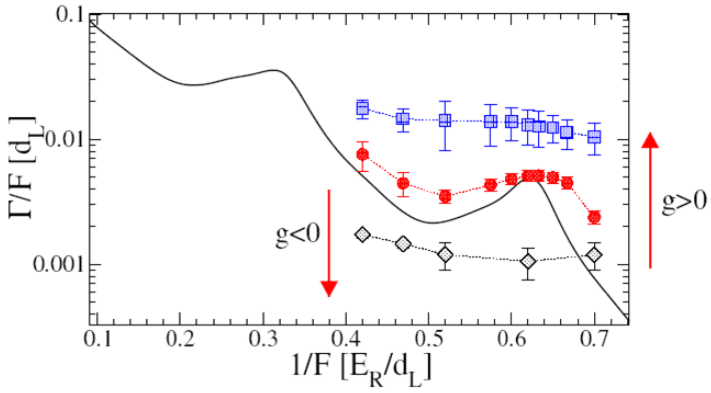

Figure 4.13: Numerical simulation of resonantly enhanced tunneling with nonlinearity. When this is increased, the resonance peak is destroyed both in the cases of repulsive ($g > 0$) and attractive ($g < 0$) interactions. From Ref. [75].

nonlinearity affects the phenomena. The effects of nonlinearity can in general be well approximated by considering the system as evolving within an effective potential [52, 70, 79]:

$$V_{eff} = \frac{V_0}{1 + 4C} \tag{4.18}$$

where C is the parameter introduced in Eq. (4.16) that takes into account the "strength" of the nonlinearity. In our experiment $C > 0$ because the atom-atom interactions are repulsive. Therefore the nonlinearity reduces the potential experienced by the atoms, causing a decrease of the height of the barrier that the atoms have to tunnel through. This leads to an increase in the tunneling rate Γ, i.e., the lifetime of the Wannier-Stark states is reduced.

The effect of the nonlinearity in resonantly enhanced tunneling has been studied in ref. [75] by numerical integration of the 3D Gross-Pitaevskii equation (4.15). Fig. (4.13) shows the results of ref. [75]. As expected the tunneling rate is increased in the case of repulsive interactions and decreased in the case of attractive interactions, independently of the force. An even more evident effect is the destruction of the resonance peak. This effect is difficult to interpret in an intuitive way. Two effects that could broaden the width of the peak can be pointed out. The first is the enhancement of the width of the Wannier-Stark states. This occurs because the effective potential (4.18) is lower than the linear one, i.e., the energy gap decreases for increasing C, leading therefore to an increase of Γ. The second effect is the inhomogeneity in the lattice filling, resulting in a different nonlinearity C on each lattice site depending on its number of atoms. This causes a different displacement

of the energy levels in each lattice site and therefore the resonance condition (4.13) is no longer well defined all along the lattice.

4.6.1 Destruction of the resonant tunneling

The experiments in the nonlinear regime were performed by using an optical lattice with constant: $d_L = 0.620$nm, and by increasing the radial frequency ν_{rad} of the dipolar confinement. Nonlinearities up to $C = 6 \cdot 10^{-2}$ were reached for $\nu_{rad} = 250\,\mathrm{Hz}$. The loading of the lattice was performed in a longer time compared to the experiments with weak nonlinearity in order to take into account the time-scale of the atom-atom interactions [80]. This is defined as [81]: $\tau_{NL} = \hbar/\mu$ where μ is the chemical potential, proportional to the condensate peak density and hence to the parameter C. In order not to excite collective modes, the lattice was loaded in $5 - 10\,\mathrm{ms}$ [69].

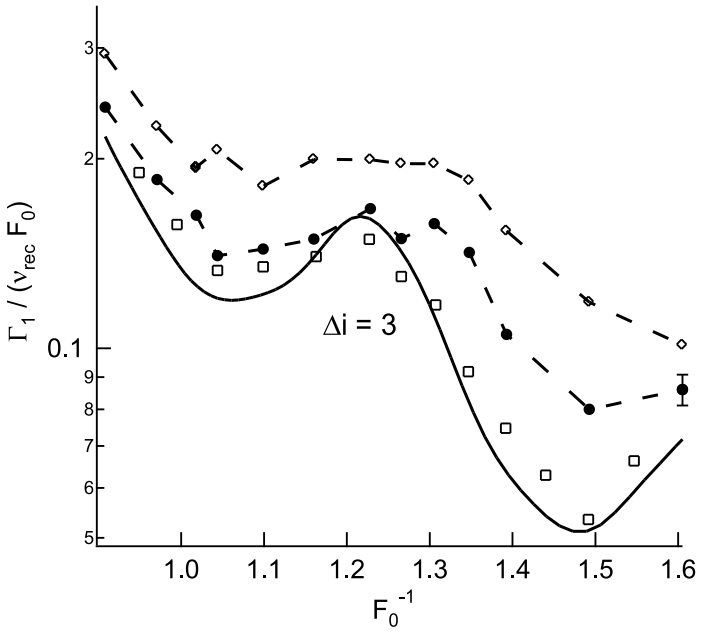

Figure 4.14: Measurement of the tunneling rate close to a resonance peak for three different nonlinearities: $C = 0.024$ (empty squares), $C = 0.035$ (filled circles), $C = 0.057$ (empty diamonds). The lattice depth was $V_0/E_{rec} = 2.5$. The resonance is of order $\Delta i = 3$.

Fig.(4.14) shows the effects of nonlinearity in the measurement of the tunneling rate close to a resonance peak. The tunneling rate was measured for three different values of C: $C = 0.024$, $C = 0.035$, $C = 0.057$. The nonlinearity was changed by varying the number of atoms and the radial frequency of the dipolar trap. Both expected behaviors were observed: a general enhancement, independent of the force, of Γ when C was increased, and a

broadening of the resonance peak that almost disappeared for the strongest nonlinearity. The experiment agrees thus with the theoretical predictions of Ref [75]. The evidence of the latter effect was highlighted in a second experiment, where the tunneling rate was measured off and on resonance, i.e., by imposing two different forces, as a function of C. This measurement is reported in Fig.(4.15). The tunneling rates on and off resonance exhibited different behaviors when the nonlinearity was changed.

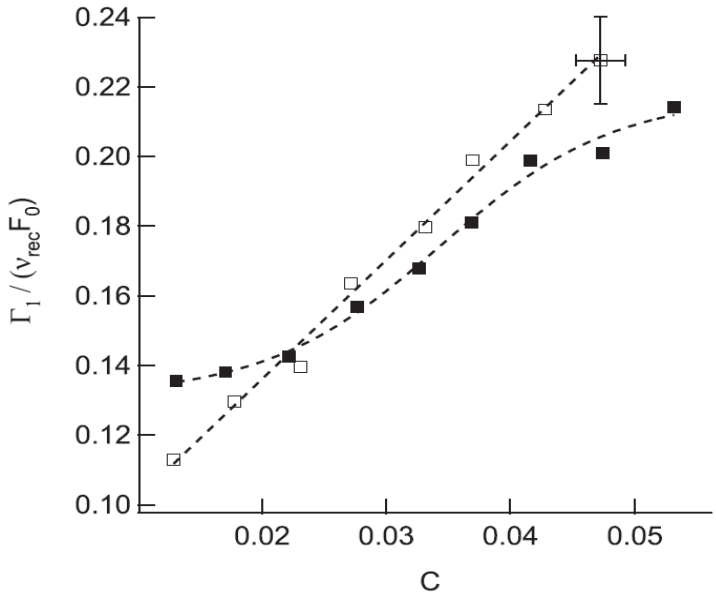

Figure 4.15: Measurement of the tunneling rate as a function of C in a lattice of depth $V_0/E_{rec} = 2.5$ and for two values of the force: on the resonance peak at $F_0^{-1} = 1.21$ (filled squares), off the resonance peak at $F_0^{-1} = 1.03$ (empty squares). The lines are fits to guide the eyes.

4.6.2 Tunneling vs time

A second prediction of Ref. [75] about nonlinearity-induced effects on the tunneling rate regards its dependence on time. The numerical simulations predict an exponential decay of the survival probability $P_{sur} = N_{drag}/N_{tot}$ as expected by the Landau-Zener theory in the linear case. In the nonlinear case a faster decay and a deviation from the exponential behavior is predicted. In order to prove these behaviors experimentally, we measured the probability P_{sur} of remaining in the fundamental band for different times of acceleration t_{acc} in the weakly and strongly nonlinear regimes. In the first case we had $C = 8 \cdot 10^{-3}$, while in the latter one $C = 3.7 \cdot 10^{-2}$, and the lattice depth was $V_0/E_{rec} = 3$. Both measurements are reported in Fig. (4.16) with the

theoretical predictions evaluated as in Ref. [75] for the parameters of our experiment. The survival probability in the nonlinear case decayed clearly faster than in the linear case. However, the predicted non-exponential behavior was not observed. This was interpreted as being due to our limit in the maximum value of t_{acc} that we can realize in the experiment. In fact the agreement of the theoretical and the experimental data in Fig.(4.16) is satisfactory, but a strong deviation from the exponential decay was only expected for $t_{acc} > 10\tau_B$.

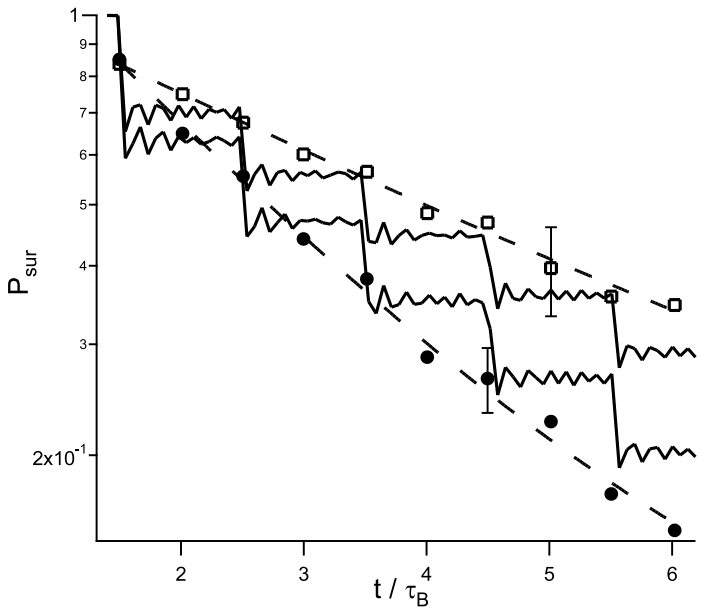

Figure 4.16: Measurement of the survival probability $P_{sur} = N_{drag}/N_{tot}$ from the fundamental to the first excited band as a function of the time of acceleration t_{acc}. The lattice depth was $V_0/E_{rec} = 3$, and the force $F_0 = 1.68$.

Chapter 5

Dynamical control of matter-wave tunneling

In this chapter the experimental control of the interwell tunneling in a strongly driven optical lattice is reported. This effect has been observed both by measuring the condensate expansion in *in situ* experiments and by observing its interference pattern in time-of-flight experiments. By the latter procedure it was demonstrated that the coherence of the sample is preserved during the driving. Apart from the intrinsic interest in managing the tunneling parameter, the results discussed here open the possibility of realizing the superfluid-Mott insulator phase transition in a strongly driven optical lattice [82, 83].

5.1 The driven optical lattice

In Chapter 2 the Bose-Hubbard Hamiltonian has been introduced in order to describe the behavior of cold atoms in an optical lattice:

$$\hat{H}_{BH} = -J \sum_{\langle i,j \rangle} \left(\hat{c}_i^\dagger \hat{c}_j + \hat{c}_j^\dagger \hat{c}_i \right) + \frac{U}{2} \sum_j \hat{n}_j \left(\hat{n}_j - 1 \right) = \hat{H}_{tun} + \hat{H}_{int}, \qquad (5.1)$$

where the sum over $\langle i, j \rangle$ is taken over nearest neighbors sites, $\hat{n}_i$ is the number operator of the i-th site, and $\hat{c}_i^\dagger$, $\hat{c}_i$ are the boson creation and annihilation operators at site i obeying the usual commutation relations: $[\hat{c}_i, \hat{c}_j^\dagger] = \delta_{i,j}$, $[\hat{c}_i^\dagger, \hat{c}_j^\dagger] = [\hat{c}_i, \hat{c}_j] = 0 \ \forall i, j$. The Hamiltonian (5.1) depends only on the parameters U and J: $U \propto V_0^{3/4}$ is the energy contribution due to the interaction between two or more atoms occupying the same lattice site; $J \propto V_0^{3/4} \exp(-2(V_0/E_{rec})^{1/2})$ is the energy cost associated with one atom tunneling from one lattice site to another one, and is usually referred to as the kinetic term.

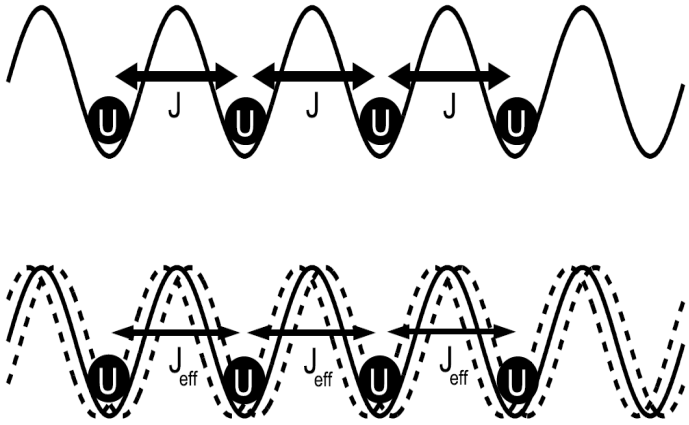

Figure 5.1: Sketch of the dynamical suppression of tunneling. In the Bose-Hubbard model, the parameters that characterize an optical lattice are the interaction energy U and the tunneling energy J. When the lattice is "shaken" (by modulating one of the frequencies of the two lattice beams), the tunneling parameter J changes to an effective J_{eff}.

In the experiments described in this chapter the lattice was frequency modulated, leading to a sinusoidal motion referred to as "shaking" in this thesis. This corresponds to a contribution in the Hamiltonian [82, 84]:

$$\hat{H}_{FM}(t) = K\cos(\omega t)\sum_j j\hat{n}_j \tag{5.2}$$

where K is the modulation amplitude and ω its frequency. The full Hamiltonian then reads:

$$\hat{H}_T(t) = \hat{H}_{BH} + \hat{H}_{FM}(t) = \hat{H}(t+T) \tag{5.3}$$

where $T = 2\pi/\omega$. As stressed in Eq.(5.3), the full Hamiltonian is now periodic in time with period T. A good strategy for this theoretical problem is to use a semiclassical approach by the so-called Floquet theory [85]. Following this theory, the Schrödinger equation

$$i\hbar\frac{\partial}{\partial t}|\psi_n(t)\rangle = \hat{H}_T|\psi_n(t)\rangle \tag{5.4}$$

has solutions of the form:

$$|\psi_n(t)\rangle = |u_n(t)\rangle\exp\left[-i\frac{\epsilon_n t}{\hbar}\right] \tag{5.5}$$

where the so-called *Floquet mode* $|u_n(t)\rangle = |u_n(t+T)\rangle$ is again periodic in time with period T. The energy ϵ_n is called a *quasienergy* because of the

formal analogy with the quasimomentum in the Bloch problem in a spatially periodic Hamiltonian. By substituting the Floquet solution (5.5) into the Schrödinger equation (5.4) one arrives at the following relation for the Floquet mode [86]:

$$\left(\hat{H}_T(t) - i\hbar\frac{\partial}{\partial t}\right)|u_n(t)\rangle = \epsilon_n|u_n(t)\rangle. \tag{5.6}$$

This result is crucial in the development of the theory. Eq.(5.6) can be interpreted as an eigenvalue problem by defining the Hamiltonian $\hat{\mathcal{H}} = \hat{H}_T - i\hbar\partial/\partial t$ in an extended Hilbert space $\mathcal{R}\otimes\mathcal{T}$, where $\mathcal{T}$ is the space of the time periodic functions of period T and $\mathcal{R}$ is the Hilbert space of square integrable functions on the configuration space. The space $\mathcal{T}$ is a Hilbert space whose inner product is defined as:

$$\langle f|g\rangle = \frac{1}{T}\int_0^T f^*(t)g(t)dt. \tag{5.7}$$

In this way the problem (5.6) can be solved using all theorems characteristic for time-independent Schrödinger theory in the composite Hilbert space $\mathcal{R}\otimes\mathcal{T}$ whose inner product is:

$$\langle\langle h|s\rangle\rangle = \frac{1}{T}\int_0^T \langle h(\mathbf{r},t)|s(\mathbf{r},t)\rangle dt = \frac{1}{T}\int_0^T\int h^*(\mathbf{r},t)s(\mathbf{r},t)d\mathbf{r}dt. \tag{5.8}$$

It is important to note that if $|u_n(t)\rangle$ is a solution of Eq.(5.6) with eigenvalue ϵ_n, then $|u_{n,m}(t)\rangle = |u_n(t)\rangle\exp(im\omega t)$ is also a solution of Eq.(5.6) with eigenvalue $\epsilon_n + m\hbar\omega$, where $m = \pm1, \pm2, ...$ The quasienergy spectrum has a Brillouin-zone-like structure, where the width of one zone is $\hbar\omega$.

It can be demonstrated that the Floquet modes within the first Brillouin zone and for a fixed time t $|u_{n,0}(t)\rangle$ form a complete set in the Hilbert space $\mathcal{R}$ [87]. In the physical system of M atoms loaded in N sites of an optical lattice, a natural basis in the $\mathcal{R}$ space is given by all the combinations of Fock states $|\{n_j\}\rangle$, where $j = 1, .., N$ and $\sum_j n_j = M$ (n_j is the number of atoms in the j-th site). The Floquet basis in the $\mathcal{R}\otimes\mathcal{T}$ space is then given by [82]:

$$|u_{n,m}(t)\rangle = |\{n_j\}, m\rangle = |\{n_j\}\rangle\exp\left[-i\frac{K}{\hbar\omega}\sin(\omega t)\sum_j jn_j + im\omega t\right]. \tag{5.9}$$

The final step in order to solve the eigenvalue problem (5.6) is to write the Hamiltonian $\hat{\mathcal{H}} = \hat{H}_T - i\hbar\partial/\partial t$ in the Floquet basis (5.9) and to diagonalize it. This has the form:

$$\begin{aligned}\langle\langle\{n'_j\}, m'|\hat{H}_T - \hbar\partial/\partial t|\{n_j\}, m\rangle\rangle = \\ = \delta_{m',m}[\langle\{n'_j\}, m'|\hat{H}_{int}|\{n_j\}, m\rangle] \\ + s^{m'-m}\mathcal{J}_{m'-m}(K/(\hbar\omega))\langle\{n'_j\}, m'|\hat{H}_{tun}|\{n_j\}, m\rangle\end{aligned} \tag{5.10}$$

where $s = \sum_j (n'_j - n_j)j$, and $\mathcal{J}_{m'-m}$ is the Bessel function of order $m' - m$. This matrix is formed by diagonal blocks for different Brillouin zones m that are coupled by nondiagonal terms. It can be shown that the coupling between these diagonal blocks can be ignored if the distance between the blocks, i.e. $\hbar\omega$, is much larger than the other energies, i.e., the tunneling and the interaction energy: $\hbar\omega \gg \max(J, U)$. Within this approximation only terms with $m = m'$ are important, and Eq.(5.10) becomes:

$$\langle\langle\{n'_j\}, m|\hat{H}_T - \hbar\partial/\partial t|\{n_j\}, m\rangle\rangle = [\langle\{n'_j\}|\hat{H}_{int} + \mathcal{J}_0(K/(\hbar\omega))\hat{H}_{tun}|\{n'_j\}\rangle]. \tag{5.11}$$

This Equation corresponds to the eigenvalue problem of the Bose-Hubbard Hamiltonian (5.1) *without frequency modulation* of the lattice where the tunneling parameter J is substituted by an *effective tunneling* J_{eff} given by:

$$J_{eff} = \mathcal{J}_0(K_0)J \tag{5.12}$$

where $K_0 = K/(\hbar\omega)$.

This result is very general, because the same theoretical approach can be used to describe any experiment in which a physical system is subjected to a strong time periodic driving potential. A beautiful example in the literature is an experiment reported in 1970 by Haroche *et al.* [88], where the Zeeman hyperfine spectrum of ^{87}Rb and ^{1}H was measured in the presence of a static magnetic field B and an orthogonal radio-frequency field $B_1 \cos(\omega t)$. A variation of the peak positions in the atomic spectrum was observed when the oscillating field was present. The experimental data were fitted very well by substituting the Landé g-factor with an "effective" one $\bar{g}_F$: $\bar{g}_f = g_f \mathcal{J}_0(g_F \mu_B B/\omega)$ [89]. Although this effect was interpreted by the authors within the "dressed-atom" approach, the experiment can be perfectly described within the Floquet theory by use of the same procedure introduced above [90].

Signatures of tunneling suppression in time periodic driven systems has been observed in a number of experiments [91, 92, 93], and recently dynamical localization and coherent suppression of tunneling have been demonstrated using light propagating in coupled waveguide arrays [94, 95]. So far, however, an exact experimental realization of the Bose-Hubbard Hamiltonian with a time-periodic potential (5.3) has not been reported.

5.1.1 Band distortion in a shaken lattice

The calculation presented previously showed that the main effect of the lattice shaking regarded the tunneling J, which has to be substituted in the Bose-Hubbard Hamiltonian by the effective tunneling J_{eff}. It is interesting to study now how the shaking affects the energy spectrum of the lattice, i.e.,

the energy bands. This can be done by using a simple model, consisting of a single particle loaded in an infinite lattice (a single particle means that there are no interactions). The Hamiltonian of the system is, within the tight binding model:

$$\hat{H} = -J \sum_{l=-\infty}^{\infty} (|l+1\rangle\langle l| + |l\rangle\langle l+1|) + K\cos(\omega t) \sum_{l=-\infty}^{\infty} l|l\rangle\langle l| \tag{5.13}$$

where $|l\rangle$ is the Wannier state centered at the l-th site. The solution of this problem can be found within the Floquet theory and by use of the Houston functions [90] (a different procedure leading to the same result was used by Ref. [96]). However, if the shaking amplitude is weak compared to the scale of energy of the undriven lattice, i.e. if $K \ll J$, one can approximate the energy spectrum by the energy bands of the unshaken lattice $E_n(q(t))$. Thus the effect of the shaking reduces to a change in time of the quasimomentum $q(t)$ through the relation:

$$\dot{q}(t) = F(t) \tag{5.14}$$

where $F(t) = K/d_L \cos(\omega t)$. Integrating the relation (5.14) one finds the dependence of the quasimomentum q in time:

$$q(t) = q_0 + \frac{K}{d_L\omega}\sin(\omega t). \tag{5.15}$$

The fundamental energy band $E_0(q(t))$ can hence be written substituting the quasimomentum of Eq.(5.15):

$$\begin{aligned} E_0(q(t)) &= -2J\cos\left(\frac{q(t)}{\hbar k_L}\pi\right) = -2J\cos\left(\frac{q_0}{\hbar k_L}\pi + \frac{K\pi}{d_L\omega\hbar k_L}\sin(\omega t)\right) \\ &= -2J\cos\left(\frac{q_0}{\hbar k_L}\pi + K_0\sin(\omega t)\right) \\ &= -2J\cos\left(\frac{q_0}{\hbar k_L}\pi\right)\cos\left(K_0\sin(\omega t)\right) + 2J\sin\left(\frac{q_0}{\hbar k_L}\pi\right)\sin\left(K_0\sin(\omega t)\right) \end{aligned} \tag{5.16}$$

The shape of the band can therefore be calculated by integrating Eq.(5.16) in time over a period of the shaking $T = 2\pi/\omega$. The integral of the $\sin(\sin(\cdot))$ term on the right hand side of Eq.(5.16) is zero; therefore, the fundamental band $E_0(q)$ is:

$$\begin{aligned} E_0(q) &= -2J\mathcal{J}_0(K_0)\cos\left(\frac{q}{\hbar k_L}\pi\right) \\ &= -2J_{eff}\cos\left(\frac{q}{\hbar k_L}\pi\right). \end{aligned} \tag{5.17}$$

The fundamental band of the shaken lattice corresponds hence to the fundamental band of the unshaken lattice but with the tunneling J (reflecting the band width) substituted by its effective value J_{eff}.

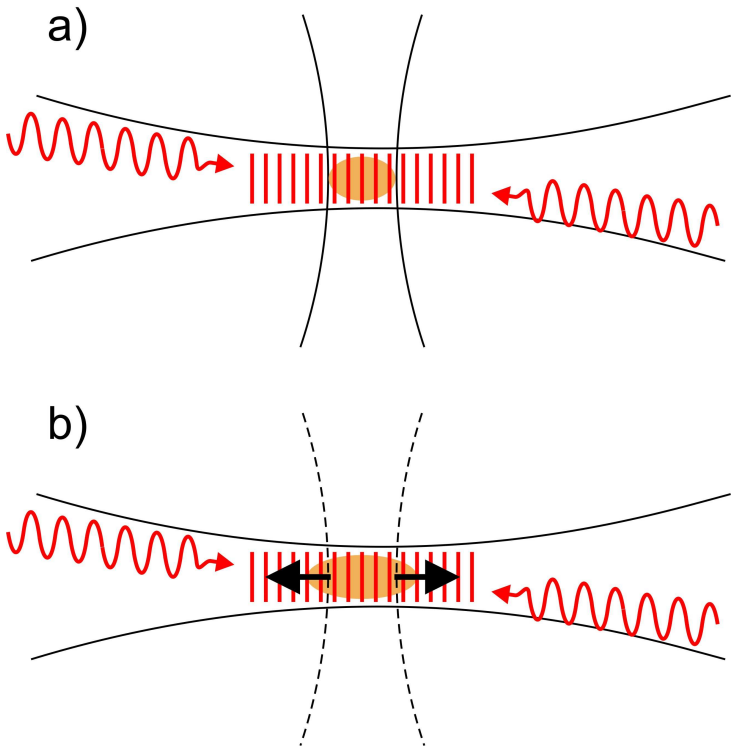

Figure 5.2: Scheme of the experimental procedure. a) The atoms were confined by two laser beams in a cigar shaped trap, and loaded into a lattice that was almost collinear with one of the dipolar beams. b) The dipolar beam orthogonal to the lattice was turned off suddenly, and the atoms started to expand along the lattice. This expansion was observed in an *in situ* measurement

5.2 In situ measurements

The aim of our experiment is to demonstrate that the interwell tunneling in an optical lattice can be controlled coherently by modulating it in frequency. This section is dedicated to showing the measurements that demonstrate how the tunneling J varies by applying the frequency modulation according to Eq. (5.12).

5.2.1 Experimental procedure

In order to measure how the tunneling changes in a strongly driven optical lattice, we designed an experiment in which the single particle tunneling J can be indirectly estimated by observing the dynamics of the whole cloud.

In our experiment, once the BECs were created inside the dipolar trap, the power of the two dipolar beams was changed in order to obtain cigar shaped condensates. This operation took 50 ms in order to assure adiabaticity, and the frequencies of the elongated trap were $\nu_{long} = 20\,\text{Hz}$ and $\nu_{rad} = 80\,\text{Hz}$. Once the atoms were in this trap, two counterpropagating, independent laser beams at the same frequency were ramped up linearly in 50 ms in order to adiabatically load a one-dimensional lattice of depth V_0. The two lattice beams were almost collinear to the dipolar beam aligned with the longitudinal axis of the cigar-shaped trap (see Fig. (5.2)). Once the lattice was ramped up, the dipolar beam orthogonal with respect to the lattice was turned off. The longitudinal frequency ν_{long} of the trap passed hence suddenly from the initial 20 Hz to $\sim 3\,\text{Hz}$ (this weak confinement being caused by the focusing of the dipolar beam collinear with the lattice). Because of this change in the confinement frequency, the atoms started to expand along the lattice. The atoms were allowed to expand for a time t_{exp}, after which they were released both from the lattice and the dipolar confinement, and finally imaged after 0.3 ms. This very short time was chosen in order to make the effect of expansion in free space negligible. This kind of measurement is usually called *in situ*, and the BECs are observed in real space instead of the momentum space as in the *time-of-flight* measurements. In the *in situ* measurements we observed the width of the cloud σ_{long} in the longitudinal direction.

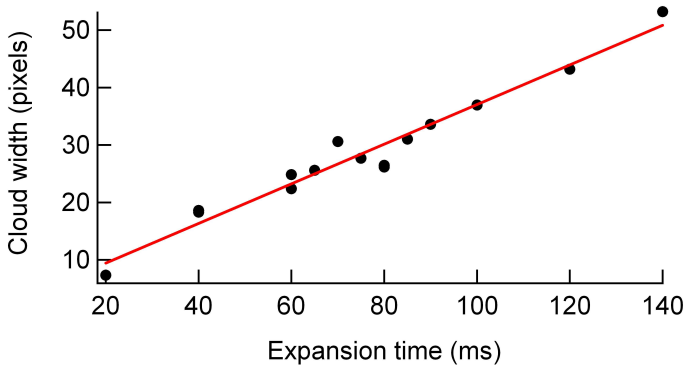

Figure 5.3: Linear expansion of the condensate in an optical lattice. In this measurement the lattice depth was $V_0 = 3E_{erec}$ and the lattice was not driven.

The expansion rate $r = d\sigma_{long}/dt$ of the condensate along the lattice is

linked to the interwell tunneling and can be determined by measuring the width of the cloud in the elongated direction for different values of t_{exp}. When no frequency modulation was applied during the experiment, this measurement was done by fitting the cloud width σ_{long} with a single gaussian. An example of the measurement of the expansion rate is presented in figure (5.3). The expansion was almost linear and its rate r was extracted with a linear fit of the experimental data. The same measurement was performed for different values of the lattice depth V_0: a plot of the expansion rate versus V_0 is shown in figure (5.4), where it is expressed in units of the lattice constant d_L. The data have been fitted with the function $r/d_L = \alpha J/h$, where J is the theoretical formula for the tunneling [41, 42]:

$$J = \frac{4}{\sqrt{\pi}} E_{rec} \left(\frac{V_0}{E_{rec}}\right)^{3/4} \exp\left(-2\sqrt{\frac{V_0}{E_{rec}}}\right), \tag{5.18}$$

and α is a factor used for the fit. The fit involved all the points except the one for $V_0 = 0$, and the factor has been found to be $\alpha = (6.29 \pm 0.15)$. This measurement proves that the expansion rate has the same dependence on V_0 as the expected tunneling rate J/h and can, therefore, be used as a tool to estimate the value of J.

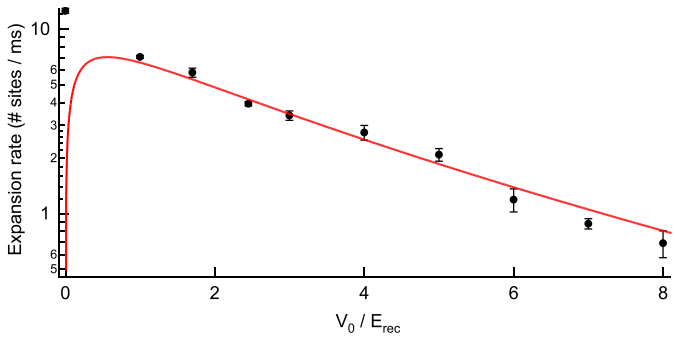

Figure 5.4: Expansion rate as a function of the lattice depth. The expansion is measured in units of lattice constant d_L. The red line is a fit with the theoretical function $r/d_L = \alpha J/h$ with $\alpha = (6.29 \pm 0.15)$.

5.2.2 Tunneling in a strongly driven lattice

The experimental investigation of tunneling in a strongly driven lattice was done by observing the expansion of the condensate in a shaken lattice. When ν_{long} was suddenly reduced, the shaking was abruptly switched on. The lattice was shaken during all the expansion time t_{exp}. The shaking was realized by modulating the radio-frequency (RF) source of one of the acousto-optic

modulators that were placed in the optical path of the two lattice beams. The two RF sources were two Agilent 3325A synthesizers, phase locked to an internal reference, and whose output frequency was centered around 72 MHz. By detuning the frequency of one of the synthesizers by $\Delta\nu$, it was possible to move the lattice at a velocity $v = d_L\Delta\nu$ or to accelerate it with an acceleration $a = d_L(d\Delta\nu/dt)$.

The shaking of the lattice was realized by imposing $\Delta\nu = d_L\Delta\nu_{max}\sin(\omega t)$, where $\Delta\nu_{max}$ was the maximum detuning between the two lattice beams. In

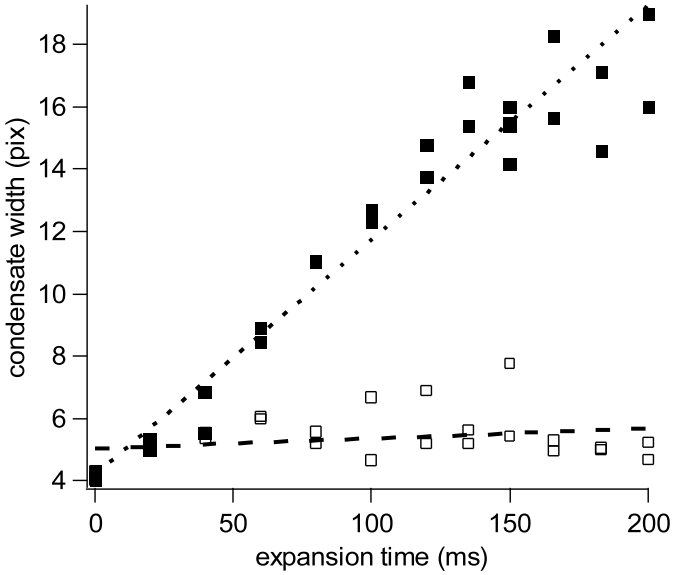

Figure 5.5: Expansion of the condensate in a lattice of depth $V_0/E_{rec} = 6$ without (full squares) and with (empty squares) strong driving. For the empty squares the shaking parameter was $K_0 = 2.3$.

the rest frame of the shaken lattice the atoms experienced a force:

$$F(t) = m\omega d_L\Delta\nu_{max}\cos(\omega t) = F_{max}\cos(\omega t). \tag{5.19}$$

The amplitude of the shaking K appearing in the Hamiltonian (5.2) is linked to the force (5.19) by the relation:

$$K = F_{max}d_L, \tag{5.20}$$

so the argument of the Bessel function $\mathcal{J}_0$ in Eq. (5.12) reads:

$$K_0 = \frac{K}{\hbar\omega} = \frac{md_L^2\Delta\nu_{max}}{\hbar} = \frac{\pi^2\Delta\nu_{max}}{2\omega_{rec}}. \tag{5.21}$$

The maximum displacement of the lattice in the laboratory frame is:

$$\Delta x_{max} = \frac{2}{\pi^2}\frac{\omega_{rec}}{\omega}K_0 d_L. \tag{5.22}$$

For a typical modulation frequency $\omega/(2\pi) = 3\,\mathrm{KHz}$ this was $\Delta x_{max} \sim 0.5\, d_L$ for $K_0 = 2.4$. When the modulation is applied, the tunneling and hence

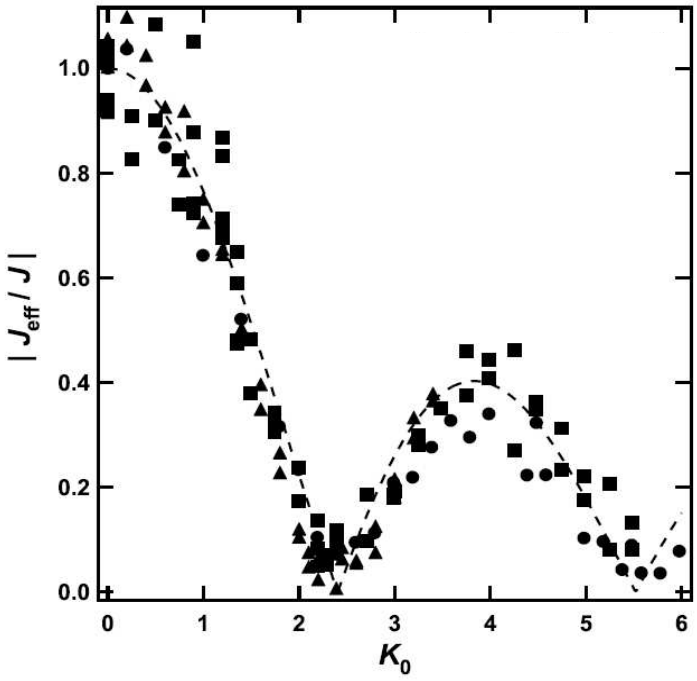

Figure 5.6: Measurement of the ratio J_{eff}/J for different values of K_0. The experimental data agree very well with the theoretical prediction given by formula (5.12). The different shapes of the points correspond to different lattice depths and different frequencies of modulation at which the measurement was performed; circles: $V_0/E_{rec} = 6$, $\omega/(2\pi) = 0.5KHz$; squares: $V_0/E_{rec} = 6$, $\omega/(2\pi) = 1.0KHz$; triangles: $V_0/E_{rec} = 4$, $\omega/(2\pi) = 1KHz$

the expansion rate of the condensate along the lattice, is expected to be reduced according to the relation (5.12). The effective tunneling J_{eff} cannot be measured directly. However, if $r(K_0)$ is the expansion rate of the sample in a shaken lattice with modulation amplitude $K_0/(\hbar\omega)$,and $r(0)$ the expansion rate without frequency modulation, these two quantities satisfy the relation:

$$\frac{J_{eff}}{J} = \frac{r(K_0)}{r(0)}. \tag{5.23}$$

Therefore, in our experiments we measured the ratio on the right-hand side of Eq.(5.23), from which the effective tunneling J_{eff} can be calculated. The assumption (5.23) is based on the result presented in figure (5.4) that has been previously discussed. An example of the condensate expansion in the regimes of shaken and unshaken lattice is presented in figure (5.5). There the lattice was shaken with $K_0 = 2.3$. By repeating the measurement of figure

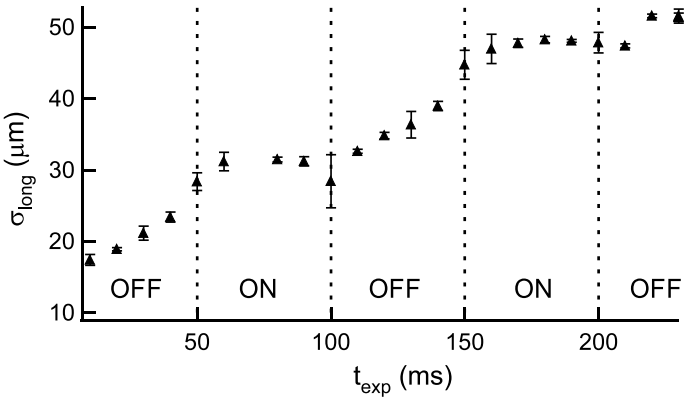

Figure 5.7: Expansion of the condensate in the lattice in different regimes of stationary (off) and driven (on) lattice. The driving was applied only in distinct time intervals, with $K_0 = 2.4$ and $\omega/(2\pi) = 1KHz$. The lattice depth was $V_0/E_{rec} = 6$.

(5.5) for different values of K_0 we were able to verify the relation (5.12). This measurement is presented in figure (5.6). This figure demonstrates a very good agreement between the theoretical prediction and the experimental data. The theoretical curve in Fig. (5.6) contains no free parameters. As expected, the smallest value for the tunneling was found for $K_0 = 2.4$, i.e., the first zero of the zeroth order Bessel function. Suppression of tunneling up to a factor of 25 was observed. However, this estimate has to be considered as a lower bound of the real tunneling suppression achievable by this technique, because we were limited by the experimental resolution in the measurement of the sample width, which was approximately 1/2 pixel. A similar result was obtained in an array of double wells by Ref. [97].

The feasibility of tunneling suppression was demonstrated in a "toy" experiment, where the shaking with $K_0 = 2.4$ was applied at different time intervals in order to "freeze" the expansion of the cloud when desired.

5.2.3 Effects of the shaking frequency

In the first paragraph of the chapter it was stated that the effect of frequency modulation on an optical lattice results in a substitution of the tunneling J by an effective J_{eff}, whose value is governed by the zero-th order Bessel function. This was possible under the hypothesis of a shaking frequency that was much larger than the tunneling and interaction energies J and U:

$$\hbar\omega \gg \max(J, U). \tag{5.24}$$

In our experiment, all the measurements we performed with a one dimen-

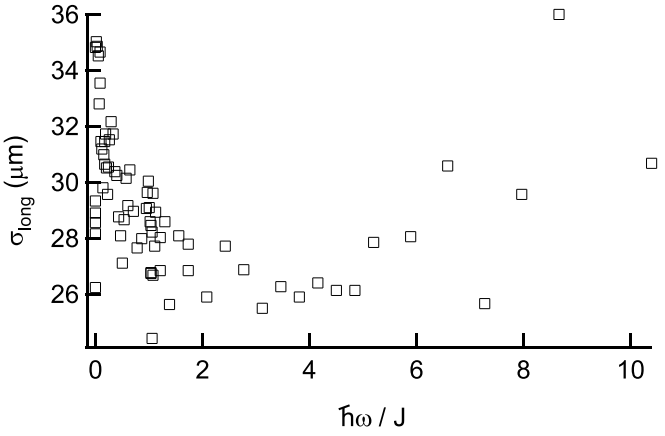

Figure 5.8: Measurement of the width of the cloud at the end of the expansion σ_{long} in a shaken lattice with $K_0 = 2.0$ fixed for different values of the shaking frequency ω. The lattice depth was $V_0/E_{rec} = 9$, corresponding to a tunneling energy $J/h \simeq 90\,\mathrm{Hz}$. The time of the expansion was $t_{exp} = 200\,\mathrm{ms}$.

sional optical lattice up to $V_0/E_{rec} < 9$ deep. Therefore, $U < J$ always, and the condition (5.24) reduces to:

$$\hbar\omega \gg J. \tag{5.25}$$

The measurements presented so far were performed at $V_0/E_{rec} = 4$ and 6, corresponding to a tunneling energy of $J/h \sim 280$ and $210\,\mathrm{Hz}$ respectively, and with a minimum shaking frequency $\omega/(2\pi) = 0.5\,\mathrm{KHz}$. Therefore, the condition (5.25) was effectively satisfied. In order to observe the dependence of the tunneling suppression on the shaking frequency, we measured the width of the cloud at the end of the expansion σ_{long} for a fixed value of K_0 but for different values of ω. Apart from a region of frequency $2J/h < \omega/(2\pi) < 5J/h$ in which σ_{long} is almost constant, the size of the cloud increases both for higher and lower frequencies. While the increase in σ_{long} for $\omega/(2\pi) > 5J/h$ can be interpreted as due to an excitation of the sample, as will be explained in the next section, the behavior of σ_{long} for $\omega/(2\pi) \lesssim 2J/h$ is difficult to interpret. In fact, together with a tunneling enhancement, a strong scatter of the experimental data was observed. To our knowledge, there is no theoretical prediction for the behavior of a condensate in a shaken optical lattice at a frequency $\omega/(2\pi) < J/h$. The aim of the measurement was not to explore this regime but to verify that the limit (5.25) agrees with the experiment.

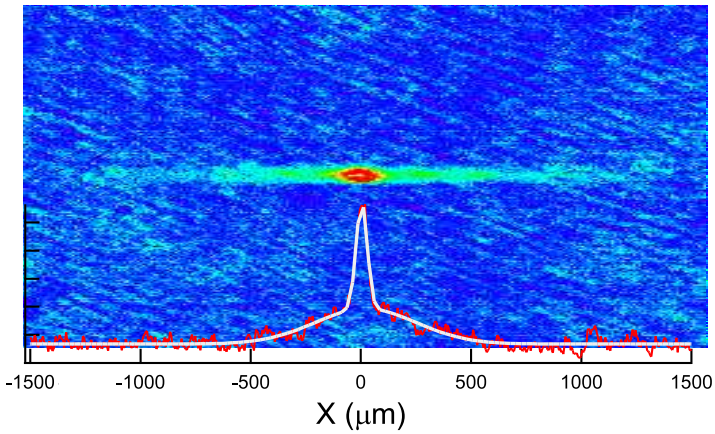

Figure 5.9: Typical image of a cloud after expansion in a shaken optical lattice. The profile was fitted by a double gaussian fit. The time of expansion was $t_{exp} = 150\,\text{ms}$, the lattice $V_0/E_{rec} = 6$ deep, the shaking frequency $\omega/2\pi = 1\,\text{KHz}$ and $K_0 = 1.5$.

5.2.4 Excitation of the sample

The physical quantity that was observed in all the *in situ* measurements was the width of the condensate σ_{long}. As stated previously, when the lattice was not shaken, σ_{long} was measured by a single gaussian fit of the cloud profile. However, when the lattice was shaken, the central peak in the atom distribution was surrounded by a broader pedestal (see Fig.(5.9)). The fraction of atoms in the pedestal increased when the frequency of the shaking was increased. For frequencies above a certain value, depending on the lattice depth, e.g. around 4 KHz at $V_0/E_{rec} = 9$ as shown in figure (5.8), the central peak was strongly suppressed, and a single gaussian fit measured mainly the pedestal distribution. This effect emerged in the distribution as a sudden rise in the cloud width. In order to verify that the atoms distributed in the pedestal were in the excited bands of the condensate, we performed a separate experiment. After the usual experimental sequence, we applied a force that allowed to separate the atoms in the fundamental band N_{fond} from the atoms in the excited bands N_{ecc}. This was possible because the force was such that only the atoms in the fundamental band were dragged by the lattice, while the atoms in the excited bands tunneled to the continuum. We tested this technique by performing a measurement analogous to the ones described in the previous chapter, by loading the sample in the fundamental or in the first excited band of the unshaken lattice and then accelerating it. Once this technique was tested, we measured the fraction of atoms in the excited band at different values of the shaking frequency ω.

It can be noted from figures (5.8, 5.10) that apart from high and low fre-

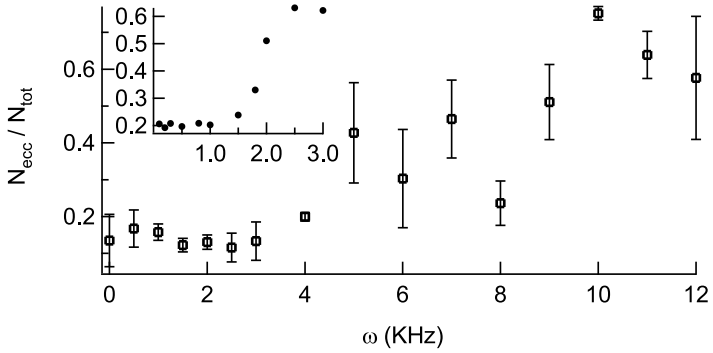

Figure 5.10: Measurement of the excited fraction of atoms versus the shaking frequency ω. For the empty squares the lattice depth was $V_0/E_{rec} = 9$ and the force $F_0 = 2.92$. The filled circles in the inset are the data for the same measurement in a $V_0/E_{rec} = 5$ deep lattice, for which $F_0 = 1.86$. In both cases the lattice was shaken for 50 ms before being accelerated.

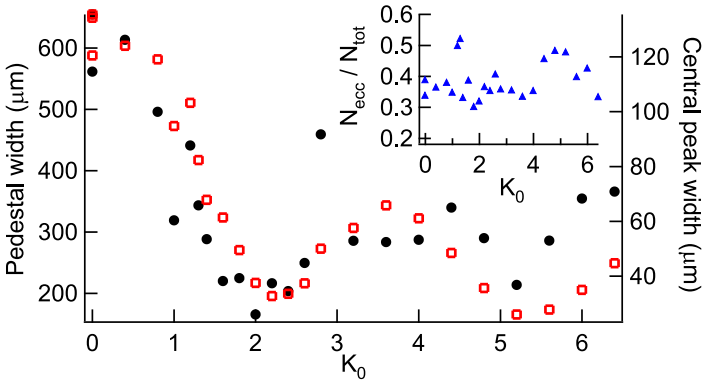

Figure 5.11: Measurement of the cloud width after 200 ms of expansion in a shaken lattice with $\omega/2\pi = 80$ Hz. The cloud width is estimated by a double gaussian fit. The larger width (pedestal distribution) is plotted with filled circles, while the narrower (central peak distribution) is plotted with empty squares. The inset is the measurement of the excited fraction of atoms for the same set of data.

quency regions where the behavior of the sample cannot be easily interpreted, there is a large *plateau* of frequencies for which excitations are negligible and the conditions imposed by theory are fulfilled. Apart from the measurements presented in this section and in the previous one, all the other measurements reported in this thesis were done by shaking the lattice at frequencies within this *plateau* region.

Once we were able to interpret the pedestal distribution as being due to atoms in the excited bands, we observed their behavior when the shaking

amplitude was varied. This results in a measurement analogous to (5.6) which is reported in figure (5.11). It can be noted that, apart from a stronger scattering of the experimental data, the behavior of the width is similar to that of (5.6). We conclude from this that the frequency modulation of the lattice also affects the interwell tunneling in the excited bands, and $|J_{eff}/J|$ in the excited bands could be described by the same Bessel function $\mathcal{J}_0$.

5.3 Time of flight measurements

The *in situ* measurements shown in the previous paragraphs demonstrated that the tunneling in a shaken lattice follows the relation (5.12), as predicted by theory. However, so far we have not addressed the problem of whether the lattice shaking affects the phase coherence of the condensate. This can be measured by observing the interference pattern of the sample in momentum space. The experimental procedure for this kind of measurements was the same as for the *in situ* measurements until the condensate was loaded into the optical lattice. At this point, the trapping frequencies were not varied anymore, i.e., the sample was *not* allowed to expand, and the lattice was shaken for a time t_{shake}. The shaking was switched on abruptly. At the end of this stage, the lattice was accelerated for $2.5\,\tau_B \sim 1\,\text{ms}$. The acceleration was chosen in order to separate the atoms in the fundamental band from the atoms in the excited bands, and ended at the band edge, i.e. at $|q| = \hbar k_L$. At the end of the acceleration the atoms were released both from the dipolar trap and the optical lattice, and they were allowed to expand and fall in free space for $t_{tof} \simeq 20\,\text{ms}$. The density profile of a typical image taken is shown in Fig.(5.12). The interference pattern of a condensate, i.e., for a coherent sample, was composed of two peaks, belonging to classes of velocity separated by $2v_{rec}$. The phase coherence of the condensate was characterized by the visibility $\mathcal{V}$ of the interference pattern, that was defined as:

$$\mathcal{V} = \frac{h_{max} - h_{min}}{h_{max} + h_{min}} \tag{5.26}$$

where h_{max} is the mean value of the condensate density at the position of the two interference peaks, and h_{min} is the mean condensate density in a region of width equal to 1/4 of the peak separation and centered around the halfway point between the two peaks (see Fig.(5.12)). For a phase coherent condensate one expects $\mathcal{V} \sim 1$, while for a dephased sample $\mathcal{V} \sim 0$.

In a first experiment, we measured the visibility (5.26) as a function of time for fixed values of the shaking amplitude K_0. Fig.(5.13) shows one of these measurements for $K_0 = 2.2$. The coherence of the sample was preserved for several tens of ms for $K_0 \leq 2.2$, while the tunneling was suppressed up to

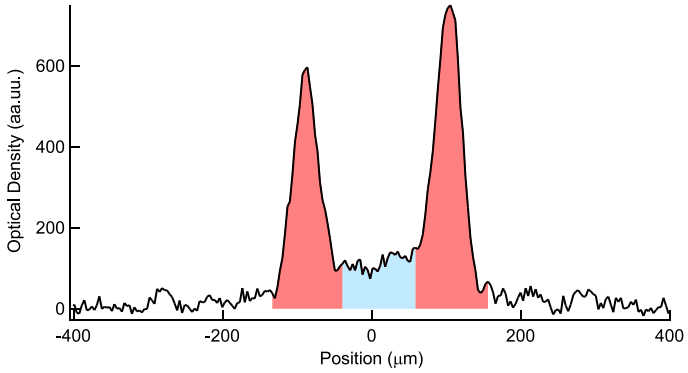

Figure 5.12: Density profile of the interference pattern created by a condensate released from the fundamental band edge, i.e. $|q| = \hbar k_L$. The visibility of the pattern is calculated using the formula (5.26), where h_{max} and h_{max} are the mean optical densities of the region highlighted in red and blue respectively.

a factor ~ 10. The experimental data for each value of K_0 were fitted with an exponential function, and the resulting characteristic times τ_{deph} of the exponential decays were extracted. The results for the extracted τ_{deph} are

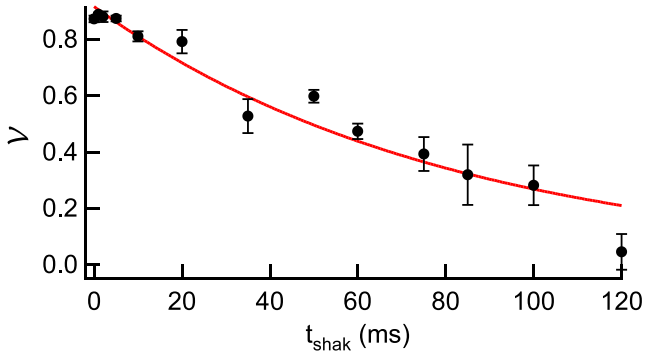

Figure 5.13: Measurement of the visibility $\mathcal{V}$ as a function of the time during which the lattice was shaken t_{shake}. The amplitude of the shaking was $K_0 = 2.2$. The solid line is an exponential fit with the offset fixed to zero.

plotted in Fig. (5.14) against K_0. A clear dip emerged for $K_0 \sim 2.4$, i.e., in proximity of the first zero of the Bessel function $\mathcal{J}_0$, for which the tunneling is strongly suppressed. When this was the case the effective tunneling was $J_{eff}/h \leq 10\,\text{Hz}$, i.e., of the same order of magnitude as in this regime the on-site interaction potential $U/h \sim 50\,\text{Hz}$. This loss of visibility can be explained as being due to the independent evolution of the local phases in distinct lattice sites [54, 80, 98].

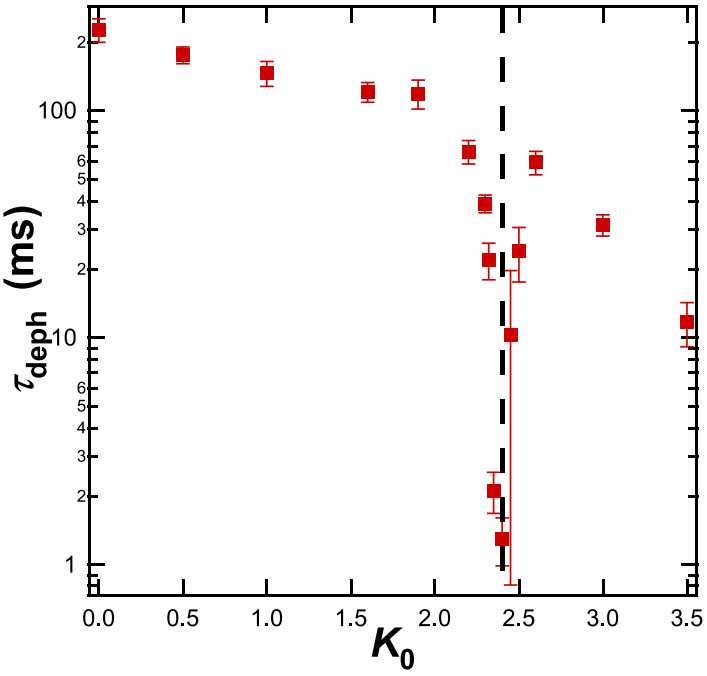

Figure 5.14: Measurement of the dephasing time τ_{deph} as a function of K_0. The figure reports the characteristic times τ_{deph} measured for different values of K_0. A clear dip is present at $K_0 = 2.4$, whose position is highlighted by the dashed line. The measurement was taken in a lattice with $V_0/E_{rec} = 9$ and with a shaking frequency $\omega = 2\pi \times 3\,\mathrm{KHz}$.

In fact for those values of K_0 the tunneling is almost completely suppressed, and the phase evolution of the wavepacket at each single site was mostly due to the on-site interactions. We checked that the on-site interaction was not affected by the lattice shaking by measuring the number of atoms in the side peaks of the interference pattern of the condensate released from the lattice at $q = 0$. In fact, the population of these side peaks depends on the width of the on-site wavefunctions and hence on the interaction U.

Finally, we explored how the phase coherence depended on the shaking frequency. This experiment was performed by measuring the characteristic time τ_{deph} of the phase coherence decay for $K_0 = 2.2$ for different values of the shaking frequency ω. This measurement is reported in Fig. (5.15). In the *in situ* experiment we observed that the suppression of tunneling was efficient until $h\omega/J \simeq 1$. However, now we observed that in order to preserve the phase coherence during the shaking much larger shaking frequencies are needed. In fact we found the optimal lattice frequency to be $h\omega/J \simeq 30$.

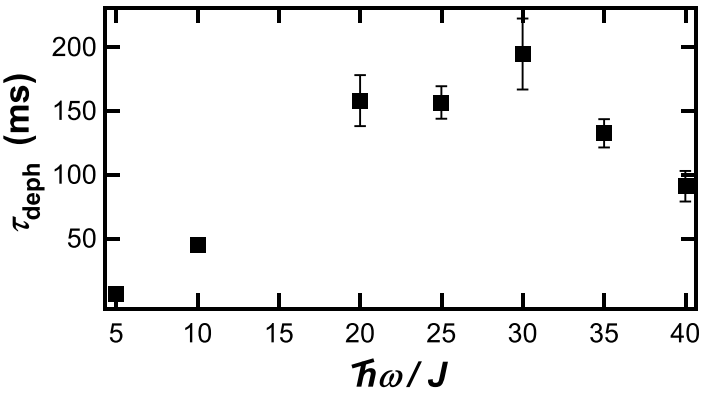

Figure 5.15: Measurement of the dephasing time τ_{deph} as a function of the shaking frequency ω. The lattice depth was $V_0/E_{rec} = 9$ and the shaking amplitude was fixed to $K_0 = 2.2$.

5.3.1 The phase inversion

In the experiment reported in Fig. (5.14) the evolution of the phase coherence was measured for K_0 varying in the range $[0, 3.5]$. However, within this range the evolution of the interference pattern was substantially different for $K_0 < 2.4$ and $K_0 > 2.4$. For $K_0 < 2.4$, the visibility decayed as shown in Fig. (5.13). For $K_0 > 2.4$, we observed an additional "shift" of the interference pattern. This emerged as a shift of $\hbar k_L$ in the plane wave decomposition of the wavefunction of the condensate when this is released from the lattice. This effect is reported in Fig.(5.16), where the images of the condensate taken at different times are shown. During the first ~ 5 ms of shaking the interference pattern evolved from the usual band edge pattern to the one experienced by atoms at the center of the fundamental band. This was confirmed by increasing the final acceleration time by $0.5\tau_B$, for which the band edge interference pattern was recovered but displaced by $\hbar k_L$ in momentum space. Then for longer values of t_{shake} the usual exponential decay of the pattern visibility was observed, and no other classes of velocity were populated.

This effect can be explained by considering that for $2.4 < K_0 < 5.5$ the zero-th order Bessel function is negative. Therefore, the effective tunneling J_{eff} becomes negative. A consequence of this change of sign is that the energy bands invert their shape: the minima of the fundamental band are now at $q = \pm\hbar k_L$, while for $q = 0$ the energy has a maximum. This effect, which can be also interpreted as a change of the sign of the effective mass m^*, causes a displacement of the interference pattern, as was observed experimentally. Thus, this measurement demonstrated that by shaking the lattice, the interesting regime of a negative tunneling can be explored.

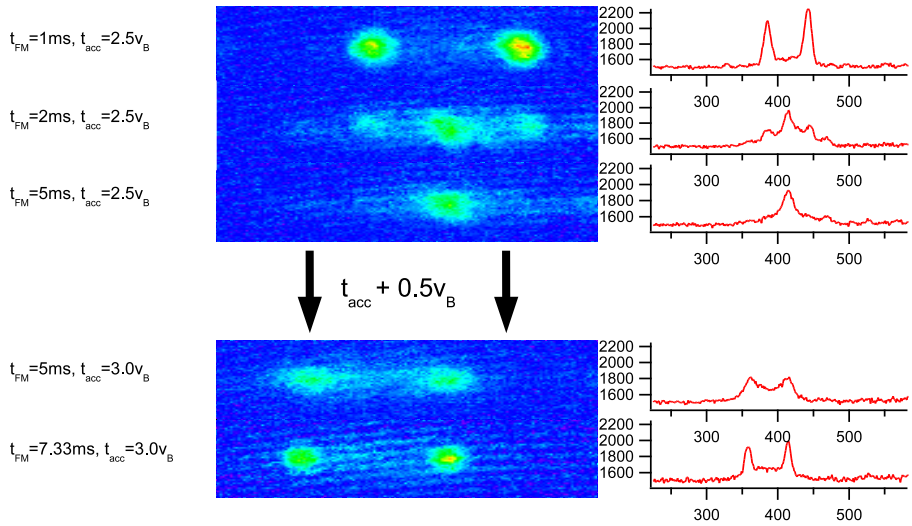

Figure 5.16: Observation of the inversion of the interference pattern. This effect emerged when the effective tunneling became negative. The lattice depth was $V_0/E_{rec} = 9$, and $\omega = 2\pi \times 3\,\mathrm{KHz}$, $K_0 = 4$.

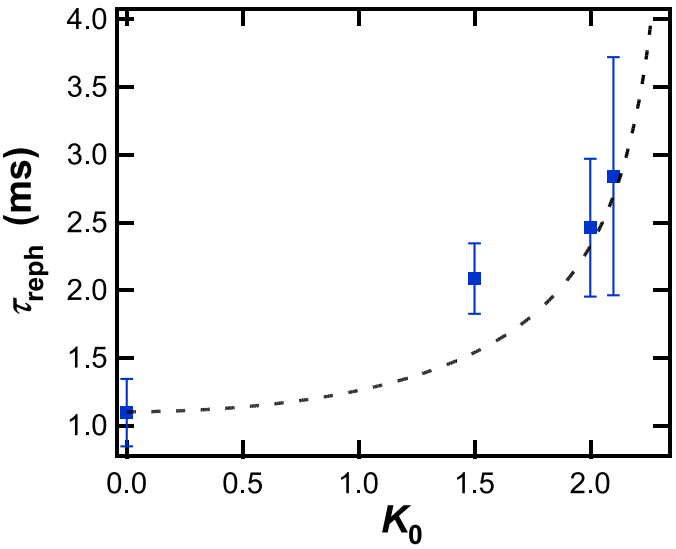

Figure 5.17: Re-phasing of the condensate. The lattice was initially shaken for 5 ms at $K_0 = 2.4$, and then allowed to evolve at a lower value of K_0. The lattice depth in the experiment was $V_0/E_{rec} = 9$, and the shaking frequency $\omega = 2\pi \times 3\,\mathrm{KHz}$. The dotted line is the theoretical prediction in a two-well model.

5.3.2 Re-phasing of the sample

In order to further confirm the phase coherence of the condensate in a shaken lattice, we performed an experiment in which the phase coherence was re-established. In this experiment the lattice was initially shaken with amplitude $K_0 = 2.4$ for 5 ms. After this time the phase coherence was completely lost. Then, the shaking amplitude was suddenly changed to a smaller value of K_0, and we observed the time evolution of the visibility. This was re-established exponentially in time. We measured the characteristic time τ_{reph} of this evolution for different values of K_0. Fig. (5.17) shows the result of this experiment. The phase coherence was re-established faster for smaller values of K_0, i.e., for higher tunneling rate J_{eff}. This behavior can be explained with an intuitive argument. The phase coherence and hence the speed of the re-phasing depends on the on-site interactions U and on the phase coupling between lattice sites that is provided by the tunneling J_{eff}. As we stated previously, the on-site interaction U was not affected by the lattice shaking. Thus, when the tunneling is suppressed, i.e., when the lattice is shaken at $K_0 = 2.4$, each site evolves independently. When the tunneling is allowed again, the phase coherence is re-established faster for higher values of the tunneling rate. In Fig. (5.17) the experimental data are compared with the inverse of the Josephson frequency as a function of the effective tunneling: $\omega_{Josephson} \propto J_{eff}^{-1/2}$, as predicted by a two-well modes [99].

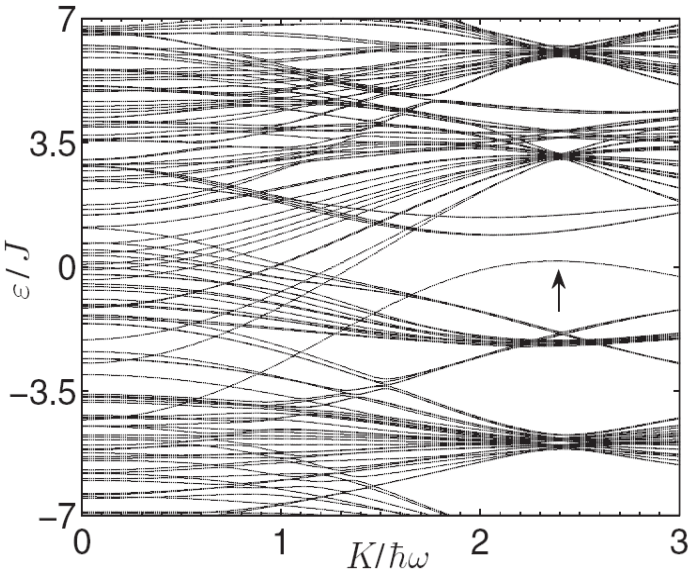

Figure 5.18: Spectrum of the quasienergies ϵ_n within the first Brillouin zone for a system of $N = 5$ atoms in $M = 5$ wells of a $V_0/E_{rec} = 3$ deep lattice. The arrow marks the ground state. From Ref. [82].

5.3.3 Adiabaticity in the shaken lattice

In the first section of this chapter the theoretical problem of a BEC in a strongly driven optical lattice has been introduced. By use of the Floquet theory, it was found that this problem can be reduced to the case of a BEC in an optical lattice at rest but with the tunneling parameter J substituted by an effective J_{eff}. However, the problem of the time evolution of an initial wavepacket has not been addressed in detail so far.

Within the Floquet theory, the eigenvalue problem (5.6) was defined in the $\mathcal{R} \otimes \mathcal{T}$ Hilbert space, which is defined as the extension of the space of the square integrable functions on configuration space $\mathcal{R}$ to the space $\mathcal{T}$ of the time periodic functions of period $T = 2\pi/\omega$. The eigenvalues of Eq.(5.6) are the quasienergies $\epsilon_{n,m}$, defined in a Brillouin-zone like spectrum of width $\hbar\omega$. Their corresponding eigenstates $|u_n(t)\rangle$ are the so-called Floquet modes, forming a basis in the $\mathcal{R} \otimes \mathcal{T}$ space. A general property of the Floquet theory is that the Floquet modes in the first Brillouin zone and for a fixed time t form a basis in the $\mathcal{R}$ space.

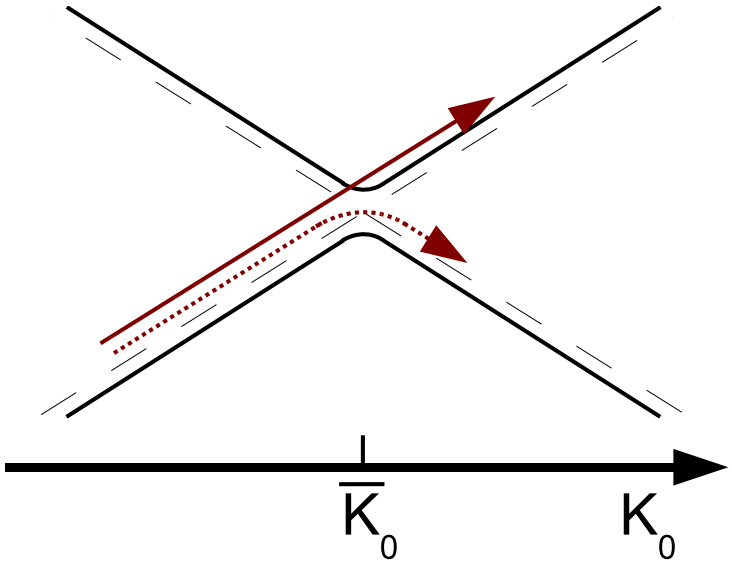

Figure 5.19: Different trajectories that the system can experience when passing through an avoided energy crossing. The solid arrow corresponds to the diabatic trajectory, i.e., the probability of tunneling through the energy gap is $r = 1$. The dotted arrow corresponds to the adiabatic trajectory, i.e., the probability of tunneling through the energy gap is $r = 0$, and the system follows the lowest energy level.

In the case of N atoms loaded into an optical lattice of M sites, the basis

in $\mathcal{R}$ is formed by the states:

$$|\{n_j\}\rangle = |n_1\rangle \otimes |n_2\rangle \otimes, ..., |n_M\rangle, \qquad \sum_{j=1}^{M} n_j = N \tag{5.27}$$

where $|n_j\rangle$ is the Fock state of n_j atoms in the j-th site. The basis is composed of all the possible combinations of atom numbers in the lattice sites. The problem of the evolution in time of a system prepared initially in one of these states is a very hard task, and a full description of the problem can be found in Ref. [82]. Here we are interested in showing qualitatively how this evolution affects the system. Fig. (5.18) shows, within the first Brillouin zone, the quasienergies ϵ_n for all the states (5.27) of a system of $N = 5$ atoms in $M = 5$ wells as a function of the shaking parameter K_0. If this system is initially prepared in its ground state at $K_0 = 0$ and then K_0 is increased to some value $K_0^{(max)}$, during its trajectory the energy level experiences many energy avoided crossings with other levels. For each of these crossings, the Landau-Zener theory predicts that there is a probability of tunneling r through the energy gap depending on how fast K_0 has changed. In particular, three regimes can be considered (see Fig.(5.19)): the system follows an adiabatic trajectory, i.e., no tunneling occurs ($r = 0$); the system follows a diabatic trajectory, i.e., the tunneling probability is $r = 1$; the system follows a trajectory that is neither adiabatic nor adiabatic, i.e. $0 < r < 1$. Referring to Fig. (5.19), in the adiabatic trajectory the system follows the lower energy state, that is not the same for $K_0 \ll \bar{K}_0$ and $K_0 \gg \bar{K}_0$, i.e., the state of the system in the $\mathcal{R}$ space changes passing through the crossing. On the other hand, in the diabatic trajectory the system changes energy level but it does not change its state in the $\mathcal{R}$ space. Finally, when the probability of tunneling is $0 < r < 1$, the state of the system becomes a coherent superposition of the two crossing states in $\mathcal{R}$. In this particular case the evolution of the system is not reversible, i.e., if the parameter K_0 is changed back to its initial value the initial state cannot be recovered. In Fig.(5.18) the energy level marked by the arrow is the ground state at $K_0 = 2.4$. This is the evolution of the ground state of the system if it follows only diabatic trajectories for all the energy crossings experienced in its evolution in parameter space. This level is well separated from the other energy levels, and moreover the tunneling is suppressed, because $K_0 = 2.4$.

Ref. [82] proposed to exploit the tunneling suppression in a shaken optical lattice in order to enter into the Mott Insulator phase. In this phase, first predicted for cold atoms in an optical lattice by Ref. [41], the number of atoms per lattice site is exactly determined, and can emerge if the filling of the lattice is homogeneous. The Mott insulator phase has been realized experimentally first by Ref. [35] loading the condensate in the ground state

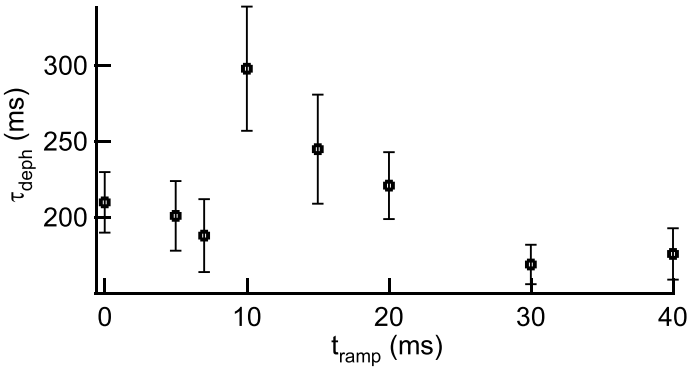

Figure 5.20: Measurement of the dephasing time τ_{deph} as a function of the ramping time t_{ramp} of the shaking parameter K_0. The lattice depth was $V_0/E_{rec} = 9$, the shaking frequency $\omega = 2\pi \times 3\,\mathrm{KHz}$, and the shaking parameter was ramped up to $K_0^{(max)} = 2.2$.

of a 3D optical lattice and then increasing adiabatically the lattice depth. Contrary to the spectrum of Fig. (5.21) of a shaken lattice, in the experiment reported by Ref. [35] the ground state does not experience any energy crossing with other levels when the lattice depth is increased. Ref. [82] found some experimental conditions in order to go from the superfluid into the Mott insulator phase by strongly driving a shallow lattice. We were not able to test these conditions in our experiment, because the mean number of atoms per lattice site was of order of several hundreds, making the transition unfeasible in our one-dimensional setup [42].

However, we performed two experiments in order to observe how the phase coherence was affected by the crossings in the energy spectrum. In a first experiment, we measured the characteristic time for the loss of phase coherence τ_{deph} in a shaken lattice whose parameter K_0 was ramped up linearly in a time t_{ramp} to a stationary value $K_0^{(max)}$. Fig. (5.20) shows the measured τ_{deph} for different values of t_{ramp}. No clear evidence of a dependence of τ_{deph} on t_{ramp} was observed.

In a second experiment, the lattice was shaken during all the experiment, i.e., both during its loading (that was $t_{lattice}$ long) and the shaking time t_{shake}. The shaking parameter K_0 was not varied during the experiment. The parameter in this case is the lattice depth. Fig.(5.21) shows the energy spectrum in parameter space for $K_0 = 1.5$. As in the case of Fig. (5.18), the system experiences many energy crossings when the parameter is varied. In the measurement reported in Fig.(5.22), the characteristic time for the loss of coherence τ_{deph} was measured for different values of the lattice ramp time $t_{lattice}$. In the case of an unshaken lattice, one expects that the coherence

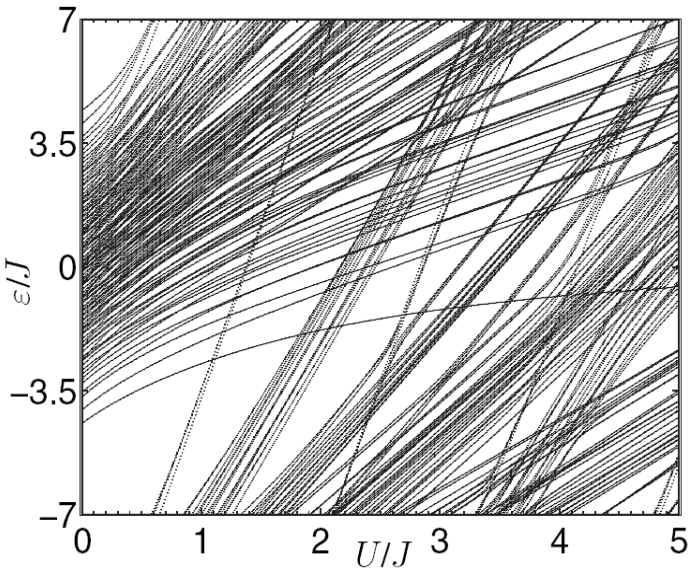

Figure 5.21: Spectrum of the quasienergies ϵ_n within the first Brillouin zone for a system of $N = 5$ atoms in $M = 5$ wells in a lattice shaken with $K_0 = 1.5$. From Ref. [82].

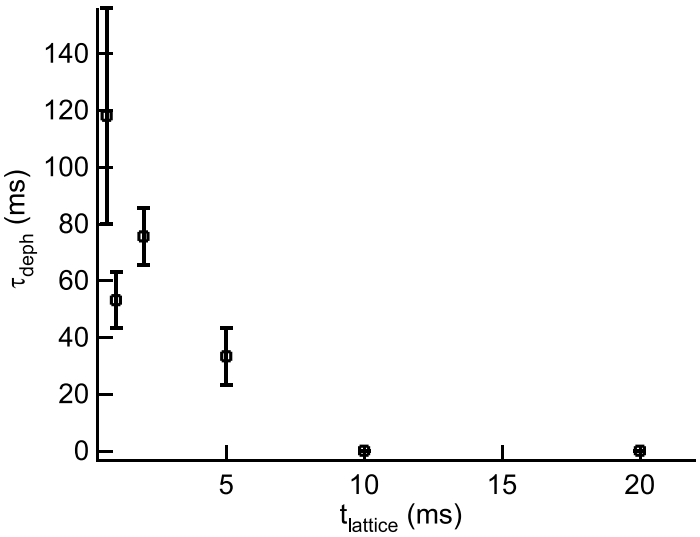

Figure 5.22: Measurement of the dephasing time τ_{deph} as a function of the ramping time $t_{lattice}$ of the lattice. The final lattice depth was $V_0/E_{rec} = 9$, the lattice shaking had frequency $\omega = 2\pi \times 3\,\mathrm{KHz}$ with $K_0 = 2.2$.

of the BEC is preserved in an adiabatic loading. Therefore, the longer the ramping time, the longer τ_{deph} should be. However, in a shaken lattice we observed a different behavior. As shown in Fig. (5.22), phase coherence was

preserved for longer time when the lattice was loaded in a shorter time. We interpreted this as an evidence of the effects of the crossings experienced by the energy levels while the lattice was loaded, i.e., while moving through one of the trajectories plotted in Fig. (5.21).

In fact, when the lattice was loaded in a shorter time, the state of the system passed with a higher velocity through the energy crossings and hence the probability of following a diabatic trajectory was higher.

Chapter 6

Photon-assisted tunneling

In the experiment described in the previous chapter the control of tunneling in an optical lattice was realized by shaking the lattice. In particular, for appropriate values of the shaking amplitude and frequency, the tunneling was strongly suppressed. In the experiment described in this chapter we first realize the suppression of tunneling in an optical lattice by use of a constant force, i.e., a linear potential, that shifts the energy levels of neighboring sites. Then, we partially restore the tunneling by shaking the lattice at appropriate frequency and amplitude. This experiment is the analogue of the *photon-assisted tunneling* observed in several solid state experiments [100, 101, 102].

6.1 Photon-assisted tunneling in an optical lattice

The physical system of a Bose-Einstein condensate loaded into an optical lattice is characterized by two parameters: the on-site interaction energy U and the inter-site tunneling energy J. The latter describes a tunneling event, and its value depends on the overlap of the single site wave functions at different lattice sites. In particular, J is maximum when all the single well energy levels are degenerate. If an additional potential (such as an external force) creates an energy shift between the lattice sites, the degeneracy is lifted and the inter-well tunneling is strongly suppressed. As stated when the resonantly enhanced tunneling was introduced, the eigenstates in this case are the Wannier-Stark states, which are localized at the lattice sites.

Photon-assisted tunneling occurs when one or more photons couple the shifted energy levels, partially restoring the tunneling. This phenomenon is very general, and it can be realized in physical systems composed of coupled energy wells whose levels are tuned out of degeneracy by an external potential. In fact, photon-assisted tunneling was first observed in supercon-

ducting junctions [100], and more recently in semiconductor superlattices [91, 102, 103] and quantum dots [101, 104]. In these systems the frequency that coupled the energy levels varied from tens of GHz to THz. In the case of an optical lattice the maximum shift between the energy levels must be of the order of the lattice depth, i.e., up to tens of KHz, in order to avoid inter-band tunneling to the continuum. The role of the photon can be played by a shaking of the lattice, which leads to sidebands to the frequency ω_L of the lattice lasers. The energy shift, on the other hand, can be provided by an external force F, that creates a linear potential along the lattice. In this case the full Hamiltonian of the system reads:

$$\begin{aligned} H = &- J \sum_{\langle i,j \rangle} \left(a_i^\dagger a_j + a_j^\dagger a_i \right) + \frac{U}{2} \sum_j n_j \left(n_j - 1 \right) + \\ &+ \Delta E \sum_j j n_j + K \cos\left(\omega t\right) \sum_j j n_j \end{aligned} \tag{6.1}$$

where:

- a_i, $a_i^\dagger$ are the bosonic annihilation and creation operators on site i,
- $n_i = a_i^\dagger a_i$ is the number operator on site i,
- $\Delta E = F d_L$ is the difference in energy between neighboring sites caused by the force F,
- K and ω are the amplitude and the frequency of the shaking.

In the Hamiltonian (6.1) the first row corresponds to the Bose-Hubbard Hamiltonian, while the two contributions in the second row are the linear potential and the shaking term, respectively. A schematic overview of the quantities involved is shown in Fig. (6.1).

Once the lattice depth V_0 and the force F are fixed, photon assisted tunneling is characterized by the last two free parameters in the Hamiltonian (6.1): the shaking amplitude K and the shaking frequency ω. The latter must be such that the energy provided by the shaking fills in the gap of the energy shift between neighboring sites. The resonance condition is thus:

$$n\hbar\omega = F d_L \tag{6.2}$$

where the integer n is the order of the photon-assisted resonance and describes how many "photons" are needed to bridge the gap $F d_L$. The dependence of the photon assisted tunneling on K can be calculated by solving the eigenvalue problem of the Hamiltonian (6.1) within the Floquet theory. The calculations are equivalent to the ones introduced in the previous chapter, where the effect of shaking the lattice was to destroy the tunneling. It

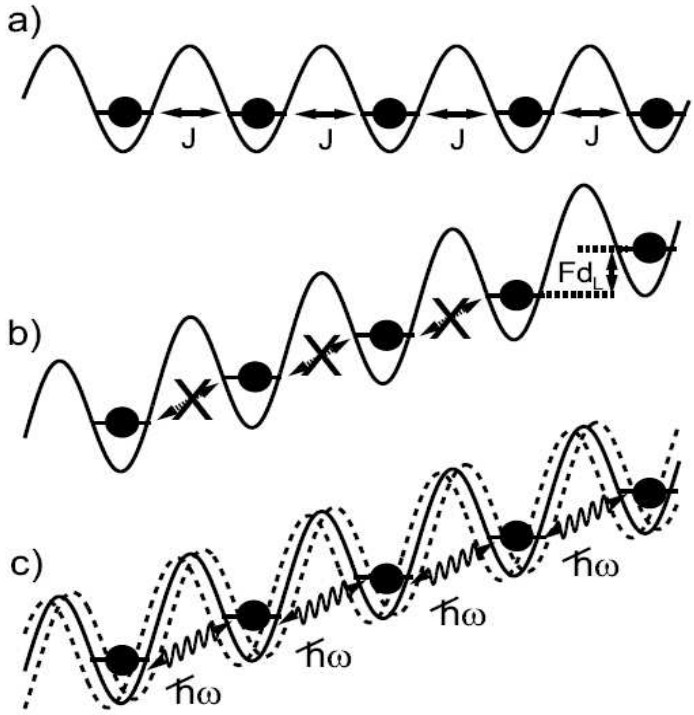

Figure 6.1: Sketch of the photon assisted tunneling in an optical lattice. a) The atoms in an optical lattice can move from site to site by tunneling. b) The inter-well tunneling is destroyed by the application of an external force F that de-couples the energy levels. c) The tunneling is partially restored by shaking the lattice at an appropriate frequency ω.

can be demonstrated [105] that if $Fd_L > J$, i.e., if the energy shift is larger than the width of the fundamental band of the unperturbed lattice, and the resonance condition (6.2) holds, then the Hamiltonian (6.1) reduces to the Bose-Hubbard Hamiltonian but with the tunneling energy J substituted by an effective one such that

$$|J_{eff}/J| = |\mathcal{J}_n(K_0)|, \tag{6.3}$$

where $\mathcal{J}_n$ is the n-th order Bessel function, n is the order of the resonance that appears in Eq.(6.2), and $K_0 = K/(\hbar\omega)$.

6.2 Experimental technique

In order to demonstrate the experimental realization of photon assisted tunneling, the physical quantity that had to be measured was the inter-well tunneling. This same quantity was measured in the "control of tunneling"

experiment described in the previous chapter. Therefore, the experimental sequence was very similar to the one followed in that experiment:

- After reaching condensation, the trap frequencies were adiabatically varied in 50 ms to a cigar shaped trap of frequencies $\nu_{rad} = 80\,\mathrm{Hz}$, $\nu_{long} = 20\,\mathrm{Hz}$
- In the longitudinal direction a one dimensional optical lattice was created by ramping up linearly in 50 ms two independent, counterpropagating laser beams of the same wavelength $\lambda = 852.2\,\mathrm{nm}$. The atoms were loaded into the fundamental band of the lattice.
- The dipolar beam responsible for the longitudinal confinement of the atoms was switched off suddenly. The dipolar frequency in this direction was now $\nu_{long} \sim 5\mathrm{Hz}$, caused mainly by the focusing of the dipolar beam. The duration of this phase t_{exp} was such that the effects of the longitudinal trapping force were negligible, and the atoms were free to expand along the lattice. This condition was experimentally tested by imposing t_{exp} such that the size of the cloud expanded linearly.
- After an expansion time t_{exp} along the lattice the atoms were released both from the lattice and the dipolar trap, and then imaged after a time of flight of 0.3 ms. This very short time assured that the effects of the expansion of the cloud in free space were negligible. The measurement was hence *in situ*, and the spatial width of the cloud was extracted by fitting its profile with a single gaussian.

The force and the sinusoidal driving were applied to the system during the expansion time t_{exp}. They were realized using the same technique introduced in the previous chapters.

The parameters that characterized the lattice shaking are the same as those introduced in the "control of tunneling" experiment: the frequency of the modulation ω and the dimensionless parameter $K_0 = K/\hbar\omega$.

In other experiments described in this thesis, the force exerted on the atoms was realized by increasing the detuning $\Delta\nu$ between the lattice beams linearly in time. In the experiment described here, the expansion time was up to 400ms, while the acceleration varied in the range 0-4ms^{-2}. For these parameters, two problems did not allow us to realize the force by ramping linearly in time the detuning $\Delta\nu$. First, the atoms would have been displaced by up to 32cm, which is roughly two orders of magnitude larger than the field of view of the CCD camera. Second, the longitudinal trap of frequency $\nu_{long} \simeq 5\,\mathrm{Hz}$ would have created a non-negligible restoring force $F_{restore}$ to the center of the dipole trap. In fact, this force had to be much smaller than the force created by the lattice acceleration $F \gg F_{restore} = m\omega_{long}^2\Delta x$,

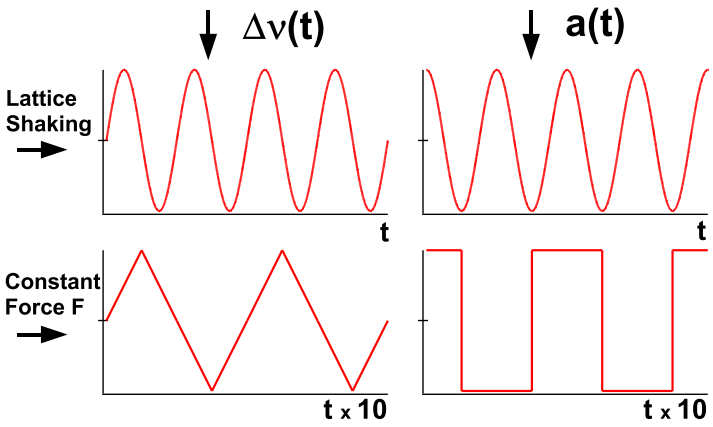

Figure 6.2: Scheme of the frequency variations involved in the experiment. The force F and the frequency modulation FM are created by varying the detuning between the two lattice beams $\Delta\nu(t)$. The corresponding acceleration $a(t)$ is plotted in the right column. The time scale for the rocking force is expanded by a factor of ten.

because the energy shift between the lattice sites had to be fixed during the experiment. We decided hence to keep the displacement Δx of the atoms below $100\,\mu$m, so that the restoring acceleration was $a_{restore} < 0.1\,\mathrm{ms}^{-2} \ll F/m$. In order to have no limitations on the expansion time t_{exp}, we applied the force with a rectangular profile, i.e. alternating in time a force F and its inverse $-F$. This force "rocked" the lattice back and forth, creating a piecewise static potential shift between neighboring lattice sites of Fd_L. The frequency of this "rocking" force ω_{rock} was always chosen to be much less than the shaking frequency: $\omega_{rock} \ll \omega$, in order to have a clear separation of the frequencies in the experiment.

In order to measure the tunneling, we used the same technique as in the "control of tunneling" experiment. Therefore we chose the time t_{exp} such that the expansion of the condensate along the lattice was approximately linear in time. The ratio between the expansion rates in the case of an unperturbed ($F = 0$, $K = 0$) and a perturbed ($F \neq 0$, $K \neq 0$) lattice corresponded to the ratio between the tunneling in these two cases: $|J_{eff}/J|$. The experimental verification of this statement and the measurement of the linear expansion of the cloud are not reported here because they are analogous to the one reported in the previous chapter.

6.3 Destruction of tunneling in a "rocked" lattice

The first experiment that was performed was the observation of the destruction of tunneling when the force was applied. In this experiment only the rocking force was implemented, and the lattice was not shaken. The tunneling was expected to be strongly suppressed when the force was such that the energy shift between neighboring lattice sites was larger than the fundamental level width. This corresponds in a first approximation to the width of the fundamental band of the lattice at rest, i.e., the tunneling J. A measurement of the tunneling for different values of the force is reported in Fig. (6.3). There the force on the horizontal axis is expressed in units of the tunneling energy J. As expected, when the force approached the tunneling energy $Fd_L/J \simeq 1$ the tunneling was strongly suppressed. In fact, for $Fd_L/J > 1$ no expansion of the cloud along the lattice was observed within the experimental error. In the measurement reported in Fig. (6.3) the lattice depth was $V_0/E_{rec} = 5$, the rocking frequency $\omega_{rock} = 2\pi \times 30\,\mathrm{Hz}$ and the expansion time $t_{exp} = 100\,\mathrm{ms}$.

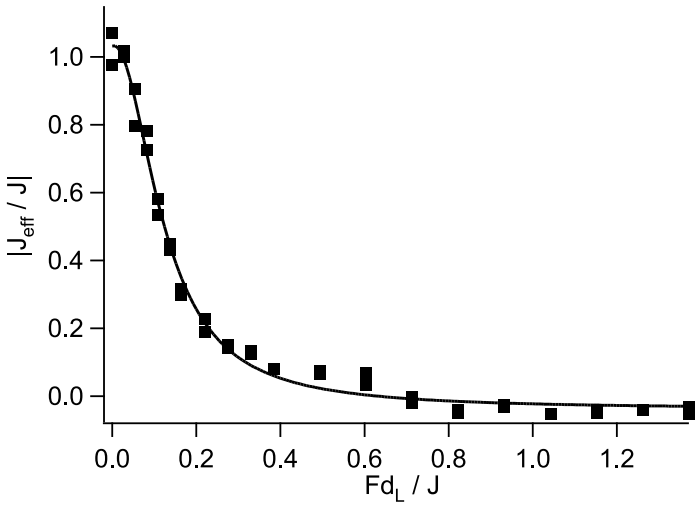

Figure 6.3: Suppression of tunneling in an optical lattice subject to a force F. When $Fd_L \approx J$ the tunneling is strongly suppressed. The solid line is a Lorentzian fit with a half-maximum half-width of 0.13.

A similar effect was observed by ref. [106], where the tunneling suppression was observed in a 3D optical lattice with one atom per lattice site. As well as in ref. [106] we fit the experimental data in Fig. (6.3) with a Lorentzian function (solid line). The half-width half-maximum we measured was 0.13.

6.4 Photon-assisted tunneling

Photon assisted tunneling occurs when the rocked lattice is shaken at a frequency that matches the energy shift between lattice sites created by the force, i.e. when the resonance condition (6.2) holds. The first experiment performed was the observation of the resonance of the first order: $n = 1$. Eq. (6.3) states that the effective tunneling J_{eff} in this case is proportional to the first order Bessel function $\mathcal{J}_1$. For this reason we set the frequency modulation amplitude $\Delta\nu_{max}$ to the first maximum of the $\mathcal{J}_1$ Bessel function at $K_0 = 1.8$. A measurement of the condensate width against the tunneling frequency is presented in Fig.(6.4) (filled circles). There the "rocking" force was $Fd_L/J = 1$, so that the tunneling was strongly suppressed. The lattice depth was $V_0/E_{rec} = 5$, and $J/h = 270\,\mathrm{Hz}$. A resonance in the tunneling was observed for the expected value of the frequency $\omega_{res} = 2\pi \times 270\,\mathrm{Hz}$. Apart from the resonance peak, two symmetric peaks were observed at $\pm 30\,\mathrm{Hz}$ from the resonance. These were interpreted as being due to the "rocking" frequency that created two sidebands at $\omega \pm \omega_{rock}$ in the overall frequency spectrum. This explanation was proved in a separate experiment where ω_{rock} was varied and the side peaks shifted with respect to the resonance peak as expected. The resolution limit in the measurement of the resonance position corresponded to t_{exp}^{-1}, i.e., the inverse of the expansion time during which the force and the shaking were applied. In the experiment reported in Fig. (6.4) this was $t_{exp} = 400\,\mathrm{ms}$. The measured width of the resonance peak was $\sim 3\,\mathrm{Hz}$, i.e., close to the resolution limit. It must be pointed out that for this value of t_{exp} the expansion of the cloud along the lattice was no longer linear in time. Therefore, it was not possible to measure the amplitude of the restored tunneling. However, the aim of this experiment was to test the resonance condition (6.2) by performing spectroscopy-like measurements, whose accuracy depended on the resolution in frequency. In order to increase the resolution we therefore increased the time t_{exp} to values for which the expansion was no longer linear. The amplitude of the effective tunneling was measured in a separate experiment that will be described in the following.

The same experiment has been performed to measure the second order resonance, i.e., $n = 2$. This measurement was initially done in the same conditions as for the $n = 1$ resonance, i.e., with $K_0 = 1.8$. However, Fig. (6.4) shows that at $\omega \simeq Fd_L/(2\hbar)$ and $K_0 = 1.8$ the second order resonance was not clearly observed. This was because according to Eq. (6.3) the effective tunneling J_{eff} was now proportional to the second order Bessel function $\mathcal{J}_2$. By setting the shaking amplitude close the maximum of the $\mathcal{J}_2$ Bessel function, i.e. $K_0 = 3.1$, the resonance peak clearly emerged. This measurement corresponds to the empty circles in Fig.(6.4). The resonance peak width was again $\sim 3\,\mathrm{Hz}$, and its position was $\omega_{res} = 2\pi \times 135\,\mathrm{Hz}$, as

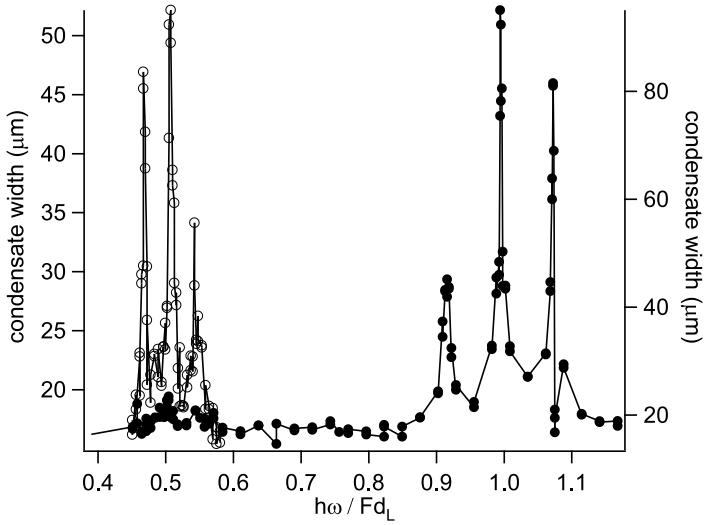

Figure 6.4: Photon-assisted tunneling resonances. The resonances were found at the expected positions, i.e., $\omega_{res} = Fd_L/(n\hbar)$ for the resonances of order $n = 1, 2$. The peaks at the sides of each resonance were due to the sidebands created in the frequency spectrum by the "rocking" frequency $\omega_{rock} = 2\pi \times 30\,\mathrm{Hz}$ of the force F. For the experimental data reported with filled circles, the amplitude of the shaking was such that $K_0 = 1.8$, i.e., close to the $\mathcal{J}_1$ maximum. In this set the $n = 1$ resonance clearly emerged, but not the $n = 2$ one. The $n = 2$ resonance was observed by setting $K_0 = 3.1$, i.e. close to the first maximum of $\mathcal{J}_2$. These data are reported in the figure with empty circles. The solid lines connect the data points as a guide to the eye.

expected. Two side peaks now emerged at a distance $\pm 15 \times 2\pi\,\mathrm{Hz}$ from the resonance peak. These peaks corresponded to a resonance condition $\hbar(2\omega \pm \omega_{rock}) = Fd_L$, so that $\omega = \omega_{res} \mp \omega_{rock}/2$. We performed the same measurement reported in Fig. (6.4) for different values of F. The position of the $n = 1$ resonance frequencies ω_{res} are plotted in Fig. (6.5) as a function of the energy shift between adjacent wells created by the force. As expected by Eq. (6.2), the resonance frequency ω_{res} varied linearly with F.

6.5 Amplitude of the photon assisted tunneling

The experiments previously described measured the dependence of photon assisted tunneling on the frequency of the shaking, finding good agreement with the theoretical prediction of Eq (6.2). The dependence of the photon assisted tunneling on the shaking amplitude predicted by Eq. (6.3) was studied

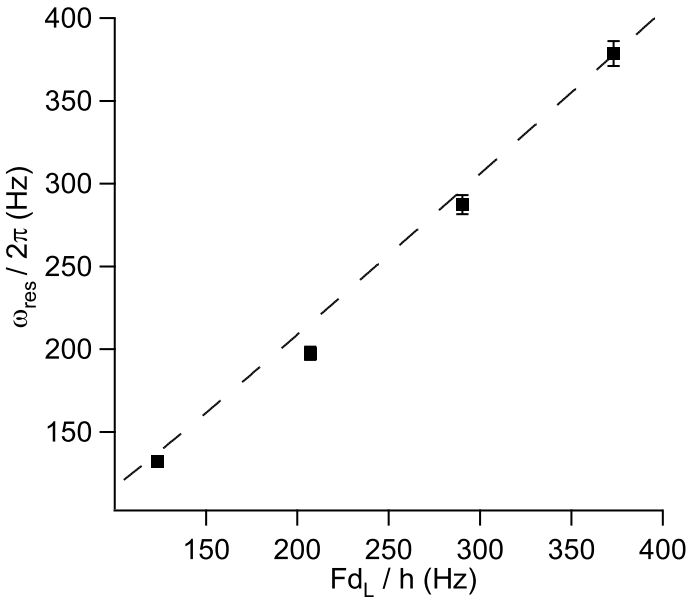

Figure 6.5: Measurement of the resonance frequencies ω_{res} for different values of the linear potential created by the force F. The dashed line is the theoretical prediction (6.2).

in an experiment in which the tunneling was measured for different amplitudes of K_0. The shaking frequency was now fixed at the center of one of the resonances measured in Fig.(6.4), i.e., $\hbar\omega/Fd_L = 1/n$ with $n = 1, 2$. The measurements of $|J_{eff}/J|$ against K_0 are reported in Fig. (6.6) for the first order resonance and in Fig. (6.7) for the second order resonance. Our first sets of experimental data are plotted there using filled squares. Both measurements were taken in a lattice of depth $V_0/E_{rec} = 5$, force $F \simeq 1.4\, Jd_L^{-1}$, and with expansion time $t_{exp} = 100\,\text{ms}$. The tunneling rate predicted by theory, i.e., $|J_{eff}/J| = |\mathcal{J}_1|$ and $|J_{eff}/J| = |\mathcal{J}_2|$ for the first and second order resonances respectively are plotted in Fig.s (6.6), (6.7) with a solid line. The measured tunneling rate agreed qualitatively with the theoretical prediction, and the maximum and the minimum values for J_{eff} were found where expected. However, there was a disagreement between theory and experiment concerning the absolute value of the effective tunneling, and a factor ~ 1.3 of difference was found between the two curves. Surprisingly, the experimental tunneling rate had a better agreement with *the square* of the expected Bessel function behavior. This is reported in Fig. (6.6), (6.7) with a dashed line. The dependence of the tunneling rate on the square of the related Bessel function is expected in the case of *sequential* tunneling [107]. Sequential tunneling occurs in systems where several energy wells are coupled, as in

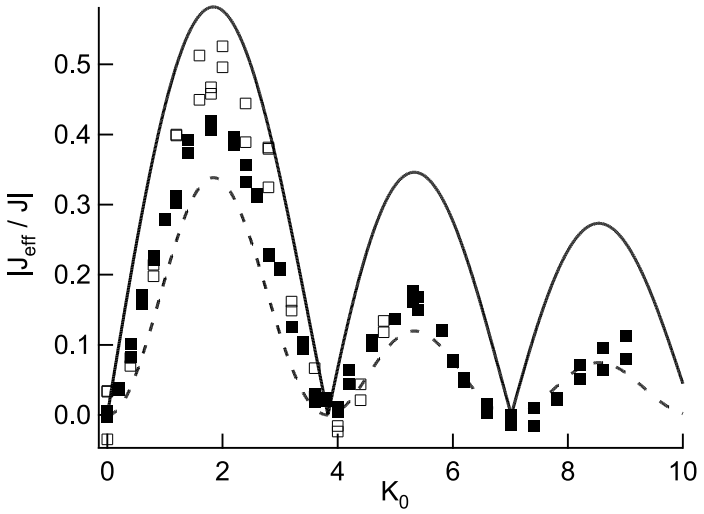

Figure 6.6: Dependence of the first order photon assisted tunneling on the shaking amplitude. The experimental data have been taken for a lattice of depth $V_0/E_{rec} = 5$, a "rocking" force of amplitude $F = 1.4J/d$ and frequency $\omega_{rock} = 2\pi \times 30\,\mathrm{Hz}$, and a shaking frequency at the first order resonance. The average number of atoms was $N \simeq 5 \cdot 10^4$ for the filled squares and $N \simeq 0.5 \cdot 10^4$ for the empty squares. The solid line is the modulus of the $\mathcal{J}_1$ Bessel function while the dashed line is its square $\mathcal{J}_1^2$.

an optical lattice, but the phase coherence is lost after each tunneling event because of some decoherence mechanism. This can be, for instance, inelastic scattering. In the case of cold atoms loaded into an optical lattice, a source of dephasing is the dynamical instability that the atoms suffer when the effective mass becomes negative [77, 78]. For atoms in the fundamental band, this corresponds to a quasimomentum q in the range $\hbar k_L/2 \lesssim |q| < \hbar k_L$ within the first Brillouin zone. In the measurements presented in Figs. (6.6), (6.7), during the "rocking" acceleration the maximum momentum reached by the atoms was $p_{max} = 6.3\,\hbar k_L$. Therefore during the experiment the atoms passed many times through unstable regions, where they spent a time $\tau_B/2$. In the measurement reported, $\tau_B \simeq 2.6\,\mathrm{ms}$, that is comparable with the time scale for which dephasing in the unstable region was observed [77, 78, 108]. In order to partially confirm that sequential tunneling might occur in our experiments, we repeated our measurements using a sample with a number of atoms that was one order of magnitude less than in the first experiment ($5 \cdot 10^3$ instead of $5 \cdot 10^4$ atoms). This allowed to decrease the nonlinearity by a factor ~ 2.5 and therefore the effects of instability. These measurements are reported with the open squares in Figs. (6.6), (6.7). Interestingly, the effective tunneling rate measured had a better agreement with the theoreti-

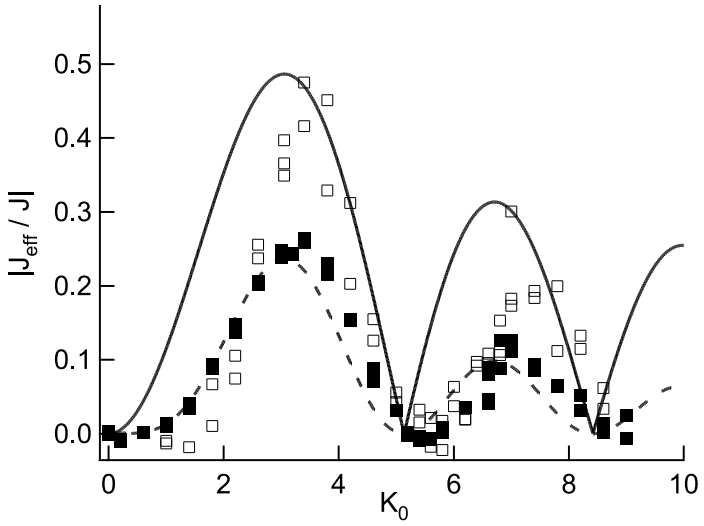

Figure 6.7: Dependence of the second order photon assisted tunneling on the shaking amplitude. The experiment has been carried out in the same experimental conditions of the experiment reported in Fig.(6.6). The average number of atoms was $N \simeq 5 \cdot 10^4$ for the filled squares and $N \simeq 0.5 \cdot 10^4$ for the empty squares. The solid line is the modulus of the $\mathcal{J}_2$ Bessel function while the dashed line is its square $\mathcal{J}_2^2$.

cal prediction for a coherent photon assisted tunneling, which supports our statement. A further confirmation of our interpretation of the disagreement between theory and experiment is given by the measurement of the control of tunneling reported in the previous chapter. There the atoms did not cross the unstable region of the energy spectrum during the lattice shaking, and the measured tunneling rate agreed with the linear Bessel function theoretical prediction. Moreover, in that experiment the sample was observed to keep its phase coherence.

Another nonlinear effect that could have been responsible for the squared Bessel function behavior of the experimental data taken with the larger number of atoms is self-trapping [109, 110]. This is a nonlinear effect that occurs when the ratio between the inter-well interaction potential and the tunneling is larger than some threshold, causing a suppression of the expansion of the atoms along the lattice. For the parameters of our experiment, the system could show self-trapping only when the tunneling was strongly suppressed, that is, for shaking amplitudes close to the Bessel functions zeros. However, the strongest deviation from the coherent photon assisted tunneling prediction were in the regions close to the Bessel function maxima. Therefore, we considered the self-trapping effects not to be responsible for the disagreement between theory and experiment. However, this effect could be studied more

in detail by tuning the scattering length, i.e., driving the system through a Feshbach resonance. In this way the interplay between sequential and coherent tunneling could be studied.

Conclusion and perspectives

The unifying theme of this thesis has been the role of quantum tunneling in a physical system of ultra-cold atoms loaded into an optical lattice. As a fundamental effect of quantum mechanics, tunneling is at the heart of many dynamical processes of atoms in a periodic potential. In the experiments described in this thesis we studied three of these processes. The results of these experiments and possible future developments are summarized in the following.

Resonantly enhanced tunneling - In this experiment the inter-band tunneling rate was measured by applying a constant force on the atoms. In a first approximation, this phenomenon can be studied by use of the Landau-Zener theory for tunneling in energy anti-crossings. A resonant enhancement of tunneling over the Landau-Zener prediction was observed when the position-dependent energy shift due to the force matched the energy gap between different energy levels. This behavior was predicted by a full theoretical analysis of the system, and the experimental data agreed with this prediction. The destruction of the tunneling resonances was observed when the atom-atom interaction was increased by changing the density of the sample. This destruction was theoretically predicted by numerical simulations. One of the limitations in our experimental investigations was given by the limited range of measurable tunneling rates. For instance, evidence of an anti-crossing between tunneling rates of different bands was observed, but we were not able to collect a full set of experimental data showing this behavior. Increasing the range of measurable tunneling rates would allow one to study both the energy and the tunneling rate anti-crossings [61]. Another aspect that has not been investigated so far is the role of phase coherence in inter-band tunneling. This could be explored by performing the experiment with a partially thermal sample instead of a BEC. Finally, the theoretical prediction of Ref. [75] on the destruction of the tunneling resonances in a nonlinear sample was tested only for a repulsive interaction between atoms. Using Feshbach resonances would allow one to investigate the inter-band tunneling in the attractive interaction regime.

Dynamical control of matter wave tunneling - In this experiment a sinusoidal driving of the lattice was used to control the tunneling between degenerate energy levels belonging to neighboring lattice sites. As expressed by the Bose-Hubbard model, the intra-band, or inter-well tunneling and the atom-atom interactions are the two parameters that characterize the behavior of atoms in an optical lattice. The driving of the lattice allowed us to control the tunneling independently of the atom-atom interactions. We studied the dependence of the inter-well tunneling both on the strength and on the frequency of the driving. As far as the driving amplitude is concerned, our experimental data were in good agreement with the theoretical expectation, while for the dependence on the driving frequency there are no theoretical predictions, as far as we know. Suppression of tunneling by up to a factor 25 was observed for particular values of the driving amplitude. Moreover, when the driving amplitude was set within a certain range, an inversion of the sign of the tunneling parameter was observed. The coherence of the sample in the driven lattice was studied by observing the interference pattern of the atoms in a time-of-flight experiment. We found a range of values for the shaking amplitude and frequency within which the phase coherence was preserved. For instance, when the tunneling was suppressed by a factor 10, the phase coherence was preserved for several tens of ms. The maintenance of the phase coherence in a shaken lattice suggest the possibility of entering into the Mott insulator phase by suppressing the tunneling in a driven lattice, as suggested by Ref. [82]. This intriguing experiment could be performed only in a 3D lattice, thus an upgrade of the experimental hardware would be needed. In such an experiment, it would be possible to explore if the energy anti-crossings that characterize the energy spectrum can affect the realization of the superfluid-Mott insulator phase transition, and in general it would be possible to study the adiabaticity of Floquet states.

Photon assisted tunneling - In this experiment a constant force was used to suppress almost completely the inter-well tunneling by shifting the energy levels with respect to each others and hence reducing resonant tunneling. The tunneling was then partially restored by bridging the energy gap between neighboring sites through a driving of the lattice. For a given value of the constant force, we observed the dependence of the tunneling both on the frequency and the amplitude of the driving. The dependence of the tunneling on the frequency agreed well with the theoretical prediction. However, the dependence of the tunneling on the driving amplitude agreed with the theoretical prediction only qualitatively. The quantitative difference between theory and experimental data was interpreted as being due to a loss of phase coherence in the sample because of the dynamical instabilities experienced by the atoms during their dynamics. In fact, the experimental data were bet-

ter in agreement with the theoretical prediction for a sequential rather than coherent tunneling. Sequential tunneling is an effect for which, after each inter-well tunneling event, the intra-well atom-atom interactions destroy the phase information carried by the tunneled atom. In order to partially confirm this interpretation, we performed the same experiment with a smaller number of atoms in the BEC, in order to decrease the interaction effects. As expected, the tunneling measured in this experiment was better in agreement with the theoretical prediction for a coherent tunneling regime. The emergence of sequential tunneling could be confirmed by using a Feshbach resonance, in order to decrease the interactions. If our prediction were confirmed, it would be possible to explore the cross-over between sequential and coherence tunneling in a controlled way.

Appendix A

Resonantly enhanced tunneling

This appendix contains a reprint of Ref. [68]: C. Sias, A. Zenesini, H. Lignier, S. Wimberger, D. Ciampini, O. Morsch, and E. Arimondo, *Resonantly Enhanced Tunneling of Bose-Einstein Condensates in Periodic Potentials*, *Phys. Rev. Lett.* **98**, 120403 (2007)

Resonantly Enhanced Tunneling of Bose-Einstein Condensates in Periodic Potentials

C. Sias, A. Zenesini, H. Lignier, S. Wimberger, D. Ciampini, O. Morsch, and E. Arimondo
Dipartimento di Fisica "E. Fermi," CNR-INFM, Largo Pontecorvo 3, 56127 Pisa, Italy
(Received 22 December 2006; published 23 March 2007)

We report on measurements of resonantly enhanced tunneling of Bose-Einstein condensates loaded into an optical lattice. By controlling the initial conditions of our system we were able to observe resonant tunneling in the ground and the first two excited states of the lattice wells. We also investigated the effect of the intrinsic nonlinearity of the condensate on the tunneling resonances.

DOI: 10.1103/PhysRevLett.98.120403 PACS numbers: 03.65.Xp, 03.75.Lm

Resonantly enhanced tunneling (RET) is a quantum effect in which the probability for tunneling of a particle between two potential wells is increased when the quantized energies of the initial and final states of the process coincide. In spite of the fundamental nature of this effect [1] and the practical interest [2], it has been difficult to observe experimentally in solid state structures. Since the 1970s, much progress has been made in constructing solid state systems such as superlattices [3–5] and quantum wells [6] which enable the controlled observation of RET [7].

In recent years, ultracold atoms in optical lattices [8] have been increasingly used to simulate solid state systems. Optical lattices are easy to realize in the laboratory, and their parameters can be perfectly controlled both statically and dynamically. Also, more complicated potentials can be realized by adding further lattice beams [9]. This makes them attractive as model systems for crystal lattices, and in the past few years cold atoms and Bose-Einstein condensates (BECs) in optical lattices have been used to simulate phenomena such as Bloch oscillations [10] and the Mott insulator transition [11]. In this Letter we show that BECs in accelerated optical lattice potentials are ideally suited to studying RET. While in solid state measurements of RET only a few potential wells were used and the periodic structures had to be grown for each realization, in our experiment the condensate is distributed over several tens of wells and the parameters of the lattice can be freely chosen. Moreover, we are able to control the initial conditions of the system and thus observe RET in any chosen energy level and can also add nonlinearity to the system.

A schematic representation of RET is shown in Fig. 1. In a tilted periodic potential, atoms can escape by tunneling to the continuum via higher-lying levels. The tilt of the potential is proportional to the force F acting on the atoms, and in general the tunneling rate Γ_{LZ} can be calculated using the Landau-Zener formula [12]. However, when the tilt-induced energy difference $Fd_L\Delta i$ between wells i and $i + \Delta i$ matches the separation between two quantized energy levels, the tunneling probability is resonantly enhanced and the Landau-Zener formula no longer gives the correct result, as previously investigated in [13] for cold atoms in optical lattices. While for the parameters of our experiment the enhancement over the Landau-Zener prediction was around a factor of 2 [see theoretical and experimental results of Fig. 2(a)], in general it can be several orders of magnitude.

The starting point of our experiments is a BEC of ^{87}Rb atoms, held in an optical dipole trap whose frequencies can be adjusted to realize a cigar-shaped condensate. The BECs are created using a hybrid approach in which evaporative cooling is initially effected in a magnetic time-orbiting potential (TOP) trap and subsequently in a crossed dipole trap. The dipole trap is realized using two intersecting Gaussian laser beams at 1030 nm wavelength and a power of around 1 W per beam focused to waists of 50 μm. After obtaining pure condensates of around 5×10^4 atoms the powers of the trap beams are adjusted in order to obtain an elongated condensate with the desired trap frequencies ($\approx$20 Hz in the longitudinal direction and 80–250 Hz radially).

Subsequently, the BECs held in the dipole trap are loaded into an optical lattice created by two Gaussian laser beams ($\lambda = 852$ nm) with 120 μm waist intersecting at an angle θ. The resulting periodic potential $V(x) = V_0 \sin^2(\pi x/d_L)$ has a lattice spacing $d_L = \lambda/(2\sin(\theta/2))$ and its depth V_0 is measured in units of the recoil energy

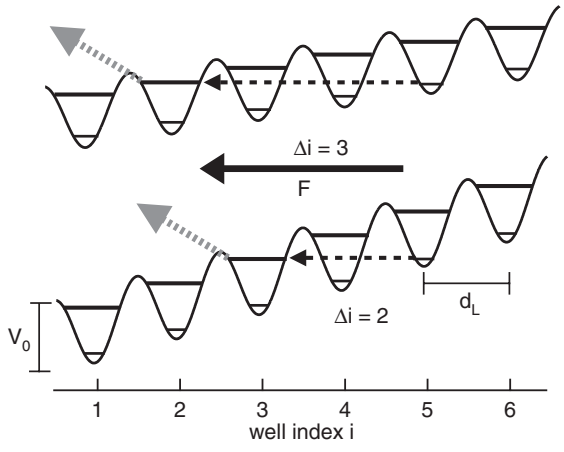

FIG. 1. Explanation of resonantly enhanced tunneling. Tunneling of atoms out of a tilted lattice is resonantly enhanced when the energy difference between lattice wells matches the distance between the energy levels in the wells.

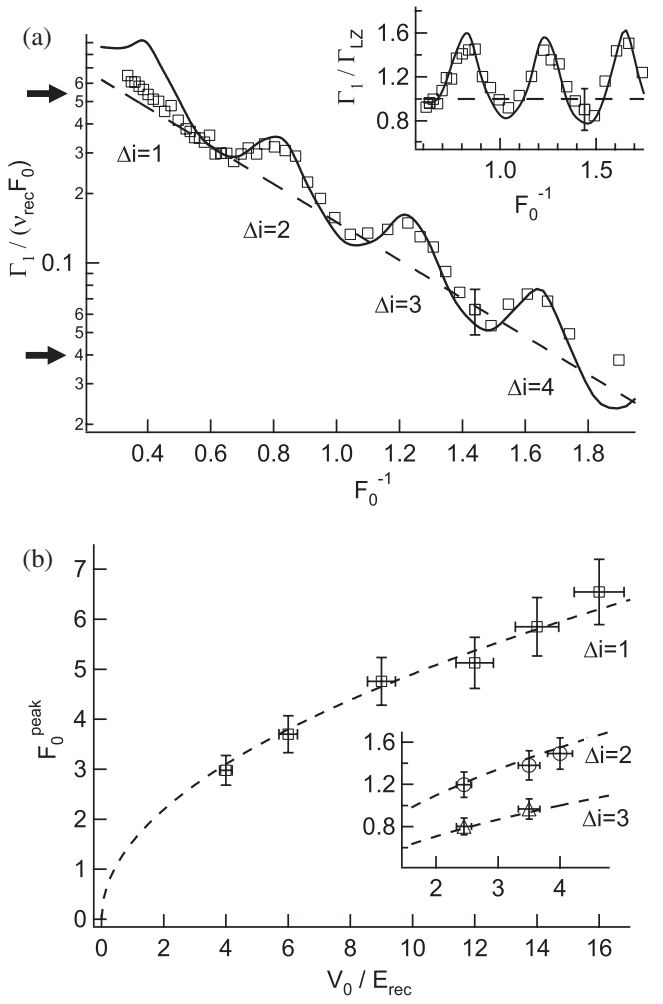

FIG. 2. Tunneling resonances in an accelerated optical lattice. (a) Tunneling resonances of the $n = 1$ lowest energy level for $V_0 = 2.5E_{\mathrm{rec}}$. The arrows indicate the upper and lower limits for our precise measurement of Γ_n. Inset: Deviation from the Landau-Zener prediction. For clarity, in both graphs only one representative error bar is shown. (b) Positions of the $\Delta i = 1$ resonance peaks as a function of the lattice depth. Only data points for which the resonance is clearly visible [e.g., not $\Delta i = 1$ of (a)] are included. Inset: Positions of the peaks for $\Delta i = 2$ and 3.

$E_{\mathrm{rec}} = \hbar^2\pi^2/(2md_L^2)$, where m is the mass of the Rb atoms. In the present experiment, we used $d_L = 0.426\ \mu$m (for $V_0/E_{\mathrm{rec}} = 6$, 4, 9, and 16) and $d_L = 0.620\ \mu$m (for $V_0/E_{\mathrm{rec}} = 2.5$, 10, 12, and 14). By introducing a frequency difference $\Delta\nu$ between the two lattice beams (using acousto-optic modulators which also control the power of the beams), the optical lattice can be moved at a velocity $v = d_L\Delta\nu$ or accelerated with an acceleration $a = d_L(d\Delta\nu/dt)$.

A ramp from 0 to V_0 in around 1 ms loads the BEC adiabatically into the optical lattice [14]. For loading the ground-state levels, the lattice velocity is $v = 0$ during the ramp. For the first and second excited levels, during the ramp the lattice is moved at a finite velocity calculated from the conservation of energy and quasimomentum [16]. Finally, the optical lattice is accelerated with acceleration a for an integer number of Bloch oscillation cycles. In the rest frame of the lattice, this results in a force $F = ma$ on the condensate. Atoms that are dragged along by the accelerated lattice acquire a larger final velocity than those that have undergone tunneling, and are spatially separated from the latter by releasing the BEC from the dipole trap and lattice at the end of the acceleration period and allowing it to fall under gravity for 5–20 ms. After the time of flight, the atoms are detected by absorptive imaging on a CCD camera using a resonant flash.

From the dragged fraction $N_{\mathrm{drag}}/N_{\mathrm{tot}}$, we then determine the tunneling rate Γ_n in the asymptotic decay law

$$N_{\mathrm{drag}}(t) = N_{\mathrm{tot}}\exp(-\Gamma_n t), \tag{1}$$

where the subscript n indicates the dependence of the tunnneling rate on the local energy level n in which the atoms are initially prepared (ground state: $n = 1$, first excited state: $n = 2$, etc.). In the experiments reported in this work, the number of bound states in the wells was small (2–4, depending on the lattice depth), so after the first tunneling event, the probability for tunneling to the next bound state or the continuum was close to unity.

The resolution of our tunneling measurement is given by the minimum number of atoms that we can distinguish from the background noise in our CCD images, which varies between 500 and 1000 atoms, depending on the width of the observed region. With our condensate number, and taking into account the minimum acceleration time limited by the need to spatially separate the two fractions after time of flight and the maximum acceleration time limited by the field of view of the CCD camera, this results in a maximum $\Gamma_n/\nu_{\mathrm{rec}}$ of ≈ 1 and a minimum of $\approx 1 \times 10^{-2}$, with the recoil frequency $\nu_{\mathrm{rec}} = E_{\mathrm{rec}}/h$.

A typical plot of the tunneling rate Γ_1 out of the ground state as a function of F_0^{-1} (where $F_0 = Fd_L/E_{\mathrm{rec}}$ is the dimensionless force) in the linear regime is shown in Fig. 2(a). This regime is reached either by choosing small radial dipole trap frequencies or by releasing the BEC from the trap before the acceleration phase and thus letting it expand. In both cases, the density and hence the interaction energy of the BEC is reduced. Superimposed on the overall exponential decay of Γ_1/F_0 with F_0^{-1}, one clearly sees the resonant tunneling peaks corresponding to $\Delta i = 2$, 3, and 4 (for this choice of parameters, the $\Delta i = 1$ peak lay outside our experimental resolution). In order to highlight the deviation from the Landau-Zener prediction, in the inset of Fig. 2(a) we plot $\Gamma_1/\Gamma_{\mathrm{LZ}}$, where the Landau-Zener tunneling rate Γ_{LZ} is given by [12,16]

$$\Gamma_{\mathrm{LZ}} = \nu_{\mathrm{rec}}F_0 e^{-[\pi^2(V_0/E_{\mathrm{rec}})^2/32F_0]}. \tag{2}$$

The experimental results are in good agreement with numerical solutions obtained by diagonalizing the Hamiltonian of the open decaying system [17,18]. Figure 2(b) sum-

marizes our results for the positions of the ground-state resonances $\Delta i = 1$, 2, and 3 as a function of the lattice depth together with a theoretical fit assuming the separation of the lowest energy levels to be

$$\Delta E = \alpha E_{\mathrm{rec}} \sqrt{V_0 / E_{\mathrm{rec}}}. \quad (3)$$

Independently of Δi, the best fit is achieved for $\alpha = 1.5$, to be compared with $\alpha = 2$ for the harmonic oscillator approximation. A value $\alpha < 2$ is to be expected since our lattice wells only contain a few bound states and are, therefore, highly anharmonic.

Using BECs in optical lattices allows us to explore resonant tunneling in regimes that are difficult or even impossible to access in solid state systems. First, we can prepare the condensates in the excited levels of the lattice wells before the acceleration. Again, tunneling resonances are clearly visible, and the experimental results agree with theoretical calculations. The accessibility of higher energy levels allows us to experimentally determine the decay rates at resonance of two strongly coupled levels. Although our experimental resolution does not allow us to measure the decay rates in two different levels for the same set of parameters F_0 and V_0, we are able to compare the ground and excited state decay rates Γ_1 and Γ_2 with the theoretical predictions for two different parameter sets, as shown in Fig. 3. This figure reveals the anticrossing of the decay rates of strongly coupled levels as a function of our control parameter F_0. These results demonstrate a peculiar behavior of the Wannier-Stark states studied theoretically [6,19] and more recently rephrased within a general context of crossings and anticrossings for the real and imaginary parts of the eigenvalues of non-Hermitian Hamiltonians [20]. Our data confirm the predictions of [17] that the anticrossings modify the decay rates of the two perturbing states in different ways.

Additionally, by exploiting the intrinsic nonlinearity of the condensate due to atom-atom interactions, we can study RET in the nonlinear regime, as simulated in [21]. In order to realize this regime, we carry out the acceleration experiments in radially tighter traps (radial frequency $\gtrsim 100$ Hz) and hence at larger condensate densities. Figure 4(a) shows the results for increasing values of the nonlinear parameter [22]

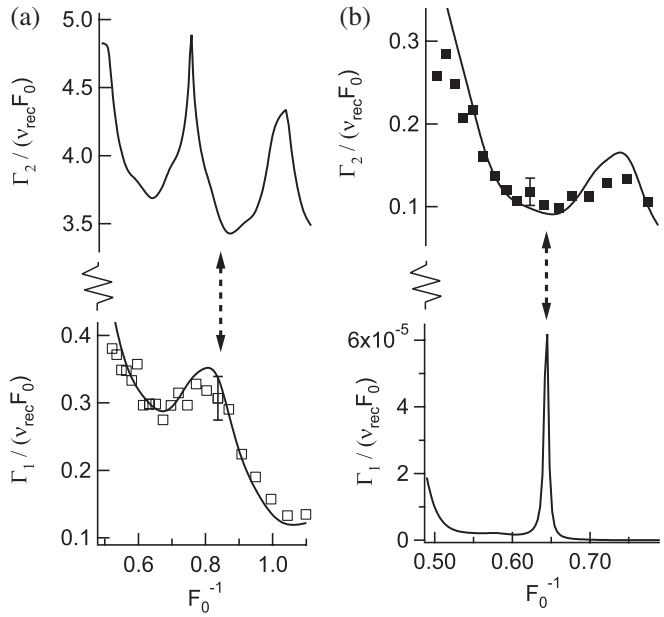

FIG. 3. Anticrossing scenario of the RET rates. (a) Theoretical plot of $\Gamma_{1,2}$ for $V_0 = 2.5 E_{\mathrm{rec}}$ with experimental points for Γ_1. (b) Theoretical plot of $\Gamma_{1,2}$ for $V_0 = 10 E_{\mathrm{rec}}$ with experimental points for Γ_2. For clarity, the vertical axes have been split and the Γ_n plotted on a linear scale, and only one representative error bar is shown.

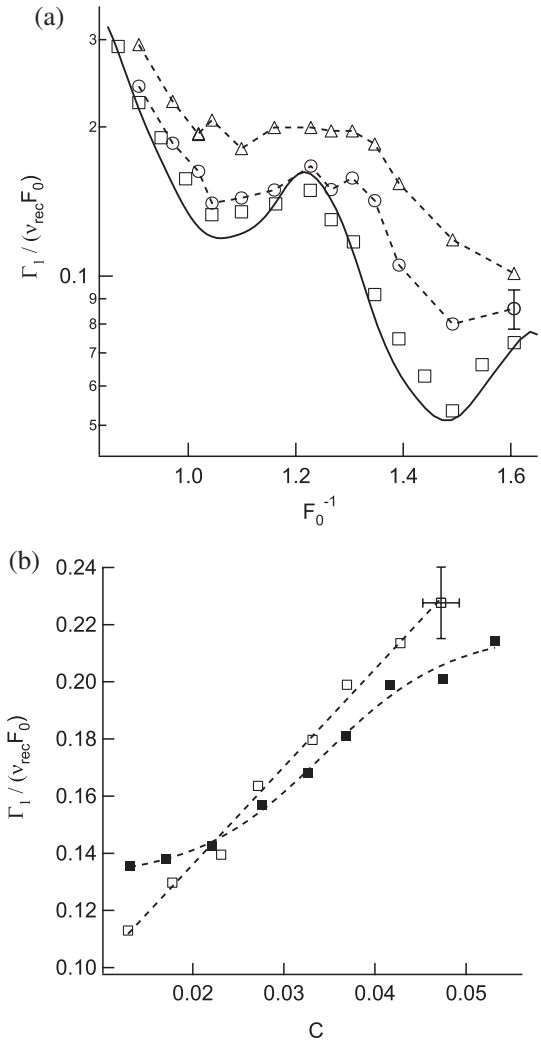

FIG. 4. Resonant tunneling in the nonlinear regime. (a) Resonance $\Delta i = 3$ for $V_0 = 2.5 E_{\mathrm{rec}}$ with $C = 0.024$ (squares), $C = 0.035$ (circles) and $C = 0.057$ (triangles). The solid line is the theoretical prediction for $C = 0$; the dashed lines are guides to the eye. (b) Dependence on C of the tunneling rate at the position of the peak $F_0^{-1} = 1.21$ (solid symbols) and of the trough $F_0^{-1} = 1.03$ (open symbols). The dashed lines are fits to guide the eye. For clarity, in (a) and (b) only one typical error bar is shown.

$$C = \frac{n_0 a_s d_L^2}{\pi}, \quad (4)$$

where n_0 is the peak condensate density and a_s the s-wave scattering length. Two effects are visible: First, the overall (off-resonant) level of Γ_1 increases linearly with C. This is in agreement with our earlier experiments on nonlinear Landau-Zener tunneling [22,23] and can be explained describing the condensate evolution within a nonlinearity-dependent effective potential $V_{\text{eff}} = V_0/(1 + 4C)$ [24]. Second, with increasing nonlinearity, the contrast of the RET peak is decreased and the peak eventually vanishes. This is confirmed by the different dependence on C of the on- and off-resonant values of Γ_1 [Fig. 4(b)]. We estimate that in order to significantly affect the resonant tunneling rate, the nonlinearity parameter has to be comparable to the width of the RET peak. This order-of-magnitude argument agrees with our observations.

Finally, we have experimentally tested the robustness of RET against a dephasing of the lattice wells induced by nonadiabatic loading of the BEC into the lattice in the nonlinear regime [15,25]. Even for completely dephased wells, the tunneling resonances survive.

In summary, we have measured resonantly enhanced tunneling of BECs in accelerated periodic potentials in a regime where the standard Landau-Zener description is not valid. Our results in the linear regime agree with numerical calculations, and the possibility to observe RET for arbitrary initial conditions and parameters of the periodic potential underlines the advantage of our system over solid state realizations. Furthermore, we have explored RET in the nonlinear regime and demonstrated that, as theoretically predicted, the tunneling resonances disappear for large values of the nonlinearity.

In the present setup the measurement of the tunneling rate is limited in its dynamic range by the detection geometry. A larger dynamic range can be realized by long-distance transport of BECs [26]. Our method for observing RET can also be generalized in order to study other regular or disordered potentials, the effects of noise and the presence of a thermal fraction in the condensate. Furthermore, one might exploit the tunneling resonances to explore the spatial decoherence processes and to perform precision measurements.

This work was supported by the European Community STREP Project OLAQUI, a MIUR-PRIN Project, the Sezione di Pisa dell'INFN, and the Feodor-Lynen Programme of the Alexander v. Humboldt Foundation. The authors would like to thank M. Cristiani, R. Mannella, and Y. Singh for assistance, A. Kolovsky for useful discussions, and S. Rolston for a critical reading of the manuscript.

[1] D. Bohm, *Quantum Theory* (Dover Publications, New York, 1989), p. 286.
[2] *Resonant Tunneling in Semiconductors*, edited by L. L. Chang, E. E. Mendez, and C. Tejedor (Plenum, New York, 1991).
[3] L. L. Chang, L. Esaki, and R. Tsu, Appl. Phys. Lett. **24**, 593 (1974).
[4] L. Esaki, IEEE J. Quantum Electron. **22**, 1611 (1986).
[5] S. Glutsch, Phys. Rev. B **69**, 235317 (2004).
[6] M. Wagner and H. Mizuta, Phys. Rev. B **48**, 14 393 (1993).
[7] K. Leo, *High-Field Transport in Semiconductor Superlattices* (Springer, Berlin, 2003).
[8] G. Grynberg and C. Robilliard, Phys. Rep. **355**, 335 (2001).
[9] L. Santos, M. A. Baranov, J. I. Cirac, H.-U. Everts, H. Fehrmann, and M. Lewenstein, Phys. Rev. Lett. **93**, 030601 (2004).
[10] O. Morsch and M. Oberthaler, Rev. Mod. Phys. **78**, 179 (2006), and references therein.
[11] M. Greiner, O. Mandel, T. Esslinger, T. W. Hänsch, and I. Bloch, Nature (London) **415**, 39 (2002).
[12] L. Landau, Phys. Z. Sowjetunion **1**, 88 (1932); **2**, 46 (1932); C. Zener, Proc. R. Soc. A **137**, 696 (1932).
[13] C. F. Bharucha, K. W. Madison, P. R. Morrow, S. R. Wilkinson, B. Sundaram, and M. G. Raizen, Phys. Rev. A **55**, R857 (1997).
[14] In the nonlinear regime, i.e., when the radial trap frequency is large and hence the interaction energy of the BEC is appreciable, the speed of the ramp has to be reduced and loading times can be as long as tens of milliseconds [15].
[15] T. Gericke *et al.*, cond-mat/0603590.
[16] E. Peik, M. B. Dahan, I. Bouchoule, Y. Castin, and C. Salomon, Phys. Rev. A **55**, 2989 (1997).
[17] M. Glück, A. R. Kolovsky, and H. J. Korsch, Phys. Rev. Lett. **83**, 891 (1999).
[18] M. Glück, A. R. Kolovsky, and H. J. Korsch, Phys. Rep. **366**, 103 (2002).
[19] J. E. Avron, Ann. Phys. (N.Y.) **143**, 33 (1982).
[20] F. Keck, H. J. Korsch, and S. Mossmann, J. Phys. A **36**, 2125 (2003).
[21] S. Wimberger, R. Mannella, O. Morsch, E. Arimondo, A. R. Kolovsky, and A. Buchleitner, Phys. Rev. A **72**, 063610 (2005).
[22] O. Morsch, J. H. Müller, M. Cristiani, D. Ciampini, and E. Arimondo, Phys. Rev. Lett. **87**, 140402 (2001).
[23] M. Jona-Lasinio, O. Morsch, M. Cristiani, N. Malossi, J. H. Müller, E. Courtade, M. Anderlini, and E. Arimondo, Phys. Rev. Lett. **91**, 230406 (2003).
[24] D. I. Choi and Q. Niu, Phys. Rev. Lett. **82**, 2022 (1999).
[25] O. Morsch, J. H. Müller, D. Ciampini, M. Cristiani, P. B. Blakie, C. J. Williams, P. S. Julienne, and E. Arimondo, Phys. Rev. A **67**, 031603 (2003).
[26] S. Schmid, G. Thalhammer, K. Winkler, L. Lang, and J. H. Denschlag, New J. Phys. **8**, 159 (2006).

Appendix B

Dynamical control of matter-wave tunneling

This appendix contains a reprint of Ref. [111]: H. Lignier, C. Sias, D. Ciampini, Y. Singh, A. Zenesini, O. Morsch, and E. Arimondo, *Dynamical Control of Matter-Wave Tunneling in Periodic Potentials*, *Phys. Rev. Lett.* **99**, 220403 (2007)

Dynamical Control of Matter-Wave Tunneling in Periodic Potentials

H. Lignier, C. Sias, D. Ciampini, Y. Singh, A. Zenesini, O. Morsch, and E. Arimondo

CNR-INFM, Dipartimento di Fisica "E. Fermi," Università di Pisa, Largo Pontecorvo 3, 56127 Pisa, Italy

(Received 3 July 2007; published 27 November 2007)

We report on measurements of dynamical suppression of interwell tunneling of a Bose-Einstein condensate (BEC) in a strongly driven optical lattice. The strong driving is a sinusoidal shaking of the lattice corresponding to a time-varying linear potential, and the tunneling is measured by letting the BEC freely expand in the lattice. The measured tunneling rate is reduced and, for certain values of the shaking parameter, completely suppressed. Our results are in excellent agreement with theoretical predictions. Furthermore, we have verified that, in general, the strong shaking does not destroy the phase coherence of the BEC, opening up the possibility of realizing quantum phase transitions by using the shaking strength as the control parameter.

DOI: 10.1103/PhysRevLett.99.220403 PACS numbers: 03.75.Lm, 03.65.Xp

Quantum tunneling of particles between potential wells connected by a barrier is a fundamental physical effect. While typically quantum systems decay faster when they are perturbed, if the wells are shifted with respect to each other by a time-varying linear potential (e.g., by periodically shaking them back and forth), the tunneling rate can actually be reduced and, for certain strengths of the time-varying potential, even completely suppressed [1,2].

Modifications of the dynamics of quantum systems by applying periodic potentials have been investigated in a number of contexts including the renormalization of Landé g factors in atoms [3], the micromotion of a single trapped ion [4], and the motion of electrons in semiconductor superlattices [5]. In particular, theoretical studies of double-well systems and of periodic potentials have led to the closely related concepts of coherent destruction of tunneling and dynamical localization [1,6]. In the latter, tunneling between the sites of a periodic array is inhibited by applying an oscillating potential, e.g., by shaking the array back and forth (see Fig. 1), and, as a consequence, the tunneling parameter J representing the gain in kinetic energy in a tunneling event is replaced by $|J_{\mathrm{eff}}| < |J|$. In a number of experiments, signatures of this tunneling suppression have been observed [5,7,8], and recently dynamical localization and coherent suppression of tunneling have been demonstrated using light propagating in coupled waveguide arrays [9,10]. So far, however, an exact experimental realization of the intrinsically nonlinear Bose-Hubbard model [2] driven by a time-periodic potential has not been reported.

In this Letter, we report on the observation of the dynamical tunneling suppression predicted in Refs. [2,11] using Bose-Einstein condensates (BECs) in strongly driven periodic optical potentials [12]. In contrast to other systems, the parameters of such optical lattices—potential depth, lattice spacing, driving strength, and driving frequency—can be varied over a wide range. Also, our system allows us to observe the effects of the shaking both through the real-space expansion of the BEC in the optical lattice and by performing time-of-flight experiments, in which the phase coherence of the BEC can be measured and which allow us to verify that the tunneling suppression occurs in a phase-coherent way.

Furthermore, BECs have an intrinsic nonlinear on-site interaction energy (represented by U in Fig. 1), the interplay of which with the tunneling parameter J has been shown to lead to the Mott-insulator quantum phase transition for a critical value of the ratio U/J [13,14]. It has been theoretically predicted that, for a BEC in a shaken optical lattice, this ratio can be replaced by U/J_{eff} and, hence, that it should be possible to drive the system across the quantum phase transition by varying the shaking parameter [2,11]. In this work, we demonstrate the feasibility of the key ingredients of this scheme. In particular, we show that, when tunneling in the shaken lattice is completely suppressed, the phase coherence of the BEC is lost, in agreement with the physical picture of a sudden "switch-off" of the interwell coupling and a subsequent independent evolution of the local phases due to collisions between the atoms [15,16].

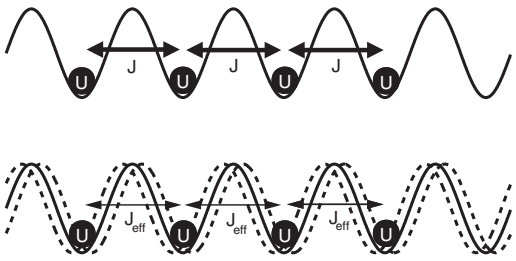

FIG. 1. Suppression of tunneling by strong driving. The dynamics of a Bose-Einstein condensate in a periodic potential is governed by the tunneling matrix element J and the on-site interaction energy U (above). If the potential is strongly shaken, tunneling between the wells is dynamically suppressed, leading to a renormalized tunneling matrix element J_{eff} (below) but leaving the interaction energy U unaffected.

Our system consisting of a Bose-Einstein condensate inside a (sinusoidally) shaken one-dimensional optical lattice is approximately described [17] by the Hamiltonian

$$\hat{H}_0 = -J\sum_{\langle i,j\rangle}(\hat{c}_i^\dagger \hat{c}_j + \hat{c}_j^\dagger \hat{c}_i) + \frac{U}{2}\sum_j \hat{n}_j(\hat{n}_j - 1) + K\cos(\omega t)\sum_j j\hat{n}_j, \quad (1)$$

where $\hat{c}_i^{(\dagger)}$ are the boson creation and annihilation operators on site i, $\hat{n}_i = \hat{c}_i^\dagger \hat{c}_i$ are the number operators, and K and ω are the strength and angular frequency of the shaking, respectively. The first two terms in the Hamiltonian describe the Bose-Hubbard model [13] with the tunneling matrix element J and the on-site interaction term U. The shaking of the lattice is expected to create a Floquet-quasienergy spectrum, in which the tunneling matrix element J is renormalized to an effective tunneling parameter [2]

$$J_{\text{eff}} = J\mathcal{J}_0(K_0), \quad (2)$$

where $\mathcal{J}_0$ is the zeroth-order ordinary Bessel function and we have introduced the dimensionless parameter $K_0 = K/\hbar\omega$.

In our experiment, we created BECs of about 5×10^4 87-rubidium atoms using a hybrid approach in which evaporative cooling was initially effected in a magnetic time-orbiting potential trap and subsequently in a crossed dipole trap. The dipole trap was realized by using two intersecting Gaussian laser beams at 1030 nm wavelength and a power of around 1 W per beam focused to waists of 50 μm. After obtaining pure condensates of around 5×10^4 atoms, the powers of the trap beams were adjusted in order to obtain elongated condensates with the desired trap frequencies (≈ 20 Hz in the longitudinal direction and 80 Hz radially). Along the axis of one of the dipole trap beams, a one-dimensional optical lattice potential was then added by ramping up the power of the lattice beams in 50 ms (the ramping time being chosen so as to avoid excitations of the BEC). The optical lattices used in our experiments were created using two counterpropagating Gaussian laser beams ($\lambda = 852$ nm) with 120 μm waist and a resulting optical lattice spacing $d_L = \lambda/2 = 0.426$ μm. The depth V_0 of the resulting periodic potential is measured in units of $E_{\text{rec}} = \hbar^2\pi^2/(2md_L^2)$, where m is the mass of the Rb atoms. By introducing a frequency difference $\Delta\nu$ between the two lattice beams (using acousto-optic modulators which also control the power of the beams), the optical lattice could be moved at a velocity $v = d_L\Delta\nu$ or accelerated with an acceleration $a = d_L\frac{d\Delta\nu}{dt}$. In order to periodically shake the lattice, $\Delta\nu$ was sinusoidally modulated with angular frequency ω, leading to a time-varying velocity $v(t) = d_L\Delta\nu_{\max}\sin(\omega t)$ and, hence, to an effective time-varying force in the lattice frame

$$F(t) = m\omega d_L\Delta\nu_{\max}\cos(\omega t) = F_{\max}\cos(\omega t). \quad (3)$$

The peak shaking force $F_{\max}$ is related to the shaking strength K in Eq. (1) by $K = F_{\max}d_L$, and hence

$$K_0 = \frac{K}{\hbar\omega} = \frac{md_L^2\Delta\nu_{\max}}{\hbar} = \frac{\pi^2\Delta\nu_{\max}}{2\omega_{\text{rec}}}. \quad (4)$$

The spatial shaking amplitude $\Delta x_{\max}$ can then be written as $\Delta x_{\max} = (2/\pi^2)(\omega_{\text{rec}}/\omega)K_0 d_L$, so for a typical shaking frequency $\omega/2\pi = 3$ kHz we have $\Delta x_{\max} \approx 0.5 d_L$ at $K_0 = 2.4$.

After loading the BECs into the optical lattice, the frequency modulation of one of the lattice beams creating the shaking was switched on either suddenly or using a linear ramp with a time scale of a few milliseconds. Finally, in order to measure the effective tunneling rate $|J_{\text{eff}}|$ between the lattice wells (where the modulus indicates that we are not sensitive to the sign of J, in contrast to the time-of-flight experiments described below), we then switched off the dipole trap beam that confined the BEC along the direction of the optical lattice, leaving only the radially confining beam switched on (the trap frequency of that beam along the lattice direction was on the order of a few hertz and hence negligible on the time scales of our expansion experiments, which were typically less than 200 ms). The BEC was now free to expand along the lattice direction through interwell tunneling, and its *in situ* width was measured using a resonant flash, the shadow cast by which was imaged onto a CCD chip. The observed density distribution was then fitted with one or two Gaussians.

In a preliminary experiment without shaking ($K_0 = 0$), we verified that, for our expansion times, the growth in the condensate width σ_x along the lattice direction was to a good approximation linear and that the dependence of $d\sigma_x/dt$ on the lattice depth (up to $V_0/E_{\text{rec}} = 9$) followed the expression for $J(V_0/E_{\text{rec}})$ in the lowest energy band [18]

$$J\left(\frac{V_0}{E_{\text{rec}}}\right) = \frac{4E_{\text{rec}}}{\sqrt{\pi}}\left(\frac{V_0}{E_{\text{rec}}}\right)^{3/4} e^{-2\sqrt{V_0/E_{\text{rec}}}}, \quad (5)$$

which is a good approximation for our range of lattice depths. This enabled us to confirm that $d\sigma_x/dt$ measured at a fixed time was directly related to J and, in a shaken lattice, to $|J_{\text{eff}}(K_0)|$. We also verified that, for our parameters U and J, the condensate was not in the self-trapping regime [19]. The results of our measurements of $|J_{\text{eff}}(K_0)/J|$ for various lattice depths V_0 and driving frequencies ω are summarized in Fig. 2. We found a universal behavior of $|J_{\text{eff}}/J|$ that is in very good agreement with the Bessel-function rescaling of Eq. (2). We were able to measure $|J_{\text{eff}}/J|$ for K_0 up to 12, albeit agreement with theory beyond $K_0 \approx 6$ was not as good, with the experimental values lying consistently below the theoretical curve. For the zeros of the $\mathcal{J}_0$ Bessel function at $K_0 \approx 2.4$ and 5.5, complete suppression of tunneling was observed (within

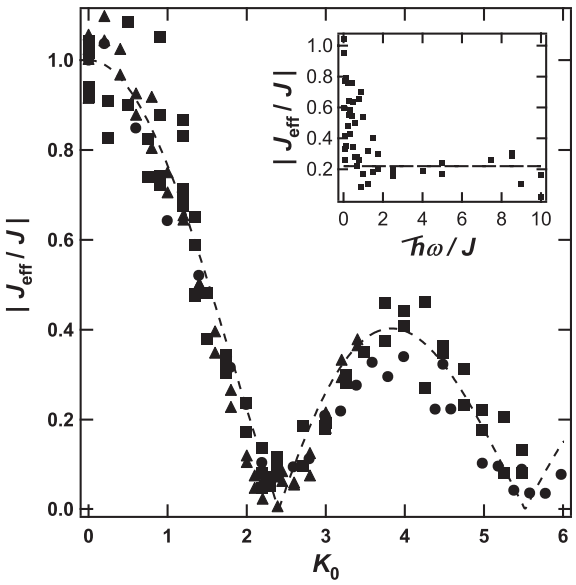

FIG. 2. Dynamical suppression of tunneling in an optical lattice. Shown here is $|J_{\rm eff}/J|$ as a function of the shaking parameter K_0 for $V_0/E_{\rm rec} = 6$, $\omega/2\pi = 1$ kHz (squares), $V_0/E_{\rm rec} = 6$, $\omega/2\pi = 0.5$ kHz (circles), and $V_0/E_{\rm rec} = 4$, $\omega/2\pi = 1$ kHz (triangles). The dashed line is the theoretical prediction. Inset: $|J_{\rm eff}/J|$ as a function of ω for $K_0 = 2.0$ and $V_0/E_{\rm rec} = 9$ corresponding to $J/h = 90$ Hz.

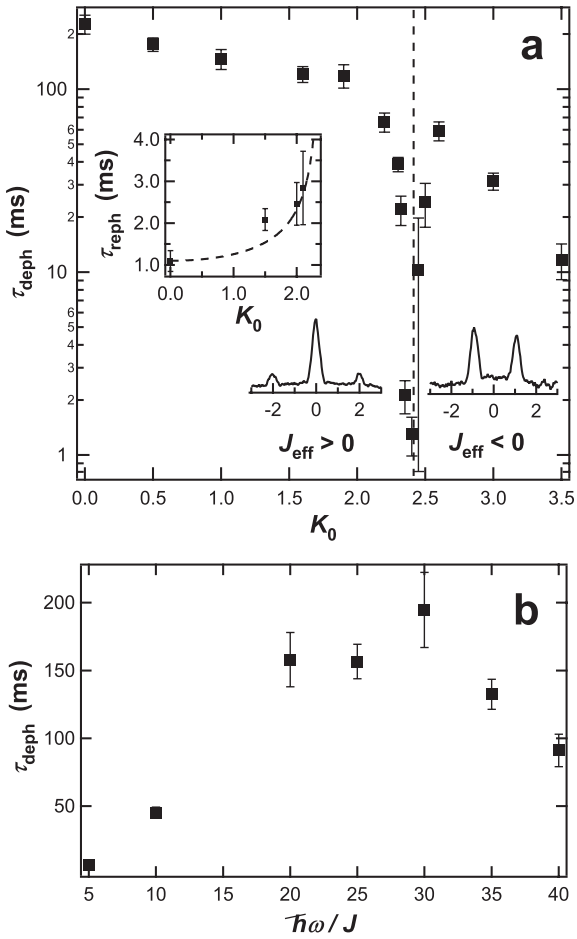

FIG. 3. Phase coherence in a shaken lattice. (a) Dephasing time $\tau_{\rm deph}$ of the condensate as a function of K_0 for $V_0/E_{\rm rec} = 9$ and $\omega/2\pi = 3$ kHz. The vertical dashed line marks the position of $K_0 = 2.4$ dividing the regions with $J_{\rm eff} > 0$ (left) and $J_{\rm eff} < 0$ (right). In both regions, a typical (vertically integrated) interference pattern without final acceleration to the zone edge is shown (the x axis is scaled in units of the recoil momentum $p_{\rm rec} = h/d_L$.) Inset: Rephasing time after dephasing at $K_0 = 2.4$ and subsequent reduction of K_0. (b) Dephasing time as a function of $\hbar\omega/J$ for $K_0 = 2.2$.

our experimental resolution, we could measure a suppression by at least a factor of 25).

We also checked the behavior of $|J_{\rm eff}/J|$ as a function of ω for a fixed value of $K_0 = 2$ (see inset in Fig. 2) and found that, over a wide range of frequencies between $\hbar\omega/J \approx 0.3$ and $\hbar\omega/J \approx 30$, the tunneling suppression works, although for $\hbar\omega/J \lesssim 1$ we found that $|J_{\rm eff}(K_0)/J|$ deviated from the Bessel function near the zero points, where the suppression was less efficient than expected. In the limit of large shaking frequencies ($\omega/2\pi \gtrsim 3$ kHz, to be compared with the typical mean separation of $\approx$15 kHz between the two lowest energy bands at $V_0/E_{\rm rec} = 9$), we observed excitations of the condensate to the first excited band of the lattice. In our *in situ* expansion measurements, these band excitations (typically less than 30% for $K_0 > 3$ and less than 10% for $K_0 < 3$) were visible in the condensate profile as a broad Gaussian pedestal below the near-Gaussian profile of the ground-state condensate atoms. From the widths of those pedestals, we inferred that $|J_{\rm eff}/J|$ of the atoms in the excited band also followed the Bessel-function rescaling of Eq. (2) and that the ratios of the tunneling rates in the two bands agreed with theoretical models.

We now turn to the phase coherence of the BEC in the shaken lattice, which was made visible by switching off the dipole trap and lattice beams and letting the BEC fall under gravity for 20 ms. This resulted in an interference pattern whose visibility reflected the condensate coherence [20]. In the region between the first two zeros of the Bessel function, where $\mathcal{J}_0 < 0$, we found an interference pattern [see Fig. 3(a)] that was shifted by half a Brillouin zone. This shift can be interpreted as an inversion of the curvature of the (quasi)energy band at the center of the Brillouin zone when the effective tunneling parameter is negative. We then quantified the visibility $\mathcal{V} = (h_{\rm max} - h_{\rm min})/(h_{\rm max} + h_{\rm min})$ of the interference pattern after shaking the condensate in the lattice for a fixed time between 1 and $\approx$ 200 ms and finally accelerating the lattice to the edge of the Brillouin zone. In the expression for $\mathcal{V}$, $h_{\rm max}$ is the mean value of the condensate density at the position of the two interference peaks, and $h_{\rm min}$ is the condensate density in a region of width equal to about 1/4 of the peak separation centered about the halfway point between the two peaks. For a perfectly phase-coherent condensate, $\mathcal{V} \approx 1$,

whereas for a strongly dephased condensate, $\mathcal{V} \approx 0$. For $K_0 \lesssim 2.2$, the BEC phase coherence was maintained for several tens of milliseconds, demonstrating that the tunneling could be suppressed by a factor of up to 10 over hundreds of shaking cycles without significantly disturbing the BEC.

This result is expressed more quantitatively in Fig. 3(a). Here the condensate was held in the lattice ($V_0/E_{\mathrm{rec}} = 9$), and the shaking was switched on suddenly at $t = 0$ (we found no significantly different behavior when K_0 was linearly ramped in a few milliseconds). Thereafter, $\mathcal{V}$ was measured as a function of time, and the decay time constant τ_{deph} of the resulting near-exponential function was extracted. Apart from a slow overall decrease in τ_{deph} for increasing K_0, a sharp dip around $K_0 = 2.4$ is visible. In this region, $|J_{\mathrm{eff}}/J| < 1/20$ and, hence, $|J_{\mathrm{eff}}/h| \lesssim 10$ Hz, which for our experimental parameters is comparable to the on-site interaction U/h (we checked that the widths of the on-site wave functions and hence U were independent of K_0 by analyzing the side peaks in the interference pattern). This means that neighboring lattice sites are effectively decoupled and the local phases evolve independently due to interatomic collisions, leading to a dephasing of the array [14,16]. By increasing the dipole trap frequency (and hence U), we verified that τ_{deph} decreases as expected. We also studied a rephasing of the BEC when, after an initial dephasing at $K_0 = 2.4$, the value of the shaking parameter was reduced below 2.4. The time constant τ_{reph} of the subsequent rephasing of the condensate (mediated by interwell tunneling and on-site collisions) increased with decreasing J_{eff} [see the inset in Fig. 3(a), where we compare τ_{reph} with the inverse of the generalized Josephson frequency $\omega^{-1}_{\mathrm{Josephson}} \propto J^{-1/2}_{\mathrm{eff}}$ predicted by the two-well model [16,21]].

Finally, we investigated the dependence of τ_{deph} on the shaking frequency ω [see Fig. 3(b)]. Interestingly, while the tunneling suppression as observed *in situ* works even for $\hbar\omega/J \approx 1$, in order to maintain the phase coherence of the condensate, much larger shaking frequencies are needed. Indeed, for our system there exists an optimum shaking frequency of $\hbar\omega/J \approx 30$.

In summary, we have measured the dynamical suppression of tunneling of a BEC in strongly shaken optical lattices and found excellent agreement with theoretical predictions. Our results show that the tunneling suppression occurs in a phase-coherent way and can, therefore, be used as a tool to control the tunneling matrix element while leaving the on-site interaction energy unchanged (in contrast to the usual technique of increasing the lattice depth, which changes both) and without disturbing the condensate. This might ultimately lead to the possibility of controlling quantum phase transitions by strong driving of the lattice. In this context, it will be important to investigate the question of adiabaticity when dynamically changing the shaking parameter. Furthermore, our system also opens up other avenues of research such as the realization of exact dynamical localization using discontinuous shaking waveforms [8,22] or tunneling suppression in superlattices [23].

This work was supported by OLAQUI and MIUR through PRIN2005. The authors thank Sandro Wimberger for useful discussions.

Note added in proof.—Similar results have been obtained in an array of double wells by Kierig and co-workers [24].

[1] F. Grossmann, T. Dittrich, P. Jung, and P. Hänggi, Phys. Rev. Lett. **67**, 516 (1991).
[2] A. Eckardt, C. Weiss, and M. Holthaus, Phys. Rev. Lett. **95**, 260404 (2005).
[3] S. Haroche, C. Cohen-Tannoudji, C. Audoin, and J. P. Schermann, Phys. Rev. Lett. **24**, 861 (1970).
[4] Ch. Raab, J. Eschner, J. Bolle, H. Oberst, F. Schmidt-Kaler, and R. Blatt, Phys. Rev. Lett. **85**, 538 (2000).
[5] B. J. Keay *et al.*, Phys. Rev. Lett. **75**, 4102 (1995).
[6] D. H. Dunlap and V. M. Kenkre, Phys. Rev. B **34**, 3625 (1986).
[7] K. W. Madison, M. C. Fischer, R. B. Diener, Q. Niu, and M. G. Raizen, Phys. Rev. Lett. **81**, 5093 (1998).
[8] R. Iyer, J. S. Aitchison, J. Wan, M. M. Dignam, and C. M. de Sterke, Opt. Express **15**, 3212 (2007).
[9] S. Longhi *et al.*, Phys. Rev. Lett. **96**, 243901 (2006).
[10] G. Della Valle *et al.*, Phys. Rev. Lett. **98**, 263601 (2007).
[11] C. E. Creffield and T. S. Monteiro, Phys. Rev. Lett. **96**, 210403 (2006).
[12] O. Morsch and M. Oberthaler, Rev. Mod. Phys. **78**, 179 (2006).
[13] M. P. Fisher, P. B. Weichman, G. Grinstein, and D. S. Fisher, Phys. Rev. B **40**, 546 (1989); D. Jaksch, C. Bruder, J. I. Cirac, C. W. Gardiner, and P. Zoller, Phys. Rev. Lett. **81**, 3108 (1998).
[14] M. Greiner, O. Mandel, T. Esslinger, T. W. Hänsch, and I. Bloch, Nature (London) **415**, 39 (2002).
[15] M. Greiner, O. Mandel, T. W. Hänsch, and I. Bloch, Nature (London) **419**, 51 (2002).
[16] W. Li, A. K. Tuchman, H.-C. Chien, and M. A. Kasevich, Phys. Rev. Lett. **98**, 040402 (2007).
[17] For most parameter values, our experiment is closer to the mean-field regime. However, tunneling suppression is also found when numerically integrating the linear Schrödinger equation, so it seems to be a general effect that occurs in all regimes [S. Wimberger (private communication)].
[18] W. Zwerger, J. Opt. B **5**, S9 (2003).
[19] Th. Anker *et al.*, Phys. Rev. Lett. **94**, 020403 (2005).
[20] O. Morsch *et al.*, Phys. Rev. A **67**, 031603 (2003).
[21] A. Smerzi, S. Fantoni, S. Giovanazzi, and S. R. Shenoy, Phys. Rev. Lett. **79**, 4950 (1997).
[22] M. M. Dignam and C. M. de Sterke, Phys. Rev. Lett. **88**, 046806 (2002).
[23] C. E. Creffield, Phys. Rev. Lett. **99**, 110501 (2007).
[24] E. Kierig *et al.*, in *Proceedings of DPG-Tagung 2007* (Deutsche Physikalische Gesellschaft e.V., Berlin, 2007), Abstract No. Q.21.7.

Appendix C

Photon-assisted tunneling

This appendix contains a reprint of Ref. [112]: C. Sias, H. Lignier, Y. Singh, A. Zenesini, D. Ciampini, O. Morsch, and E. Arimondo, *Observation of photon-assisted tunneling in optical lattices*, accepted for publication in *Phys. Rev. Lett.*

Observation of photon-assisted tunneling in optical lattices

C. Sias, H. Lignier, Y. P. Singh, A. Zenesini, D. Ciampini, O. Morsch and E. Arimondo
CNR-INFM, Dipartimento di Fisica 'E. Fermi', Largo Pontecorvo 3, 56127 Pisa, Italy

We have observed tunneling suppression and photon-assisted tunneling of Bose-Einstein condensates in an optical lattice subjected to a constant force plus a sinusoidal shaking. For a sufficiently large constant force, the ground energy levels of the lattice are shifted out of resonance and tunneling is suppressed; when the shaking is switched on, the levels are coupled by low-frequency photons and tunneling resumes. Our results agree well with theoretical predictions and demonstrate the usefulness of optical lattices for studying solid-state phenomena.

PACS numbers: 03.65.Xp, 03.75.Lm

A number of experiments in recent years have shown that Bose-Einstein condensates (BECs) [1] loaded into optical lattices are well suited to simulating solid state systems [2, 3]. Optical lattices are created by crossing two or more laser beams, and the resulting periodic potential landscapes (arising from the ac-Stark shift exerted on the condensate atoms) are intrinsically defect-free, their lattice wells have controllable depths, and it is possible to move or accelerate the entire structure. This flexibility has made it possible to study dynamical effects such as Bloch oscillations [4] and resonant tunneling [5] as well as ground-state quantum properties such as the Mott-insulator transition [6]. More recently, the coherent suppression of inter-well tunneling by strong driving of the lattice has been demonstrated [7]. In this Letter, we explore an effect [8] that is analogous to photon-assisted tunneling in solids and arises from the interplay between static acceleration and strong driving of the lattice. We observe two regimes, a linear and a nonlinear one, with different dependencies of the observed tunneling on the theoretically predicted behaviour.

Photon-assisted tunneling occurs when adjacent potential wells whose ground states are tuned out of resonance by a static potential are coupled by photons (see Fig. 1). The static force leads to a suppression of resonant tunneling between the ground states. This suppression and the related Wannier-Stark localization of the wavefunction have been intensively discussed in the theoretical literature [9, 10]. In this work, we report a direct measurement of this suppression based on the spatial tunneling of the condensate atoms. When photons of an appropriate frequency are present whose energy bridges the gap created by the static potential, tunneling is (partly) restored. In solid state systems, the photons are typically in the microwave frequency range and the static potential is provided by an electric bias field applied to the structure. So far, photon-assisted tunneling has been observed in superconducting diodes [11], semiconductor superlattices [12, 13, 14] and quantum dots [15, 16].

Our system consists of a BEC inside a one-dimensional optical lattice. The static potential is provided by a constant acceleration of the lattice, resulting in a constant force F in the lattice rest frame and hence in a potential difference $\Delta E = Fd_L$ between adjacent wells a distance d_L apart. The role of the photons is played by a periodic shaking of the lattice at frequency ω that leads to the creation of sidebands around the carrier frequency of the laser beam. In the limit of sufficiently deep lattice wells and neglecting higher-lying energy levels, our system can be described by the Hamiltonian [8]

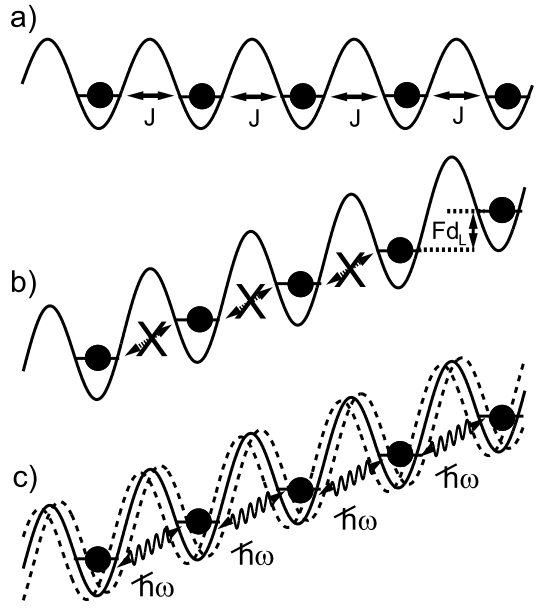

FIG. 1: Photon-assisted tunneling. (a) In an optical lattice at rest, the ground-state levels are resonantly coupled, leading to a tunneling energy J. (b) When a linear potential is applied, e.g. by accelerating the lattice, the levels are shifted out of resonance and tunneling is suppressed. (c) If the lattice is now periodically shaken at an appropriate frequency, the levels can again be coupled through photons of energy $\hbar\omega$ and tunneling is partially restored.

$$\hat{H}_0 = -\ J\sum_{\langle i,j\rangle}(\hat{c}_i^\dagger\hat{c}_j + \hat{c}_j^\dagger\hat{c}_i) + \frac{U}{2}\sum_j \hat{n}_j(\hat{n}_j - 1) + \quad (1)$$
$$+\ \Delta E\sum_j j\hat{n}_j + K\cos(\omega t)\sum_j j\hat{n}_j,$$

where $\hat{c}_i^{(\dagger)}$ are the boson creation and annihilation operators on site i, $\hat{n}_i = \hat{c}_i^\dagger \hat{c}_i$ are the number operators, and K and ω are the strength and angular frequency of the shaking, respectively. The first line of this equation is the Bose-Hubbard model [17] with the tunneling matrix element J and the on-site interaction term U (in a BEC, the on-site interaction is due to atom-atom collisions and hence proportional to the s-wave scattering length and the density of the BEC). In the second line, the first term describes the constant potential, whereas the second term represents the sinusoidal shaking of the lattice. While for a sufficiently strong linear potential inter-well tunneling is suppressed, leading to Wannier-Stark localization, recent theoretical work [8] predicts that the shaking term can partially restore it, leading to an effective tunneling rate

$$|J_{\rm eff}(K_0)/J| = |\mathcal{J}_n(K_0)| \tag{2}$$

when the resonance condition

$$n\hbar\omega = F d_L \tag{3}$$

is satisfied, where n is an integer denoting the order of the photon-assisted resonance, $\mathcal{J}_n$ is the n-th order ordinary Bessel function, and $K_0 = K/\hbar\omega$ is the dimensionless parameter characterizing the shaking amplitude.

In our experiment we produced BECs of ^{87}Rb containing around 5×10^4 atoms in a crossed optical dipole trap. The two dipole traps were created by gaussian laser beams at 1030 nm wavelength and a power of around 1 W per beam focused to waists of 50 μm, and the frequencies of the resulting trapping potentials could be controlled independently. Subsequently, the BECs held in the dipole trap were loaded into an optical lattice created by two counter-propagating gaussian laser beams ($\lambda = 852\,$nm) with 120 μm waists by ramping up the power of the lattice beams in about 50 ms. The resulting periodic potential $V(x) = V_0 \sin^2(\pi x/d_L)$ had a lattice spacing $d_L = \lambda/2 = 426\,$nm and its depth V_0 was measured in units of the recoil energy $E_{\rm rec} = \hbar^2\pi^2/(2md_L^2)$, where m is the mass of the Rb atoms. By introducing a frequency difference $\Delta\nu$ between the two lattice beams (using acousto-optic modulators, which also control the power of the beams), the optical lattice could be moved at a velocity $v = d_L\Delta\nu$ or accelerated with an acceleration $a = d_L\frac{d\Delta\nu}{dt}$. In order to periodically shake the lattice, $\Delta\nu$ was sinusoidally varied with frequency ω and amplitude $\Delta\nu_{\rm max}$ leading to a time-varying force (in the rest frame of the lattice)

$$F(t) = m\omega d_L \Delta\nu_{\rm max}\cos(\omega t) = F_{\rm max}\cos(\omega t). \tag{4}$$

The dimensionless shaking parameter K_0 is then given by

$$K_0 = K/\hbar\omega = m d_L^2 \Delta\nu_{\rm max}/\hbar = \pi^2\Delta\nu_{\rm max}/2\omega_{\rm rec}. \tag{5}$$

Our method for measuring the effective tunneling parameter $|J_{\rm eff}/J|$ (where the modulus indicates that this measurement is not sensitive to the sign of $J_{\rm eff}$) is based on the free expansion of the BEC [7, 18] confined only radially but free to move along the direction of the lattice (the dipole trap frequency in that direction being on the order of a few Hz and hence negligible for our purposes). After condensation was reached in the crossed dipole trap and the optical lattice had been ramped up, the trapping beam perpendicular to the lattice direction was suddenly switched off. Subsequently, the in-situ width of the BEC in the lattice direction was measured by flashing on a resonant beam and imaging the shadow cast by the BEC on a CCD camera. In the experiments with an accelerated and / or shaken lattice, $|J_{\rm eff}/J|$ was determined by measuring the expansion for the same lattice depth both in the driven case and without the driving.

In a preliminary experiment, we studied the tunneling suppression caused by shifting adjacent ground states out of resonance through a constant force F acting on the BEC inside a lattice that was subjected to an acceleration a. Typical accelerations in our experiment were between 0 and 4 ms^{-2}, meaning that for an expansion time of 400 ms the lattice (and therefore the BEC) would have been displaced by up to 32 cm, two orders of magnitude more than the field-of-view of our imaging system. Also, a displacement of more than 100 μm along the lattice direction would have led to a restoring force of the longitudinal harmonic trap created by the radial dipole trap beam corresponding to an acceleration $a_{\rm restore} > 0.1\,$ms^{-2}. Therefore, in order to be able to achieve a high resolution in our measurements of the expansion rate (and hence J) of the condensate, implying a long expansion time, whilst keeping the displacement of the lattice below $\approx 100\,\mu$m, we used a rectangular acceleration profile that alternated between $+a$ and $-a$ and therefore 'rocked' the lattice back and forth. In this way, the modulus of the resulting force and hence the energy shift between adjacent wells was constant, while the mean position of the lattice (and hence the BEC) remained close to the center of the dipole trap. In order to separate the frequency regimes of the rocking and the shaking motion, we chose a 'rocking frequency' of 30 Hz, which was much smaller than the resonant frequencies for photon-assisted tunneling (typically around $150 - 400\,$Hz).

Figure 2 (a) shows the results of our measurements of $|J_{\rm eff}|$ in an accelerated (rocked) lattice. As expected, when the energy difference Fd_L between adjacent levels is increased, resonant tunneling is reduced and, for $Fd_L \approx J$, completely suppressed (as recently also observed for single-atom tunneling in a double-well structure [19]). In this limit, the energy levels in the individual wells can be viewed as Wannier-Stark levels. Our data are fitted very well by a Lorentzian, but to our knowledge there is no analytical prediction for such a dependence in the theoretical literature. In [10], an expression for the wavefunction in a tilted lattice as a function of the applied force is given, but an analytical calculation of $J_{\rm eff}(F)$ has yet to be done.

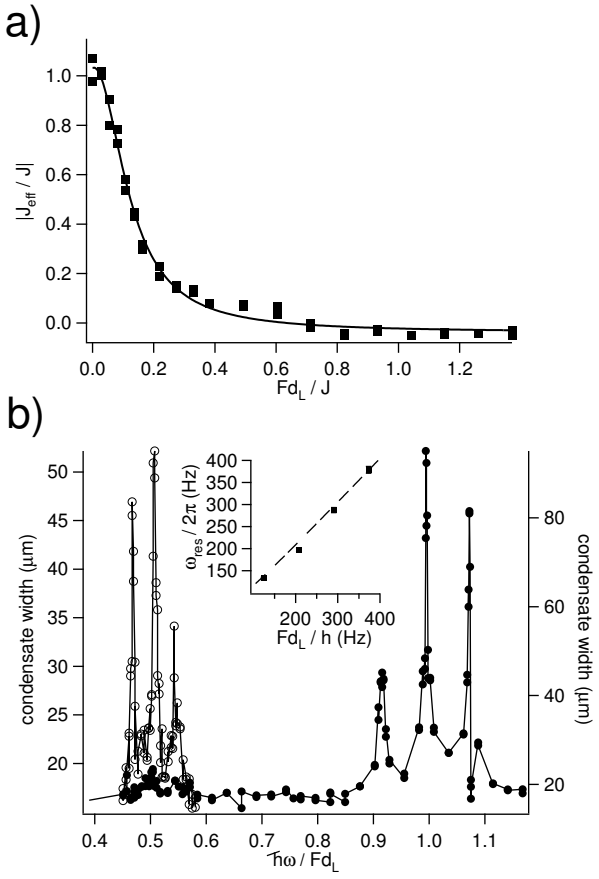

FIG. 2: (a) Suppression of tunneling by a linear potential. Shown here is the normalized effective tunneling parameter $|J_{\rm eff}/J|$ as a function of the linear potential Fd_L in units of the tunneling energy. When $Fd_L/J \approx 1$, the ground state levels are shifted out of resonance and tunneling is suppressed almost completely. The solid line is a Lorentzian fit with a half-maximum half-width of 0.13. (b) Photon-assisted tunneling resonances in a shaken lattice. For a fixed linear potential $Fd_L/h = 380\,$Hz, the condensate width after 400 ms of free expansion is plotted as a function of the normalized shaking frequency $\hbar\omega/Fd_L$. The fixed shaking parameter was $K_0 = 1.8$ for the one-photon resonance (solid circles) and $K_0 = 3.1$ for the two-photon resonance (open circles), corresponding to the first maximum of the $\mathcal{J}_1$ and $\mathcal{J}_2$ Bessel functions, respectively. For both graphs, $V_0/E_{\rm rec} = 5$ and $J/h = 380\,$Hz.

Tunneling between the on-site levels shifted out of resonance by the static acceleration can be partially restored by sinusoidally shaking the lattice at a frequency ω satisfying the resonance condition of Eq. 3. The shaking of the lattice effectively creates low-frequency 'photons' that bridge the energy gap between adjacent wells with n such photons (see Fig. 1 (c)). Figure 2 (b) shows the condensate width after 400 ms of free expansion inside a rocked lattice with $Fd_L/J = 1$ as a function of the shaking frequency ω. One clearly sees two photon-assisted tunneling peaks at $\hbar\omega = Fd_L$ (for $K_0 = 1.8$, where $\mathcal{J}_1(K_0)$ has its first maximum) and at $2\hbar\omega = Fd_L$ (for $K_0 = 3.1$, the first maximum of $\mathcal{J}_2(K_0)$). The peaks are extremely narrow, with a width of $\approx 3\,$Hz (when we repeated the experiment with smaller values of Fd_L, this width increased slightly). The two side-peaks of each peak are evidence of additional photon-assisted tunneling events due to the rocking motion of the lattice (for the two-photon resonance at $2\hbar\omega = Fd_L$, the side-peaks are at half the distance to the main peak compared to the one-photon case, as expected).

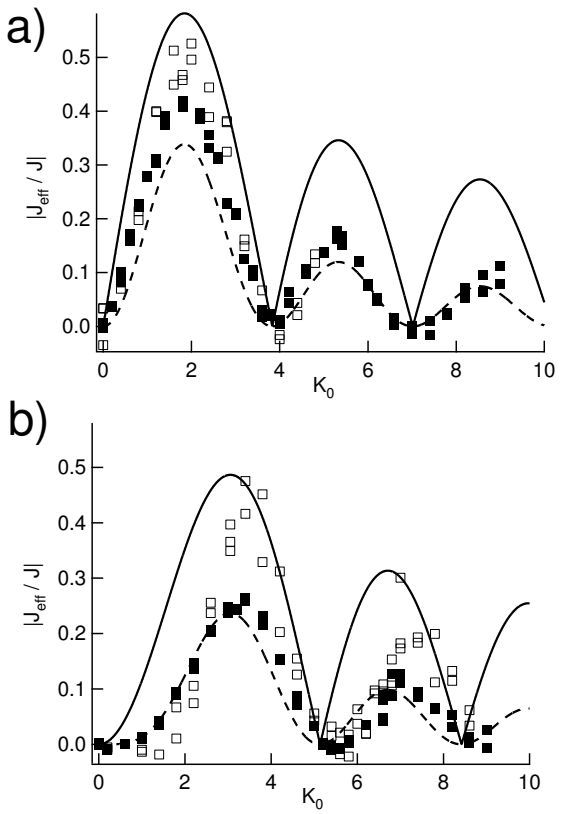

FIG. 3: Photon-assisted tunneling as a function of the shaking parameter K_0. Shown here are the one-photon resonance at $\omega/2\pi = 380\,$Hz (a) and the two-photon resonance at $\omega/2\pi = 190\,$Hz (b). In both graphs, the full and open squares are the measurements for $N \approx 5\times10^4$ and $N \approx 0.5\times10^4$, respectively. The solid lines are the moduli of the $\mathcal{J}_1(K_0)$ and $\mathcal{J}_2(K_0)$ Bessel functions, respectively, whereas the dashed lines are the squares of these functions. The lattice depth $V_0/E_{\rm rec} = 5$ and the constant force $Fd_L/h = 380\,$Hz in this experiment, with a free expansion time $t = 100\,$ms.

Finally, we studied the dependence of the effective tunneling rate on the shaking parameter K_0. Figure 3 summarizes our results for the one-photon and two-photon resonances. Theory predicts [8] that the effective tunneling rates $|J_{\rm eff}/J|$ for resonances of n-th order should vary as an n-th order ordinary Bessel function (see Eq. 2). While qualitative agreement between experiment and theory is good, with the positions of the maxima and minima of the one- and two-photon resonances as a function of K_0 coinciding perfectly with theoretical predictions, the absolute values of $|J_{\rm eff}/J|$ lie consistently

below the theoretical curves by a factor of about 1.3.

Interestingly, quantitative agreement between experiment and theory is better if we use the squares of the Bessel functions rather than their moduli. A dependence of the photon-assisted tunneling rate on the square of the Bessel function is expected, e.g., for experiments on Josephson junctions irradiated by microwaves and, more generally, if the tunneling in a multi-well structure is sequential rather than coherent. The difference between coherent and sequential tunneling has been extensively studied in the theoretical literature [20]. Sequential tunneling would require a dephasing mechanism between two successive tunneling events. In our experiments, such a mechanism could be the dynamical instability inside the optical lattice [21, 22, 23]: owing to the constant applied acceleration a, the BEC moves through the Brillouin zone and hence through the dynamically unstable region within the Brillouin zone between about $0.5\,p_{\rm rec}$ (where $p_{\rm rec} = \pi\hbar/d_L$ is the recoil momentum) and the zone edge. For the values of the intrinsic nonlinearity of the BEC in our experiments (determined by the number of atoms and the trap frequencies), we found in previous experiments [21] (and have verified for this work) that the BEC loses its phase coherence after a few milliseconds inside the unstable region, which is comparable to the Bloch periods in the present experiment. Since the effective tunneling frequencies $J_{\rm eff}$ in our experiment are less than 100 Hz, the corresponding dephasing rate is almost an order of magnitude larger and hence it is likely that dephasing of neighbouring wells occurs between two tunneling events.

In future experiments one might use, e.g., Feshbach resonances in order to tune the nonlinearity and hence move from the strongly nonlinear regime to the linear regime in order to test our hypothesis. As a preliminary test, we have repeated the measurement of the one-photon assisted tunneling rate as a function of K_0 with the smallest atom number that allowed us to measure the free expansion ($N \approx 0.5 \times 10^4$), resulting in a condensate density that was about a factor of 3 smaller. Again, we obtained qualitatively similar results to the measurements with $N \approx 5\times10^4$, but this time the absolute values of $|J_{\rm eff}/J|$ agreed better with the linear Bessel-function prediction (see Fig. 3).

A further indication that dephasing might be responsible for the observed deviation from the linear Bessel functions comes from our measurements of the dynamical suppression of tunneling in a shaken lattice *without* linear acceleration [7], in which our measured values for $J_{\rm eff}/J$ agreed perfectly with the linear Bessel function prediction. In that system, the BEC does not cross the unstable region of the Brillouin zone, and we have experimentally verified that during the shaking the BEC retains its phase coherence.

If the two regimes of photon-assisted tunneling observed in our experiment do, indeed, correspond to coherent and sequential tunneling, our system is ideally suited to studying the cross-over between these two extremes in a well-controlled way. However, we also have to consider the possibility that other effects play a role. In particular, it is conceivable that a self-trapping mechanism is present that depends on the relative magnitude of the nonlinearity U and the effective tunneling parameter $J_{\rm eff}$. Self-trapping in static optical lattices has already been observed [18] and could, if present also in our strongly driven system, lead to a suppression of the tunneling rate compatible with our observations, also for the case of a static force as in Fig. 2(a). On the other hand, our system is only in a self-trapping regime (as calculated from $U/h \approx 10-30$ Hz and $J_{\rm eff}$) in a small region around the zeroes of the Bessel functions, whereas we observe the largest deviation from the linear prediction close to the local maxima.

In summary, we have demonstrated photon-assisted tunneling of BECs in a linearly accelerated and sinusoidally shaken optical lattice. Our results agree quantitatively with recent theoretical predictions and show the need for a theoretical investigation into the difference between the (roughly) linear and the nonlinear regimes for which we observe difference dependencies of the effective tunneling rate on the predicted linear Besse-function scaling.

This work was supported by OLAQUI and MIUR-PRIN. The authors would like to thank M. Holthaus for illuminating discussions.

[1] O. Morsch and M. Oberthaler, Rev. Mod. Phys. **78**, 179 (2006).
[2] I. Bloch, Nat. Phys. **1**, 23 (2005).
[3] I. Bloch, J. Dalibard, and W. Zwerger, arXiv:0704.3011 (2007).
[4] O. Morsch, J.H. Müller, M. Cristiani, D. Ciampini, and E. Arimondo, Phys. Rev. Lett. **87**, 140402 (2001).
[5] C. Sias *et al.*, Phys. Rev. Lett. **98**, 120403 (2007).
[6] M. Greiner, O. Mandel, T. Esslinger, T. W. Hänsch, and I. Bloch, Nature **415**, 39 (2002).
[7] H. Lignier *et al.*, arXiv:0707.0403 (2007).
[8] A. Eckardt, T. Jinasundera, C. Weiss, and M. Holthaus, Phys. Rev. Lett. **95**, 200401 (2005).
[9] F. Rossi, Semicond. Sci. Technol. **13**, 147 (1998).
[10] M. Glück, A. R. Kolovsky, and H. J. Korsch, Physics Reports **366**, 103 (2002).
[11] P.K. Tien and J.P. Gordon, Phys. Rev. **129**, 647 (1963).
[12] P.S.S. Guimarães *et al.*, Phys. Rev. Lett. **70**, 3792 (1993).
[13] B.J. Keay *et al.*, Phys. Rev. Lett. **75**, 4098 (1995).
[14] B.J. Keay *et al.*, Phys. Rev. Lett. **75**, 4102 (1995).
[15] L.P. Kouwenhoven *et al.*, Phys. Rev. Lett. **73**, 3443 (1994).
[16] T.H. Oosterkamp, L.P. Kouwenhoven, A.E.A. Koolen, N.C. van der Vaart, and C.J.P.M. Harmans, Phys. Rev.

Lett. **78**, 1536 (1997).
[17] D. Jaksch, C. Bruder, J. I. Cirac, C. W. Gardiner, and P. Zoller, Phys. Rev. Lett. **81**, 3108 (1998).
[18] Th. Anker *et al.*, Phys. Rev. Lett. **94**, 0204003 (2005).
[19] S. Fölling *et al.*, Nature **448**, 1029 (2007).
[20] M. Büttiker, IBM J. Res. Develop. **32**, 63 (1988).
[21] M. Cristiani, *et al.* Opt. Express **12**, 4 (2004).
[22] L. Fallani, *et al.*, Phys. Rev. Lett. **93**, 140406 (2004).
[23] J. Mun, *et al.*, arXiv:0706.3946 (2007).

Bibliography

[1] Bose, S. *Z. Phys.* **26**, 178 (1924).

[2] Einstein, A. *Sitzber. Kgl. Preuss. Akad. Wiss.* , 261 (1924).

[3] Einstein, A. *Sitzber. Kgl. Preuss. Akad. Wiss.* , 3 (1925).

[4] Cohen-Tannoudji, C. *Rev. Mod. Phys.* **70**(3), 707 (1998).

[5] Chu, S. *Rev. Mod. Phys.* **70**(3), 685 (1998).

[6] Phillips, W. *Rev. Mod. Phys.* **70**(3), 721 (1998).

[7] Anderson, M., Ensher, J., Matthews, M., Wieman, C., and Cornell, E. *Science* **269**, 198 (1995).

[8] Davis, K., Mewes, M., Andrews, M., van Druten, N., Durfee, S., Kurn, D., and Ketterle, W. *Phys. Rev. Lett.* **75**(22), 3969 (1995).

[9] Moskowitz, P., Gould, P., Atlas, S., and Pritchard, D. *Phys. Rev. Lett.* **51**(5), 370 (1983).

[10] Gould, P., Ruff, G., and Pritchard, D. *Phys. Rev. Lett.* **56**(8), 827 (1986).

[11] Anderson, B. and Kasevich, M. *Science* **282**, 1686 (1998).

[12] Morsch, O. and Oberthaler, M. *Rev. Mod. Phys.* **78**, 179 (2004).

[13] Bloch, I. *Nature Physics* **1**, 23 (2005).

[14] Huang, K. *Statistical Mechanics*. John Wiley & Sons, Inc., third edition, (1966).

[15] Dalfovo, F., Giorgini, S., Pitaevskii, L., and Stringari, S. *Rev. Mod. Phys.* **71**(3), 463 (1999).

[16] Hänsch, T. and Schawlow, A. *Optics Commun.* **13**(1), 68 (1975).

[17] Metcalf, H. and van der Straten, P. *Laser Cooling and Trapping.* Springer, (2002).

[18] Chu, S., Hollberg, L., Bjorkholm, J., Cable, A., and Ashkin, A. *Phys. Rev. Lett.* **55**(1), 48 (1985).

[19] Wineland, D. and Itano, W. *Phys. Rev. A* **20**(4), 1521 (1979).

[20] Lett, P., Watts, R., Westbrook, C., Phillips, W., Gould, P., and Metcalf, H. *Phys. Rev. Lett.* **61**(2), 169 (1988).

[21] Dalibard, J. and Cohen-Tannoudji, C. *J. Opt. Soc. Am. B* **2**(11), 1707 (1985).

[22] Dalibard, J. and Cohen-Tannoudji, C. *J. Opt. Soc. Am. B* **6**(11), 2023 (1989).

[23] Castin, Y., Dalibard, J., and Cohen-Tannoudji, C. In *Light Induced Kinetic Effects on Atoms, Ions and Molecules,* Moi, L., Gozzini, S., Gabbanini, C., Arimondo, E., and Strumia, F., editors, 5. ETS Editrice, Pisa (1991).

[24] Raab, E., Prentiss, M., Cable, A., Chu, S., and Pritchard, D. *Phys. Rev. Lett.* **59**(23), 2631 (1987).

[25] Masuhara, N., Doyle, J., Sandberg, J., Kleppner, D., and Greytak, T. *Phys. Rev. Lett.* **61**(8), 935 (1988).

[26] Petrich, W., Anderson, M., Ensher, J., and Cornell, E. *Phys. Rev. Lett.* **74**(17), 3352 (1995).

[27] Chu, S., Bjorkholm, J., Ashkin, A., and Cable, A. *Phys. Rev. Lett.* **57**(3), 314 (1986).

[28] Arimondo, E., Lew, H., and Oka, T. *Phys. Rev. Lett.* **43**(11), 753 (1979).

[29] Gupta, S., Leanhardt, A., Cronin, A., and Pritchard, D. *C. R. Acad. Sci. Paris* **2**(IV), 479 (2001).

[30] Martin, P., Oldaker, B., Miklich, A., and Pritchard, D. *Phys. Rev. Lett.* **60**(6), 515 (1988).

[31] Niu, Q., Zhao, X., Georgakis, G., and Raizen, M. G. *Phys. Rev. Lett.* **76**(24), 4504 (1996).

[32] Dahan, M., Peik, E., Reichel, J., Castin, Y., and Salomon, C. *Phys. Rev. Lett.* **76**(24), 4508 (1996).

[33] Wilkinson, S., Bharucha, C., Madison, K., Niu, Q., and Raizen, M. *Phys. Rev. Lett.* **76**(24), 4512 (1996).

[34] Bloch, I., Dalibard, J., and Zwerger, W. *cond-mat* , 07043011 (2007).

[35] Greiner, M., Mandel, O., Esslinger, T., Hänsch, T., and Bloch, I. *Nature* **415**, 39 (2002).

[36] Kozuma, M., Deng, L., Hagley, E., Wen, J., Lutwak, R., Helmerson, K., Rolston, S., and Phillips, W. *Phys. Rev. Lett.* **82**(5), 871 (1999).

[37] Keller, C., Schmiedmayer, J., Zeilinger, A., Nonn, T., Dürr, S., and Rempe, G. *Appl. Phys. B* **69**(4), 303 (1999).

[38] Ashcroft, N. and Mermin, N. *Solid state physics*. Saunders college, (1976).

[39] Abramowitz, M. and Stegun, I. *Handbook of mathematical funtions*, volume 55 of *Applied mathematics series*. National bureau of standards, tenth edition, (1972).

[40] Santos, L., Baranov, M., Cirac, J., Everts, H.-U., Fehrmann, H., and Lewenstein, M. *Phys. Rev. Lett.* **93**, 030601 (2004).

[41] Jaksch, D., Bruder, C., Cirac, J., Gardiner, C., and Zoller, P. *Phys. Rev. Lett.* **81**(15), 3108 (1998).

[42] Zwerger, W. *J. Opt. B: Quantum Semiclass. Opt.* **5**, S9 (2003).

[43] Inouye, S., Andrews, M., Stenger, J., Miesner, H.-J., Stamper-Kurn, D., and Ketterle, W. *Nature* **392**, 151 (1998).

[44] Courteille, P., Freeland, R., Heinzen, D., van Abeelen, F., and Verhaar, B. *Phys. Rev. Lett.* **81**(1), 69 (1998).

[45] Sakurai, J. *Modern Quantum Mechanics*. Addison-Wesley, (1985).

[46] Bloch, F. *Z. Phys.* **52**, 555 (1929).

[47] Feldmann, J., Leo, K., Shan, J., Miller, D., Cunningham, J., Meier, T., von Plessen, G., Schulze, A., Thomas, P., and Schmitt-Rink, S. *Phys. Rev. B* **46**(11), 7252 (1992).

[48] Leo, K., Haring Bolivar, P., Brüggemann, F., Schwedler, R., and Köhler, K. *Solid State Commun.* **84**, 943 (1992).

[49] Waschke, C., Roskos, H., Schwedler, R., Leo, K., Kurz, H., and Köhler, K. *Phys. Rev. Lett.* **70**(21), 3319 (1993).

[50] Peik, E., Dahan, M., Bouchoule, I., Castin, Y., and Salomon, C. *Phys. Rev. A* **55**(4), 2989 (1997).

[51] Peik, E., Dahan, M., Batelaan, H., Castin, Y., and Salomon, C. *Appl. Phys. B* **65**, 685 (1997).

[52] Morsch, O., Müller, J., Cristiani, M., Ciampini, D., and Arimondo, E. *Phys. Rev. Lett.* **87**(14), 140402 (2001).

[53] Denschlag, J., Simsarian, J., Häffner, H., McKenzie, C., Browaeys, A., Cho, D., Helmerson, K., Rolston, S., and Phillips, W. *J. Phys. B: At. Mol. Opt. Phys.* **35**, 3095 (2002).

[54] Greiner, M., Mandel, O., Hänsch, T., and Bloch, I. *Nature* **419**, 51 (2002).

[55] Mellish, A., Duffy, G., McKenzie, C., Geursen, R., and Wilson, A. *Phys. Rev. A* **68**, 051601(R) (2003).

[56] Cristiani, M., Morsch, O., Müller, J., Ciampini, D., and Arimondo, E. *Phys. Rev. A* **65**(6), 063612 (2002).

[57] Pedri, P., Pitaevskii, L., Stringari, S., Fort, C., Burger, S., Cataliotti, F., Maddaloni, P., Minardi, F., and Inguscio, M. *Phys. Rev. Lett.* **87**(22), 220401 (2001).

[58] Slater, J. *Phys. Rev.* **87**(5), 807 (1952).

[59] Landau, L. *Phys. Z. Sowjetunion* **2**, 46 (1932).

[60] Zener, C. *Proc. R. Soc. London, Ser. A* **137**, 696 (1932).

[61] Glück, M., Kolovsky, A., and Korsch, H. *Phys. Rep.* **366**(3), 103 (2002).

[62] Glück, M., Kolovsky, A., and Korsch, H. *Phys. Rev. Lett.* **83**(5), 891 (1999).

[63] Chang, L., Esaki, L., and Tsu, R. *Appl. Phys. Lett.* **24**, 593 (1974).

[64] Esaki, L. *IEEE J. Quantum Electron.* **22**(9), 1611 (1986).

[65] Glutsch, S. *Phys. Rev. B* **69**(23), 235317 (2004).

[66] Wagner, M. and Mizuta, H. *Phys. Rev. B* **48**(19), 14393 (1993).

[67] Bharucha, C., Madison, K., Morrow, P., Wilkinson, S., Sundaram, B., and Raizen, M. G. *Phys. Rev. A* **55**(2), R857 (1997).

[68] Sias, C., Zenesini, A., Lignier, H., Wimberger, S., Ciampini, D., Morsch, O., and E., A. *Phys. Rev. Lett.* **98**, 120403 (2007).

[69] Gericke, T., Gerbier, F., Widera, A., Fölling, S., Mandel, O., and Bloch, I. *e-print* , condmat/0603590.

[70] Choi, D. I. and Niu, Q. *Phys. Rev. Lett.* **82**(10), 2022 (1999).

[71] Avron, J. *Ann. Phys. (N.Y.)* **366**, 103 (1982).

[72] Glück, M., Kolovsky, A., and Korsch, H. *J. Opt. B: Quantum Semiclass. Opt.* **2**, 694 (2000).

[73] Keck, F., Korsch, H., and Mossmann, S. *J. Phys. A: Math. Gen.* **36**, 2125 (2003).

[74] Schmid, S., Thalhammer, G., Winkler, K., Lang, L., and Denschlag, J. *New J. Phys.* **8**, 159 (2006).

[75] Wimberger, S., Mannella, R., Morsch, O., Arimondo, E., Kolovsky, A., and Buchleitner, A. *Phys. Rev. A* **72**, 063610 (2005).

[76] Wu, B. and Niu, Q. *Phys. Rev. A* **64**(6), 061603 (2001).

[77] Cristiani, M., Morsch, O., Malossi, N., Jona-Lasinio, M., Anderlini, M., Courtade, E., and Arimondo, E. *Optics express* **12**(1), 4 (2004).

[78] Fallani, L., De Sarlo, L., Lye, J., Modugno, M., Saers, R., Fort, C., and Inguscio, M. *Phys. Rev. Lett.* **93**(14), 140406 (2004).

[79] Jona-Lasinio, M., Morsch, O., Cristiani, M., Malossi, N., Müller, J., Courtade, E., Anderlini, M., and Arimondo, E. *Phys. Rev. Lett.* **91**(23), 230406 (2003).

[80] Morsch, O., Müller, J., Ciampini, D., Cristiani, M., Blakie, P., Williams, C., Julienne, P., and Arimondo, E. *Phys. Rev. A* **67**(3), 031603(R) (2003).

[81] Trippenbach, M., Band, Y., and Julienne, P. *Phys. Rev. A* **62**, 023608 (2000).

[82] Eckardt, A., Weiss, C., and Holthaus, M. *Phys. Rev. Lett.* **95**, 260404 (2005).

[83] Creffield, C. and Monteiro, T. *Phys. Rev. Lett.* **96**, 210403 (2006).

[84] Grossmann, F., Dittrich, T., Jung, P., and Hänggi, P. *Phys. Rev. Lett.* **67**, 516 (1991).

[85] Shirley, J. *Phys. Rev.* **138**(4B), B979 (1965).

[86] Sambe, H. *Phys. Rev. A* **7**(6), 2203 (1973).

[87] Grifoni, M. and Hänggi, P. *Phys. Rep.* **304**, 229 (1998).

[88] Haroche, S. and Cohen-Tannoudji, C. *Phys. Rev. Lett.* **24**(16), 861 (1970).

[89] Cohen-Tannoudji, C. In *Cargése Lectures in Physics,* Lévy, M., editor, volume 2, 347. Gordon and Breach, Amsterdam (1968).

[90] Holthaus, M. In *Coherent Control in Atoms, Molecules, and Semiconductor,* Pötz, W. and Schroeder, W., editors, 171. Kluwer, Dordrecht (1999).

[91] Keay, B. J., Zeuner, S., Allen, S. J., Maranowski, K. D., Gossard, A. C., Bhattacharya, U., and Rodwell, M. J. W. *Phys. Rev. Lett.* **75**(22), 4102 (1995).

[92] Madison, K., Fischer, M., Diener, R., Niu, Q., and Raizen, M. G. *Phys. Rev. Lett.* **81**(23), 5093 (1998).

[93] Iyer, R., Stewart Aitchison, J., Dignam, M., and de Sterke, C. *Opt. Expr.* **15**, 3212 (2007).

[94] Longhi, S., Marangoni, M., Lobino, M., Ramponi, R., Laporta, P., Cianci, E., and Foglietti, V. *Phys. Rev. Lett.* **96**, 243901 (2006).

[95] Della Valle, G., Ornigotti, M., Cianci, E., Foglietti, V., Laporta, P., and Longhi, S. *Phys. Rev. Lett.* **98**, 263601 (2007).

[96] Dunlap, D. and Kenkre, V. *Phys. Rev. B* **34**, 3625 (1986).

[97] Kierig, E., Schietinger, A., Schnorrberger, U., Tomkovic, J., Welte, J., and Oberthaler, M. *Proceedings of TPG-Tagung 2007* (Deutsche Physikalische Gesellschaft e.V., Berlin, 2007) , Abstract No. Q 21.7 (2007).

[98] Li, W., Tuchman, A., and Chien, H.-C. anf Kasevich, M. *Phys. Rev. Lett.* **98**, 040402 (2007).

[99] Smerzi, A., Fantoni, S., Giovanazzi, S., and Shenoy, S. *Phys. Rev. Lett.* **79**(25), 4950 (1997).

[100] Tien, P. and Gordon, J. *Phys. Rev.* **129**, 647 (1963).

[101] Kouwenhoven, L. P., Jauhar, S., Orenstein, J., McEuen, P. L., Nagamune, Y., Motohisa, J., and Sakaki, H. *Phys. Rev. Lett.* **73**(25), 3443 (1994).

[102] Keay, B. J., Allen, S. J., Galán, J., Kaminski, J. P., Campman, K. L., Gossard, A. C., Bhattacharya, U., and Rodwell, M. J. W. *Phys. Rev. Lett.* **75**(22), 4098 (1995).

[103] Guimarães, P. S. S., Keay, B. J., Kaminski, J. P., Allen, S. J., Hopkins, P. F., Gossard, A. C., Florez, L. T., and Harbison, J. P. *Phys. Rev. Lett.* **70**(24), 3792 (1993).

[104] Oosterkamp, T. H., Kouwenhoven, L. P., Koolen, A. E. A., van der Vaart, N. C., and Harmans, C. J. P. M. *Phys. Rev. Lett.* **78**(8), 1536 (1997).

[105] Eckardt, A., Jinasundera, T., Weiss, C., and Holthaus, M. *Phys. Rev. Lett.* **95**, 200401 (2005).

[106] Fölling, S., Trotzky, S., Cheinet, P., Feld, M., Saers, R., Widera, A., Müller, T., and Bloch, I. *Nature* **448**, 1029 (2007).

[107] Büttiker, M. *IBM J. Res. Develop.* **32**, 63 (1988).

[108] Mun, J., Medley, P., Campbell, G., Marcassa, L., Pritchard, D., and Ketterle, W. *Phys. Rev. Lett.* **99**, 150604 (2007).

[109] Trombettoni, A. and Smerzi, A. *Phys. Rev. Lett.* **86**(11), 2353 (2001).

[110] Anker, T., Albiez, M., Gati, R., Hunsmann, S., Eiermann, B., Trombettoni, A., and Oberthaler, M. *Phys. Rev. Lett.* **94**, 020403 (2005).

[111] Lignier, H., Sias, C., Ciampini, D., Singh, Y., Zenesini, A., Morsch, O., and Arimondo, E. *Phys. Rev. Lett.* **99**, 220403 (2007).

[112] Sias, C., Lignier, H., Singh, Y., Zenesini, A., Ciampini, D., Morsch, O., and Arimondo, E. *accepted for publication in Phys. Rev. Lett.* .